MULTIFACETED INVESTIGATION OF RIBONUCLEASE MRP IN *CYANIDIOSCHYZON MEROLAE*: HEAT STRESS RESPONSE, CANONICAL rRNA PROCESSING PATHWAY, STRUCTURAL PREDICTION AND MUTATIONAL ANALYSIS

by

Sebastian Fumador

BSc., University of Health and Allied Sciences, 2020

THESIS SUBMITTED IN PARTIAL FULFILLMENT OF
THE REQUIREMENTS FOR THE DEGREE OF
MASTER OF SCIENCE
IN
BIOCHEMISTRY

UNIVERSITY OF NORTHERN BRITISH COLUMBIA

December 2024

Abstract

RNase MRP is a ribonucleoprotein complex essential for ribosome biogenesis in eukaryotes including *Saccharomyces cerevisiae* and humans. Mutations in the single genomic locus encoding its noncoding RNA component result in cartilage-hair hypoplasia (CHH), a recessively inherited developmental disorder. In *Cyanidioschyzon merolae,* the 442-nucleotide RNA component of RNase MRP is encoded within the intronic region of the CMK142T gene. Under heat stress conditions, this intronic region accumulates significantly, prompting investigations into the effects of heat stress on RNase MRP expression and its role in 5.8S rRNA processing. The impact on 5.8S rRNA processing of deleting the P19 region (Δ372–405) and the G162A mutation via homologous recombination was assessed using Northern blot analysis while computational analyses were performed to compare structural conservation and protein composition of RNase MRP in *C. merolae* with other eukaryotes. Total RNA analysis indicates that deletion of the P19 region (Δ372–405) of MRP significantly alters the stoichiometry of 5.8S rRNA forms, underscoring its importance in rRNA processing. Additionally, *C. merolae* adheres to the canonical rRNA processing pathway and while rDNA transcription is inhibited under heat stress, the stability of mature 28S and 18S rRNA remains unaffected, indicating the organism's sophisticated regulatory mechanism in ribosome biogenesis. Computational comparative genomics analyses revealed conserved structural regions in *C. merolae* RNase MRP RNA, highlighting evolutionary conservation. The complex in *C. merolae* is predicted to comprise five proteins, fewer than the eleven in *S. cerevisiae*, reflecting dramatic streamlining of RNA processing pathways which parallels findings in pre-mRNA splicing. These findings confirm the conserved function of RNase MRP in *C. merolae* and raise important questions about why the levels appear to increase under heat stress.

Table of Contents

List of Tables

List of Figures

List of Abbreviations

aa – amino acid(s)

APS – ammonium persulfate

ATP – adenosine triphosphate

bp – base pair(s)

CHH – Cartilage hair hypoplasia

C. merolae – Cyanidioschyzon merolae strain 10D

CR – Conserved Region

CAT – Chloramphenicol Acetyltransferase

dATP – deoxyadenosine triphosphate

dCTP – deoxycytidine triphosphate

dGTP – deoxyguanosine triphosphate

DMSO – dimethyl sulfoxide

DNA – deoxyribonucleic acid

dNTPs – deoxynucleotide triphosphates, consisting of dATP, dCTP, dGTP, and dTTP

dTTP – deoxythymidine triphosphate

EDTA – Ethylenediaminetetraacetic acid

ETS1 – Externally Transcribed Spacer 1

ETS2 – Externally Transcribed Spacer 2

GTP – guanosine triphosphate

Int – Integrands

ITS1 – Internally Transcribed Spacer 1

ITS2 – Internally Transcribed Spacer 2

kbp – kilobase pairs

knt – kilonucleotides

LB – Luria broth

MA2 – modified Allen's 2×

MA2G – MA2 with glycerol

MA2GU – MA2G with uracil

MCS – multiple cloning site

mRNA – mature messenger RNA

MRP – Mitochondrial RNA Processing

NaOAc – sodium acetate

NCBI – National Center for Biotechnology Information

ncRNA – non-coding RNA

Nc – Negative Control

nt – nucleotide(s)

NTPs – nucleotide triphosphates, consisting of ATP, CTP, GTP, and UTP

OD750 – optical density at 750 nm

OMPD – orotidine 5′-monophosphate decarboxylase

OPRT – orotate phosphoribosyltransferase

PCR – polymerase chain reaction

PEG – polyethylene glycol

Pop – Processing of Precursor

pre-mRNA – precursor messenger RNA

RMRP – RNase MRP

pre-tRNA – precursor tRNA

RNA – ribonucleic acid

RNA-seq – RNA sequencing

RNase – Ribonuclease

rpm – revolutions per minute

rRNA – ribosomal RNA

Sd – Sulfadiazine

SDS – Sodium Dodecyl Sulfate

snoRNA – small nucleolar ribonucleic acid

snRNA – small nuclear ribonucleic acid

snRNP – small nuclear ribonucleoprotein

TERT – telomerase reverse transcriptase

tRNA – transfer RNA

UniProt – Universal Protein Resource

UTP – uridine triphosphate

Acknowledgments

I acknowledge that this research was conducted on the traditional, unceded territory of the Lheidli T'enneh First Nation, part of the Dakelh (Carrier) peoples' territory. I am grateful for the opportunity to live, learn, and work on their lands.

I would like to express my deepest gratitude to my supervisor, Dr. Stephen Rader, for his unwavering support, guidance, and encouragement throughout my research journey. His expertise, patience, and insightful feedback have been instrumental in shaping both my thesis and my development as a scientist.

I extend my sincere appreciation to Dr. Martha Stark for her patience in training me and for her invaluable help with technical challenges and troubleshooting. Her support made an enormous difference in my lab work.

I would like to thank my Graduate Supervisory Committee, Dr. Andrea Gorrell and Dr. Michael Preston, for their valuable feedback, advice, and encouragement. Their thoughtful guidance motivated me throughout this journey, and I appreciate their unwavering support. I would also like to extend my sincere thanks to my defense chair, Dr. Catharine Schiller and my external examiner, Dr. Marlene Oeffinger.

I am grateful to my colleagues in the Rader Lab for their friendship, collaboration, and the stimulating discussions that made my time in the lab both enjoyable and intellectually enriching. Your camaraderie has been an essential part of my graduate experience.

Dedication

This thesis is dedicated to my mother, Rosemary Afi Mattey, whose unwavering love, support, and encouragement have been my constant source of strength.

Chapter 1 – Introduction

1.1 RNase MRP

RNase MRP (ribonuclease for mitochondrial RNA processing) is an essential ribonucleoprotein endoribonuclease that cleaves RNA substrates in a site-specific manner and comprises a catalytic RNA moiety and multiple (ten in *Saccharomyces cerevisiae*) protein components (Karwan et al.,1991). RNase MRP is an essential eukaryotic enzyme that has been found in practically all eukaryotes analyzed (Piccinelli *et al*., 2005). It is localized to the nucleolus and, transiently, to the cytoplasm (Esakova *et al*., 2010). RNase MRP appears to have split from the RNase P lineage early in the evolution of eukaryotes, acquiring distinct substrate specificity and cellular functions (Piccinelli *et al*., 2005; Rosenblad et al., 2006; Lopez *et al*. 2009). The catalytic (C) domain of RNase MRP RNA (Figure 1.1a) has a secondary structure resembling that of the C-domain of RNase P (Figure 1.1b) and includes elements forming a highly conserved catalytic core. The specificity (S) domain of RNase MRP RNA does not have any apparent similarities with the specificity domain of RNase P (Figures 1.1a and b). Crosslinking studies (Esakova et al., 2013) indicate the involvement of the RNase MRP S-domain in substrate recognition. Most of the RNase MRP protein components are also found in eukaryotic RNase P (Chamberlain et al., 1998); the structures of *S. cerevisiae* and human RNases P have been determined (Lan, P. et al., 2018; Wu, J. et al. 2018). *S. cerevisiae* RNase MRP and RNase P share eight proteins (Pop1, Pop3, Pop4, Pop5, Pop6, Pop7, Pop8, and Rpp1 (two copies); RNase MRP protein Snm1 has a homolog in RNase P (Rpr2), while Rmp1 is found only in RNase MRP. Shared proteins bind to both catalytic (C) and specificity (S)-domains. Yeast RNase MRP proteins Pop1, Pop3, Pop4, Pop5, Pop6, Pop7, and Pop8 have homologs in human RNase P, while Pop3, Pop4, Pop5, and Rpp1 have homologs in archaeal RNases P. RNase MRP proteins Pop1, Pop6, Pop7 are also an essential part of yeast telomerase, where they are involved in the localization of the enzyme and

form a structural module that stabilizes the binding of telomerase components Est1 and Est2 (Lemieux *et al*., 2016; Garcia *et al*. 2020).

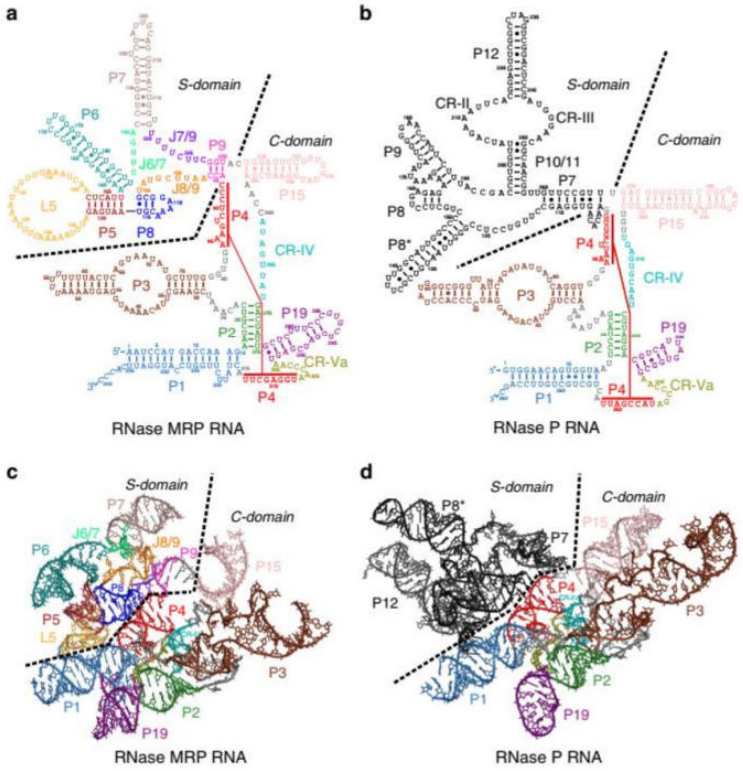

Figure 1.1. RNA components of RNase MRP and RNase P in *S. cerevisiae*. The catalytic (C-) domains of the two related enzymes are similar both in their secondary structures and in their folds, whereas the specificity (S-) domains are distinct. **a, b** Secondary structure diagrams of the RNase MRP and RNase P RNAs, respectively. **c, d** Folding of the RNase MRP and RNase P RNAs, respectively, color-coded as in (a, b). Adapted from Lan *et al*.,2018.

In a study published in 2020, a cryo-EM structure of the *S. cerevisiae* RNase MRP holoenzyme was resolved to a nominal resolution of 3.0 Å, providing new insights into its molecular architecture (Figure 1.2). It elucidates the overall structural organization of the ribonucleoprotein (RNP) complex, highlighting the arrangement of its catalytic RNA component, the substrate binding pocket, and the intricate interactions among RNase MRP components. A significant aspect of the research is the comparative analysis between RNase MRP and its evolutionary progenitor, eukaryotic RNase P. This comparison reveals that several proteins common to both

RNase MRP and RNase P undergo RNA-driven structural remodeling, enabling these ribonucleoproteins to function within distinct structural contexts (Figure 1.2) (Perederina *et al*.,2020). Notably, while the catalytic center of RNase MRP closely mirrors that of RNase P, there is a divergence in the topology of the substrate binding pocket, suggesting functional specialization within these closely related enzymes. These findings contribute to a deeper understanding of the structural and functional dynamics of RNase MRP, highlighting its role in cellular processes and its evolutionary relationship with RNase P (Perederina *et al*.,2020).

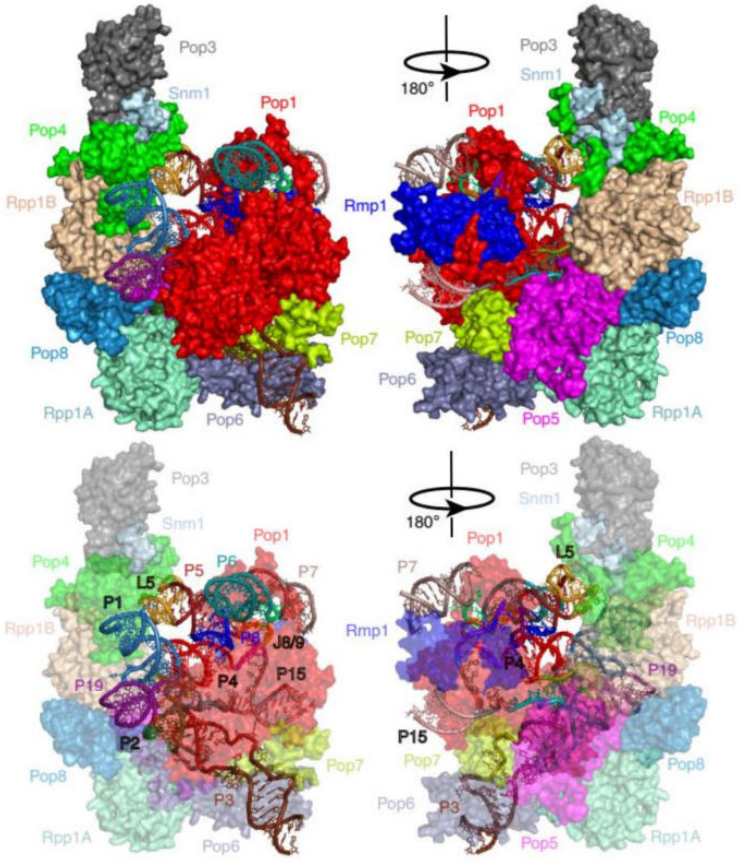

Figure 1.2. Structure of the RNase MRP holoenzyme. Protein components (shown as surfaces) are color-coded as marked; the RNA elements (shown as a cartoon) are color-coded according to Fig.1. Adapted from Perederina *et al.*, 2020.

1.2 Diseases Associated with RNase MRP

There are over 17, 000 human genetic disorders listed in the database of Online Mendelian Inheritance in Man (OMIM), and majority of these disorders relate to protein-coding genes, whereas only a few noncoding RNA genes have been linked to genetic diseases. Whilst noncoding RNA is an RNA molecule that functions without being translated into a protein, certain diseases are associated with noncoding RNAs. RNase MRP is a noncoding RNA involved in mitochondrial DNA replication (Figure 1.3a), pre-rRNA processing (Figure 1.3b and d), and processing of 5′-UTR of *CLB2* mRNA (Figure 1.3c).

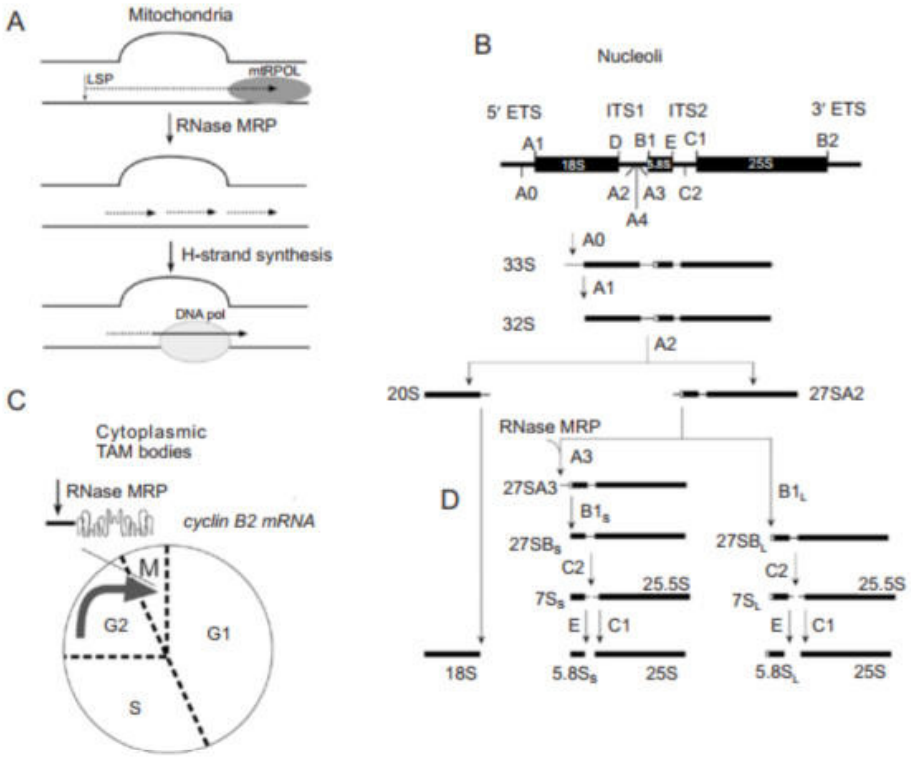

Figure 1.3. Function of the RNase MRP enzyme complex. **(a)** RNase MRP is involved in the processing of mitochondrial RNA that functions as a primer for mitochondrial DNA replication in mitochondria. Transcription starts from the light-strand promoter by mitochondrial RNA polymerase. After transcription of the heavy-strand origin of replication, the transcript remains bound to the DNA duplex and is cleaved by RNase MRP to form primers that are used for the initiation of DNA synthesis by DNA polymerase; Adapted from (Shadel et al.,1997). **(b, d)** RNase MRP functions in the pre-rRNA processing in S. cerevisiae. The 35S primary transcript is processed into mature 25S, 18S, and 5.8S rRNAs; Adapted from (Venema and Tollervey 1999). The cleavage sites (A0 through E), the external transcribed spacers (5′-ETS and 3′-ETS), and the internal transcribed spacers (ITS1 and ITS2) are indicated. The small white box marks the sequence in the long form of 5.8S rRNA, 5.8SL, that is absent in the short form, 5.8SS. RNase MRP processes the A3 site in ITS1; Adapted from (Schmitt and Clayton,1992). **(c)** RNase MRP processes the 5′-UTR of CLB2 mRNA in cytoplasmic temporal asymmetric MRP (TAM) bodies. CLB2 mRNA normally disappears rapidly as cells complete mitosis. RNase MRP mutations have an exit-from-mitosis defect and a late anaphase delay. RNase MRP specifically cleaves the CLB2 mRNA in its 5′-UTR to allow rapid 5′ to 3′ degradation by the Xrn1 nuclease. Degradation of the CLB2 mRNA by RNase MRP provides a novel way to regulate the cell cycle that complements the protein degradation machinery; Adapted from (Allison and Yong 2006).

Mutations to the single genomic locus for this noncoding transcript cause inviable yeast (Shadel et al. 2000), embryonic lethality in mice (Rosenbluh *et al*. 2011), and a spectrum of severely debilitating human diseases (Ridanpää *et al*. 2001), harkening to MRP RNA's essential role in

biology. Among these conditions is Cartilage Hair Hypoplasia (CHH), a pleiotropic human disease (Hirose *et al*.,2006). Two categories of mutations involving RNase MRP have been identified in patients with CHH. The first type is when an insertion, duplication, or triplication occurs at the promoter of the RNase MRP gene between the TATA box and the transcription initiation site. This causes the initiation of RNase MRP to be slow, or to not occur at all. The second category consists of mutations that are in the transcribed RNA made by the RNase MRP. Patients with CHH have been identified to have over 70 different mutations in the RNA transcript made by RNase MRP, whereas around 30 distinct mutations have been identified in the promoter region of the RNase MRP gene. Most CHH patients have a combination of either a promoter mutation in one allele along with an RNase MRP RNA mutation in the other allele, or a combination of two RNase MRP RNA mutations in both alleles. The fact that there is not often a mutation in the promoter region in both alleles shows the lethality of not having this RNA present that is transcribed by RNase MRP (Hermanns *et al*.,2006).

1.3 RNase MRP in *Saccharomyces cerevisiae*

In *Saccharomyces cerevisiae*, the RMRP ortholog NME1 (nuclear mitochondrial endonuclease 1) showed an essential role in cell viability, indicating a nuclear role for RNase MRP (Schmitt and Clayton 1992). RNase MRP cleaves the pre-rRNA at the B2 cleavage site in yeast pre-rRNA, which is thought to be the functional equivalent of site 2 in humans (Schmitt and Clayton 1993). Its secondary structure has been determined (Figure 1.4a). Further, conditional depletion of the RNA component of the enzyme (Figure 1.4b) showed that this is responsible for the maturation of 5.8S rRNA (Schmitt and Clayton 1992). It was found that there was a reversal in the stoichiometry of the two mature forms (long and short) of 5.8S rRNA (Figure 1.4c), a component of the large ribosomal subunit. In the MRP RNA depleted condition via the utilization of glucose-repressed GAL1 promoter, the 7-nucleotide-longer version of 5.8S rRNA was 10 times more abundant than the shorter species lacking this 7-nucleotide sequence at the 5' end, and the accumulation of an aberrant rRNA precursor (a defective RNA intermediate that deviates from the normal processing pathway) (Schmitt and Clayton 1993). These results contrasted with the normal stoichiometry in which the shorter version of 5.8S rRNA is 10-fold more abundant than the slightly longer version. Also, the NME1 temperature-sensitive mutants show the same rRNA processing defect (Figure 1.4d). Literature has revealed that a particular A to G transition at position 122 in the RNA sequence defines its functional capacity (Shadel *et al.*,2000). High-copy suppressor analysis of this point mutation led to the identification of interacting proteins, and SNM1 was the first identified protein component unique to the RNase MRP enzyme complex. The protein contains a leucine zipper motif, a zinc-cluster motif, and a serine/lysine-rich tail (Schmitt and Clayton 1994). Another role has been assigned to the RMRP by observing a delay in the progression of the cell cycle at the end of mitosis in some *nme1*

mutants (Cai *et al.,* 2002). This is caused by an increase in *CLB2* (B-type cyclin) mRNA levels leading to increased Clb2p (B-cyclin) levels and a resulting late anaphase delay. Normally, the RNase MRP complex cleaves the 5' UTR of CLB2 mRNA, which, in turn, causes rapid degradation of CLB2 mRNA and efficient cell cycle progression (Gill *et al.,* 2004).

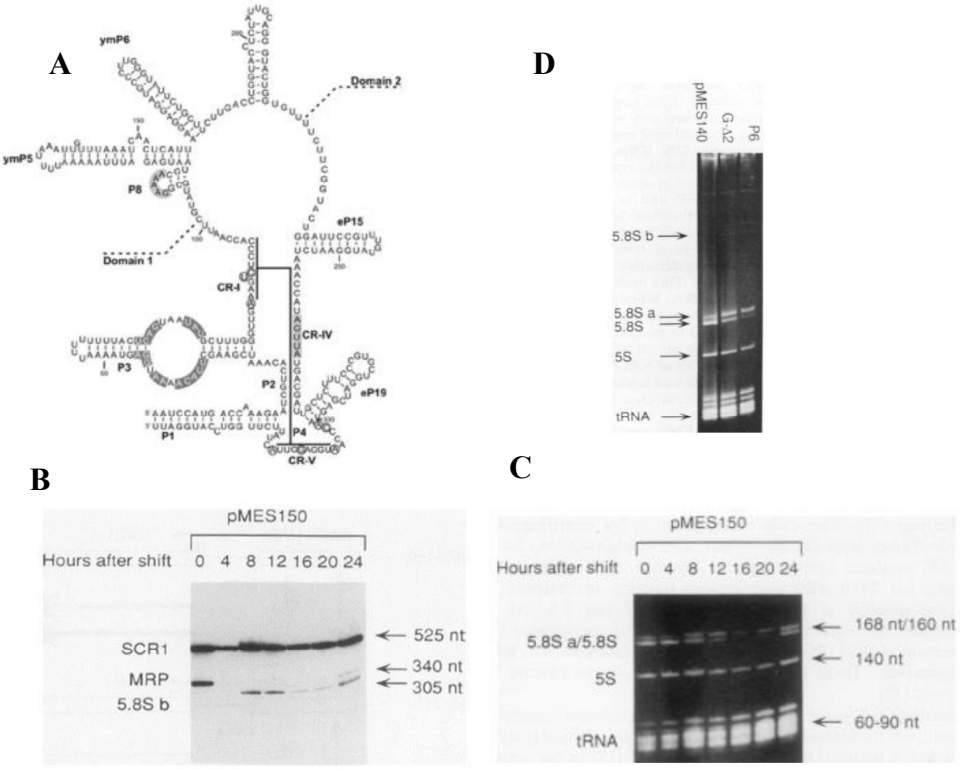

Figure 1.4. Secondary structure of S. cerevisiae RNase MRP and Shift in the ratio of the 5.8S rRNAs after either depletion of the RNase MRP RNA (NME1) or Temperature-sensitive mutations: a) Structure of S. cerevisiae's RNase MRP (Marcela et al.,2009). **(b)** Depletion was induced using a glucose-repressed GAL1 promoter. Following the shift to a glucose-containing medium, samples were collected every 4 hours for total RNA extraction. After gel electrophoresis and transfer to nylon membranes, the RNA was probed for SCR1 (yeast signal recognition particle RNA, serving as a loading control) and RNase MRP RNA (NME1), or with a probe targeting the ITS1 region of the rRNA precursor. **c)** A shift in the ratio of 5.8S rRNAs was observed following the depletion of RNase MRP RNA (NME1). RNA was isolated from yeast cells grown in glucose and analyzed by ethidium bromide staining after PAGE. No changes were detected in the tRNA or 5S rRNA profiles; however, a significant shift in the 5.8S rRNA ratio was evident. **d)** NME1 conditional mutants show the same rRNA processing defect. Yeast strains were grown at the permissive temperature (24 C) and then shifted to the nonpermissive temperature (37 C) for 6 h. Total RNA was prepared, fractionated by PAGE, and then visualized with ethidium bromide (Schmitt and Clayton 1993).

1.4 RNase MRP in Humans

In humans, the role of the RNA component of the RNase MRP complex (RMRP) in pre-rRNA processing has long been established. However, the precise details of its function were not fully understood until CRISPR/Cas9-mediated deletions of the RMRP gene provided more insights. These experiments revealed that RMRP directs the cleavage at site 2 in ITS1 of human pre-rRNA, highlighting its role in ribosomal RNA maturation (Goldfarb et al., 2017). This finding solidified RMRP's involvement in processing pre-rRNA, which is essential for ribosome assembly and cell viability. RMRP is the RNA component of the RNase MRP (ribonuclease mitochondrial RNA processing) complex, a ribonucleoprotein endonuclease. The enzyme was first identified in mice for its ability to cleave mitochondrial RNA, which serves as a primer for mitochondrial DNA replication (Chang et al., 1987). Initially thought to be primarily mitochondrial, subsequent studies showed that RMRP is nuclear-encoded and predominantly localized in the nucleolus, suggesting a broader role beyond mitochondria (Reimer et al., 1988). In humans, RMRP is 267 nucleotides long, sharing 84% sequence homology with the mouse RMRP gene. Interestingly, the conservation extends beyond the coding region, as approximately 700 nucleotides of the 5'-flanking regions are also conserved, indicating the importance of regulatory elements for the expression of RMRP (Topper and Clayton, 1990).

The high degree of sequence conservation across species, including humans, mice, rats, cows, *Xenopus*, yeast, *Arabidopsis*, and tobacco, underscores the essential nature of RMRP's function (Schmitt et al., 1993). The length of the RMRP transcript varies between species, but its conserved core structure is essential for its function. Structural models of RMRP have revealed a complex secondary structure, which helps in the assembly and functionality of the

ribonucleoprotein complex (Walker and Avis, 2004). These conserved structural elements, such as stem-loops and internal bulges, are thought to facilitate interactions with the protein subunits of RNase MRP, which in turn are required for the enzyme's catalytic activity and proper localization. In addition to its role in rRNA processing, RNase MRP has been implicated in several other cellular processes, including the regulation of cell cycle progression and mitochondrial DNA replication. For instance, mutations in the RMRP gene are associated with a variety of human diseases, including cartilage-hair hypoplasia (CHH), an autosomal recessive disorder characterized by skeletal dysplasia, immunodeficiency, and increased cancer susceptibility caused by mutations in the transcribed RNA made by RNase MRP or an insertion or duplication at the promoter of RNase MRP (Ridanpää et al., 2001). These mutations often affect the secondary structure of RMRP, leading to disrupted ribonucleoprotein assembly and altered cleavage activity, which in turn impairs ribosome biogenesis and cellular proliferation. The nucleolar localization of RMRP, observed through immunolocalization studies, further underscores its involvement in ribosome biogenesis within the nucleolus (Reimer et al., 1988). This localization is consistent with its role in pre-rRNA cleavage, where it interacts with other key factors involved in the maturation of 5.8S, 18S, and 28S rRNAs. Overall, the RNase MRP complex plays an indispensable role in human cellular function, particularly in ribosome biogenesis. The continued study of its RNA component, RMRP, is not only important for understanding fundamental aspects of rRNA processing but also for shedding light on the molecular underpinnings of human diseases associated with RMRP dysfunction.

1.5 RNase MRP in *Drosophila melanogaster*

In *Drosophila*, the expression of the *Drosophila* ortholog of MRP RNA (CR33682), which was predicted by a bioinformatics screen for MRP RNA sequences (Piccinelli *et al*. 2005)

has been reported (Figure 1.5). Characterization of a mutant strain shows that *Drosophila* MRP (dMRP) is an essential gene. dMRP mutants display a severe impairment in growth, a characteristic shared with human diseases carrying mutations in this gene (Martin and Li 2007). These phenotypic defects were attributed to impairments at different stages of rRNA processing that were observed. These include the classic defect in processing 5.8S rRNA (Figure 1.5a and b) that has been associated with human and *S. cerevisiae* RNase MRP mutants (Schmitt and Clayton 1993; Lygerou *et al*. 1996; Hermanns *et al*. 2005; Thiel *et al*. 2005), as well as a defect in early rRNA processing similar to a defect reported by Lindahl et al. 2009 in *S. cerevisiae*. Expression of dMRP RNA was detected throughout the *Drosophila* life cycle. This is consistent with its role in fundamental cellular processes such as ribosome biogenesis, mitochondrial DNA replication, and cell cycle regulation (Chang and Clayton 1987; Schmitt and Clayton 1993; Lygerou *et al*. 1996; Gill *et al*. 2004; Thiel *et al*. 2007). Results from Mary *et al*., (2010) support the idea that dMRP RNA shares structural and functional homology with conserved MRP RNA genes previously characterized in other eukaryotes. The first characterization of the ribosomal RNA processing pathway in *Drosophila* by Long and Dawid (1980) identified a single form of 5.8S rRNA. However, extensive characterization studies done by Mary *et al*., (2010) identified both long and short forms of 5.8S rRNA in normal larvae. The data also reveal similarities in rRNA processing between dMRP RNA and MRP RNA orthologs in other species. Homozygous dMRP mutants display a similar change in relative abundances of the two forms of 5.8S rRNAs, indicating a similar function for this gene in *Drosophila*. Normally, the pre-rRNA transcript is cleaved at defined sites in a consistent order to produce a defined set of rRNA intermediates that are ultimately processed into mature rRNAs.

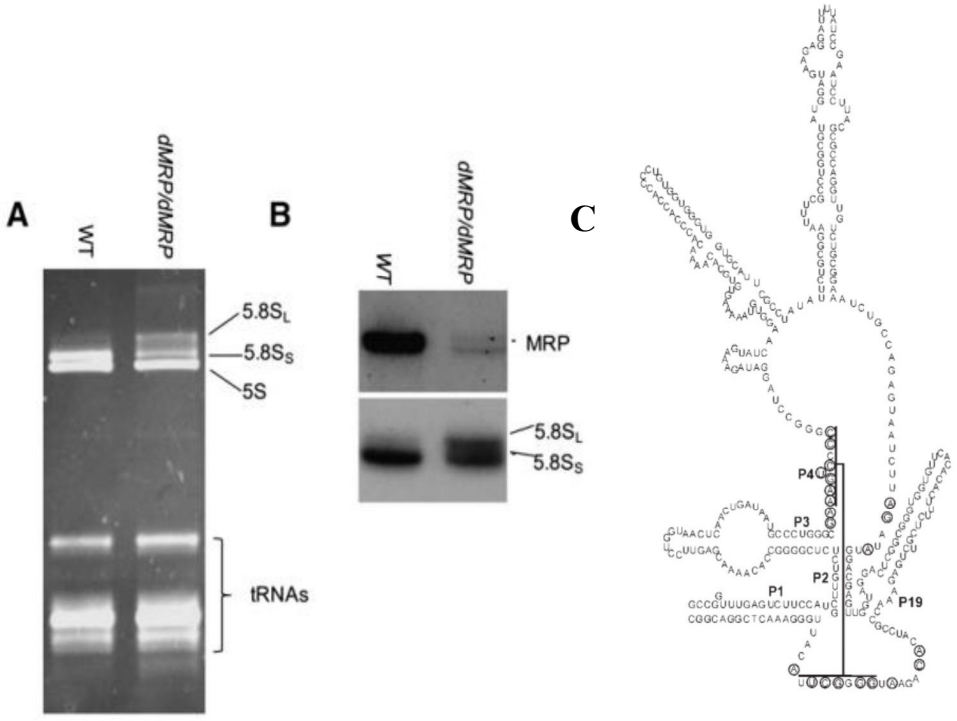

Figure 1.5. **The secondary structure of *D. melanogaster* RNase MRP and 5.8S rRNA processing impaired in dMRP mutants.** Total RNA isolated from wild-type (WT) and dMRPEY08633 mutant larvae were separated in a denaturing polyacrylamide gel and either directly analyzed by staining with ethidium bromide **(a)** or used for Northern blotting with probes specific to the dMRP RNA or 5.8 rRNA **(b).** The two forms of 5.8S rRNA are indicated (Schneider *et al*., 2010)**. (c)** Secondary structure of RNase MRP in *Drosophila melanogaster* (Piccinelli *et al*., 2005).

1.6 RNase MRP in *Cyanidioschyzon merolae*

Cyanidioschyzon merolae (C. merolae) is a thermophilic and acidophilic red alga that thrives in hot springs, characterized by extreme conditions of 45 C and a pH of 1.5. This microorganism has a cell length of ~2 µm (Matsuzaki *et al*., 2004) and a compact genome of approximately 16.5 million base pairs (Nozaki *et al*., 2007). Interestingly, concerning splicing, *C. merolae* strain 10D exhibits a simplified spliceosome, notably lacking the U1 small nuclear ribonucleoprotein (snRNP) in its spliceosome complex (Stark et al., 2015). Splicing involves the excision of introns and the ligation of exonic regions to produce mature mRNA, which is essential for protein

synthesis (Figure 1.6). However, some of these introns excised during splicing contain snoRNAs (small nucleolar RNAs), which in turn modify snRNA, tRNAs, and rRNAs (Figure 5). The reduction in splicing machinery (Stark *et al*., 2015), raises intriguing questions about the evolutionary simplification, functional adaptation, and conserved mechanisms of RNase MRP complex in *C. merolae*. Also, the organism's ability to thrive in extreme environments raises questions about the resilience and adaptability of RNase MRP under stress. *C. merolae* exhibits an extremely simple cytological genomic architecture, this feature offers advantages in cytological and biochemical studies (Fujiwara 2017) and positions *C. merolae* as a valuable model organism for elucidating the complexities of RNase MRP and its broader implications in cellular biology. Although RNase MRP has been extensively studied in a wide range of organisms, relatively little is known about this complex in *C. merolae*. However, studies have identified a putative MRP RNA gene in the *C. merolae* genome, suggesting that this organism also possesses an RNase MRP complex. It is unclear how the MRP RNA gene in *C. merolae* is processed or how the MRP RNA complex functions in this organism, however, given the conservation of MRP RNA in other eukaryotes and the importance of RNase MRP for ribosome biogenesis (Piccinelli *et al*.,2005), it seems likely that the MRP RNA complex in *C. merolae* plays a similar role in processing rRNA and maintaining cell growth and proliferation as reported in other organisms. In *C. merolae*, the MRP RNA is located in the intronic region of the non-coding CMK142T gene, as in *D. melanogaster* and *C. elegans*. Repeated efforts in our lab to delete the intronic region from the CMK142T gene have been unsuccessful (Rader Lab unpublished data), suggesting that MRP is essential.

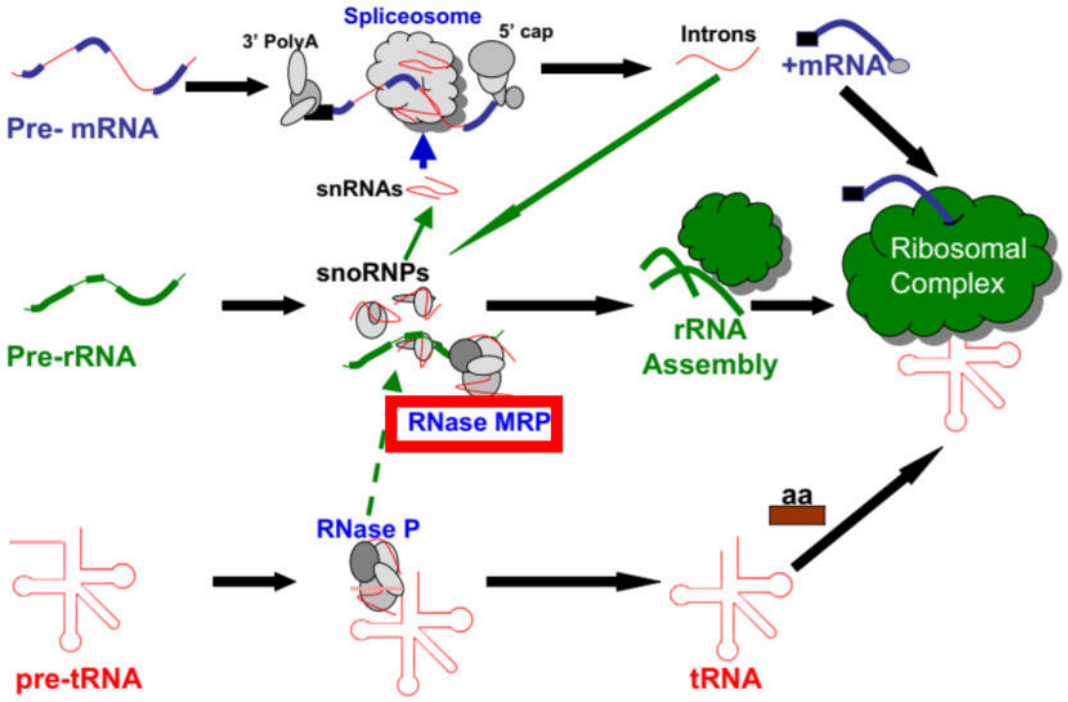

Figure 1.6. The eukaryotic RNA processing cascade integrates splicing, rRNA processing, and translation. The spliceosome, composed of snRNAs and proteins, excises introns from pre-mRNA, releasing mature mRNA and introns. Some introns harbor snoRNAs, which subsequently modify snRNAs, tRNAs, and rRNAs. RNase P cleaves pre-tRNA, while RNase MRP targets rRNA. The ribosomal complex, formed by rRNAs, facilitates the interaction between tRNAs and mature mRNAs during translation. Image adapted from Woodhams *et al*., 2007.

1.7 Heat Stress and Ribosomal RNA Biogenesis

Ribosomal RNAs (rRNAs) are the essential structural and functional components of ribosomes involved in protein synthesis. The rRNA gene clusters, referred to as rDNA, differ slightly across species: 35S in yeast, 45S in plants, and 47S in mammals. These rDNA units encode the 18S, 5.8S, and 25S rRNAs (with 28S rRNA in mammals). Each rDNA unit comprises external transcribed spacers (5'ETS and 3'ETS) and the 18S, 5.8S, and 25S/28S rRNA sequences, which are interspersed by internal transcribed spacers (ITS1 and ITS2). These rDNA units are transcribed by RNA polymerase I (Pol I) within the nucleolus, generating a single precursor transcript - 35S in yeast, 45S in plants, and 47S in mammals. This precursor rRNA undergoes a

series of processing steps, including exonucleolytic and endonucleolytic cleavages, to remove the ETS and ITS regions, ultimately yielding the mature 18S, 5.8S, and 25S/28S rRNAs. Additionally, specific RNA modifications occur at designated positions during this processing to ensure proper ribosome function (Sharma and Lafontaine 2015; Henras *et al*. 2015; Sloan *et al*. 2017; Tomecki *et al*. 2017). Environmental and cell stress conditions induce known changes in nucleolar morphology and functions (Boulon *et al*. 2010; Hayashi and Matsunaga 2019; Kalinina *et al*.,2018), however, the impact of heat stress on the processing of pre-rRNAs remains poorly investigated. In mammals, a short heat shock inhibits pre-rRNA transcription and processing into mature rRNAs (Ghosha and Jacob 1996), while 40 min exposure at 43 C causes accumulation of 30SL pre-RNAs from the ITS1-first pathway (Coccia *et al*.,2017). Heat stress is known to inhibit rDNA transcription in animal cells (Ghosha and Jacob 1996; Coccia *et al*.,2017), whereas in Drosophila, heat shocks increase RNA pol I transcription of retrotransposons located in rDNA clusters (Raje *et al*., 2018).

In *Arabidopsis thaliana*, studies have shown that heat stress disturbs nucleolar structure, inhibits pre-rRNA processing, and provokes imbalanced ribosome profiles. Upon heat stress, precursors of 18S, 5.8S, and 25S RNAs are rapidly undetectable in *A. thaliana* (Darriere *et al*., 2022).

1.8 Research Objectives

Considering the complexity of elucidating the essential function of MRP RNA in human cells, a much simpler organism with fewer components such as *C. merolae* studied in the Rader Lab is of considerable interest in investigating the function of RNase MRP in ribosome biogenesis. It has been reported in *S. cerevisiae* that at a nonpermissive temperature in temperature-sensitive mutants of the MRP RNA, there is a reduction in the catalytic activity of RNase MRP leading to a defect in the synthesis of the two forms of 5.8S rRNAs required in protein synthesis (Schmitt

and Clayton 1993). However, in *C. merolae*, the intronic region of the non-coding CMK142T gene that houses MRP, turns out to be the most accumulated when exposed to heat stress at 57 C (Rader Lab unpublished data). This raises the possibility that the accumulation of RNase MRP during heat stress at 57 C in *C. merolae* may result in a 5.8S ribosomal RNA processing defect. Also, building upon the literature review addressing the impact of heat stress on rDNA transcription and processing of mature rRNA, it's interesting to verify whether heat stress impacts these processes in *C. merolae*.

The objectives of this thesis are fourfold: First, to determine if there is a defect in 5.8S rRNA processing via Northern blot analysis, potentially due to hypothesized modulation of RNase MRP catalytic activity under heat stress and heat stress impact on mature rRNAs (28S and 18S). Second, to verify whether *C. merolae* subscribes to the canonical rRNA processing pathway and to evaluate the impact of heat stress on the precursors of this pathway. Third, to employ bioinformatics tools to predict the secondary structure of *C. merolae* RNase MRP, identify conserved regions through comparative genomics, and predict the protein constituents of the RNase MRP complex in *C. merolae*. Finally, to elucidate the function of *C. merolae* RNase MRP by conducting mutational analysis of its RNA component, using plasmid shuffling or direct replacement via homologous recombination.

Chapter 2 - Intronic Accumulation Induced by Heat Stress Does Not Modulate RNase MRP Expression in *C. merolae*, Resulting in Unaltered Stoichiometry of 5.8S rRNA

2.1 Introduction

In *C. merolae*, the intronic region of the CMK142T gene, which harbors RNase MRP, appears to accumulate under heat-stress conditions (Figure 2.1). This chapter delves into the effects of heat stress on RNase MRP expression and its catalytic function in cleaving ITS1, leading to the generation of two 5.8S rRNA isoforms. Furthermore, given that heat stress has been shown in other species to alter ribosomal profiles, the chapter examines the impact of heat stress on mature 5.8S rRNAs in *C. merolae*. Northern blot analysis was utilized in this chapter to assess the expression levels of RNase MRP and 5.8S rRNA.

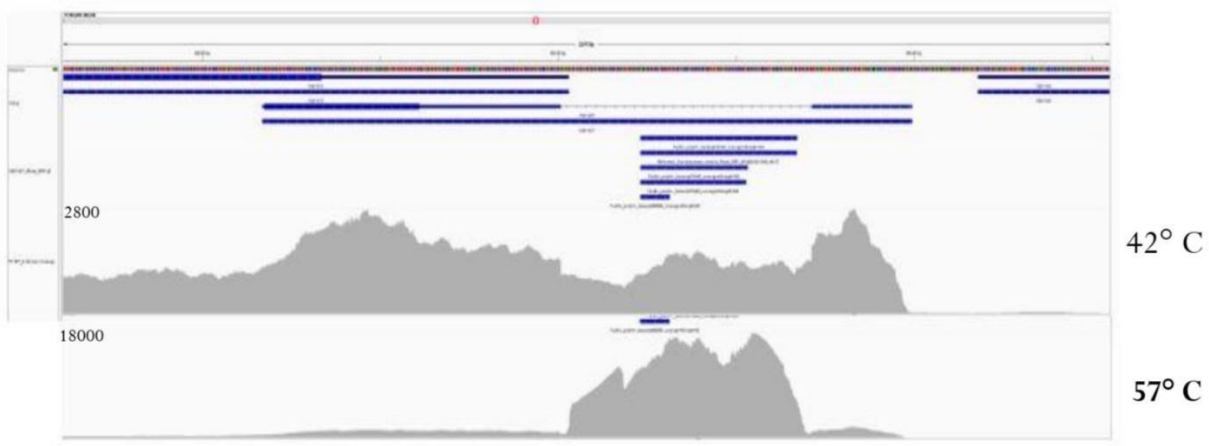

Figure 2.1. Transcriptomic data depicts *C. merolae* CMK142T intron accumulation. The intronic region of CMK142T is the first to accumulate under heat stress at 57 C. This intronic region houses the RNA component of RNase MRP (Schubert Lab unpublished data).

2.2 Materials and Methods

2.2.1 Cultivation of *C. merolae* and Subsequent Heat Stress Treatment at 57 C

The cultivation protocol for *C. merolae* was based on the method outlined by Kobayashi et al. (2010). The cells were grown in liquid MA2G medium, which consists of 40 mM $(NH4)_2SO_4$, 8 mM KH_2PO_4, 4 mM MgSO4, 1 mM CaCl2, 184 µM H_3BO_3, 100 µM FeCl3, 80 µM Na_2EDTA,

36 µM MnCl2, 6.4 µM Na2MoO4, 3.08 µM ZnCl2, 1.2 µM CuCl2, 0.68 µM CoCl2, and 50 mM glycerol. Cultures were maintained at 42 C with 2% CO_2 and continuous illumination at 90 µmol photons·m^{-2}·s^{-1}. Wild-type *C. merolae* cells were grown to an OD750 =1.0 under standard conditions. Cells were then transferred to a 57 C water bath for 1 h for heat stress or 42 C for controls.

2.2.2 Total RNA Isolation

RNA extraction was carried out using the cold phenol method with phase-lock gel (PLG) tubes. After heat stress treatment, the cells were centrifuged at 15,000g for 2 minutes, the supernatant was discarded and resuspended the cells in 300 µL of cold phenol lysis buffer (200mM Tris-HCL, pH7.5, 500mM NaCl, 10mM EDTA, 1%SDS) in a 1.5 mL Eppendorf tube. The cells were sonicated for 2 bursts of 5-10 seconds, followed by the addition of 300 µL of acid-phenol, vortexed for 5 seconds, and then spun at maximum speed (12,000-16,000g) for 20-30 seconds. The mixture of acid-phenol and cell lysate were transferred to a PLG microtube and centrifuged at 15,000g for 5 minutes. 300 µL of acid-phenol was added with gentle mixing before spinning again for 5 minutes at 15,000g. The aqueous phase was then transferred to a new Eppendorf tube, mixed with 300 µL of chloroform, vortexed for 5 seconds, and spun for 5 minutes at 15,000g. The aqueous phase was transferred to a new tube, 1 mL of 100% ethanol was added, and centrifuged at 4 C for 30 minutes at maximum speed, followed by discarding the supernatant. The pellet was washed with 180 µL of cold 70% ethanol, centrifuged for 1 minute at maximum speed, and all liquid was carefully aspirated off. The pellet was allowed to dry for about 5 minutes, or longer if needed, before being resuspended in 25 µL of dH_2O. 1 µL of the sample was used to determine the concentration with a Nanodrop spectrophotometer.

2.2.3 RNA Integrity Assessment

RNA integrity was assessed using a 2% agarose bleach gel. The gel was run at a constant voltage (120 V) for an hour for better separation of bands. Post-electrophoresis, the gel was stained with ethidium bromide, and RNA bands were visualized under UV light.

2.2.4 Fluorescence Northern Blot Analysis

Fluorescence Northern Blot Analysis was performed using either a denaturing polyacrylamide gel or a denaturing formaldehyde agarose gel.

2.2.4.1. 6%/7M Urea Denaturing Gel Preparation

To prepare a 6% denaturing polyacrylamide gel with 7M urea, 6.3 g of urea was weighed into a 50 mL beaker. 2.25 mL of 40% acrylamide (19:1 ratio) was added using a 10 mL disposable pipette, followed by 7.3 mL of deionized water (dH2O) from a dedicated bottle. After adding 750 µL of 20x Tris-Borate-EDTA (TBE) buffer and a small stir bar, the solution was mixed on a hotplate/stirrer set to 100 C until the urea completely dissolved. Once dissolved, the mixture was cooled on ice to slow down polymerization before adding 150 µL of 10% ammonium persulfate (APS), stirring with a pipette tip. 15 µL of TEMED was then added and stirred again. The amount of acrylamide and water was changed accordingly for the percentage of gel needed. The gel was then poured using the same disposable pipette, inserted the comb into the appropriate depth based on the sample volume, and allowed the gel to polymerize. The leftover gel mix was solidified, and the solidified acrylamide was discarded safely.

To prepare a 1.5% formaldehyde-agarose gel in a 150-mL volume, 2.25 g of agarose was mixed with 109.5 mL of water. The agarose was melted in a microwave and cooled to 65 C before adding 15 mL of 10x MOPS buffer and 25.5 mL of 37% formaldehyde under a chemical fume

hood. The agarose mixture was then poured into a gel tray with an inserted comb and allowed to solidify. Concurrently, sufficient 1x MOPS buffer was prepared for the gel tank reservoirs by diluting the 10x stock. After placing the gel in the tank and adding the 1x MOPS buffer to prevent drying, the gel was loaded and run immediately to minimize formaldehyde diffusion. For RNA sample preparation, 4.7 µL of each RNA sample, containing 10-30 µg of total cellular RNA, was added to a 1.5-mL microcentrifuge tube. A fresh stock of sample buffer was prepared, consisting of 660 µL ultrapure formamide, 200 µL 10x MOPS buffer, and 270 µL formaldehyde (37%). A total of 11.3 µL of this sample buffer was added to each RNA sample, followed by heating at 60 C for 5 minutes and cooling on ice. Finally, 4 µL of tracking dye was added to bring the total volume to 20 µL, and the samples were ready for electrophoresis.

2.2.4.2. Denaturing Polyacrylamide Gels for RNA Analysis

6-15% denaturing polyacrylamide gel, suitable for analyzing RNAs smaller than 1000 nucleotides was poured. Denaturing (formaldehyde) agarose gel was used for larger RNAs. The gel was pre-run for 15 minutes at 400 V in 1X TBE buffer, ensuring that urea was cleared from the wells and any trapped air was removed from the bottom of the gel using a syringe with a bent needle. Next, 1–10 µg of RNA was mixed with an equal volume of 2X formamide loading buffer, with the total volume kept under 20 µL. RNA samples were denatured at 65 C for 3 minutes, quickly spun down, and immediately placed on ice. The wells were cleared again with a syringe before loading samples using an elongated gel-loading tip, with the tip rinsed in TBE buffer between samples. The gel was then run at 400 V for 45–90 minutes, depending on the size of the RNA being analyzed. Samples were analyzed by staining with ethidium bromide or via Northern blotting.

2.2.4.3. Membrane Transfer with Semi-Dry Electroblotter/Capillary Transfer

To prepare for RNA transfer, six pieces of Whatman paper and one piece of Hybond+ nylon membrane were cut slightly larger than the gel, with the membrane labeled with the date and experiment identifier. Two pieces of Whatman paper were pre-wetted in 1X TBE, placed on the semi-dry blotter, and arranged to avoid any trapped air bubbles. The gel was carefully transferred from the glass plate to the Whatman paper, and excess gel was trimmed. The membrane was then pre-wetted, aligned with the gel, and covered with three additional pre-wetted Whatman papers. After ensuring no bubbles were present, the setup was secured for transfer, conducted at 2.5 mA/cm^2 for 30 - 45 minutes.

For a capillary RNA transfer from formaldehyde agarose gel, a few millimeters of the gel edges were trimmed with a scalpel to create a flat surface. A nylon membrane was cut approximately 2 mm larger than the gel on all sides, along with six pieces of Whatman 3MM paper and a 2-inch stack of paper towels matching the membrane size. A capillary gel-transfer system was set up on an elevated base gel tank, with two pieces of Whatman 3MM paper pre-wetted in 20X SSC layered on top. The gel was placed upside down relative to its position in the gel tank on top of the Whatman paper, and excess liquid was blotted off with Kimwipes. The nylon membrane was pre-wetted with water, then 20X SSC, and carefully positioned on the gel without allowing movement after contact. Bubbles between the gel and membrane were smoothed out with a 5-mL glass pipette or a gloved finger. A pre-wetted piece of Whatman 3MM paper was layered on top of the membrane, followed by three dry pieces of Whatman paper, a 2-inch stack of paper towels, a glass plate, and a weight. This blotting sandwich was left to transfer overnight.

2.2.4.4. RNA Cross-Linking for Membrane Stabilization Using the Strata Linker System

Using forceps, the membrane was transferred, RNA side up, onto a piece of Whatman paper and immediately cross-linked the RNA to the membrane using the auto cross-link setting on the Strata linker.

2.2.4.5. Pre-hybridization

The ULTRAhyb™–Oligo Buffer (Invitrogen, AM8663) was preheated to 42 C in a water bath until fully resolubilized. The hybridization oven was also set to 42 C. Using forceps, the blot(s) were carefully positioned in a hybridization bottle with the RNA side facing inward. Between 5-10 mL of the preheated hybridization buffer was added to the bottle, and the assembly was incubated at 42 C for 30 minutes.

2.2.4.6. Hybridization

5 pmol/mL of biotinylated oligonucleotide was incorporated into the pre-hybridization buffer, avoiding direct application onto the blot. The hybridization was conducted at 42 C for a duration ranging from 1 to 24 hours.

Table 2.1. Oligonucleotides used in Northern Blot Analysis

The oligonucleotides ordered are 5' biotinylated. oSDR2488 was designed by Dr. Martha Stark.

Oligonucleotide	Target	Sequence (5′ to 3′)
oSDR2487	Cm 5.8SrRNA	CGCTGCGAGAGCCTAGATATCCACCG
oSDR2586	Cm 28SrRNA	CGCTATCGGTCTCTCGCCGGTATTTAGCCTTAGGTGAAG
oSDR2587	Cm 18SrRNA	GTTACCATGAATCACCAGAGACCGCCGAGGCGGTTTGG
oSDR2488	Cm RNase MRP	AGCTTTGCTTACCACCGACACTCTCTG

2.2.4.7. Washing Strategies for Enhanced Specificity

For the washing step, 2x SSC, 0.5% SDS, stored at 37 C was used. The blot was initially rinsed with 5-10 mL of wash buffer to eliminate excess unhybridized probe. It was then subjected to a series of washes with approximately 20-25 mL of buffer for 30 minutes, performing three 5-minute washes at 42 C. Subsequently, the oven temperature was lowered to 20 C, and the door was left ajar while the blot was prepared for blocking.

For cases where non-specific bands were detected, more stringent washing conditions were employed to enhance specificity: first, a 5-minute wash with 2x SSC and 0.1% SDS at 42 C, followed by two 20-minute washes with 0.5x SSC and 0.1% SDS at 42 C, and, if necessary, an additional 20-minute wash with 0.1x SSC and 0.1% SDS.

2.2.4.8. Blocking Procedure for Northern Blot Analysis

Blocking was performed with 5 mL of blocking buffer (Licor, 927-70001), and the blot was incubated for 1 hour at room temperature (20 C).

2.2.4.9. Fluorescent Labeling of Northern Blot; IRDye 800CW Streptavidin Binding

To minimize the background signal, 100 µL of 10% Tween-20 (to achieve a final concentration of 0.2%) and 50 µL of 10% SDS (final concentration of 0.1%) were added to the blocking buffer before the addition of dye. In the dark, 0.5 µL of Streptavidin-IRDye 800CW conjugate (Licor, 926-32230) was introduced into the blocking buffer at a 1:10,000 dilution. For multiple tubes, a 1:100 dilution was prepared, and 50 µL was added to each tube. The blot was then incubated for 30 minutes at room temperature in the dark.

2.2.4.10. Post-Streptavidin Binding Washing

The blot was initially rinsed with 5-10 mL of PBST (1X PBS, 0.1% Tween-20) to remove the majority of unbound dye. Subsequently, it was washed with 20-25 mL of PBST for three intervals of 5 minutes each at room temperature. Finally, a single 5-minute wash with 1X PBS at room temperature was performed to remove the detergent, thereby enhancing fluorescence**.**

2.2.4.11. Detection

For imaging, the blot was placed on a piece of Whatman paper moistened with water and positioned on an acetate sheet before being placed into the Bio-Rad Imager. If the moistened Whatman paper caused any blotchiness, it was removed. To prevent the blot from drying, which would hinder stripping, Saran wrap was used if a long exposure (more than a few minutes) was necessary. The IR-Dye 800 CW setting was selected, and the image was captured using auto exposure, with a preview followed by an optimal capture. Manual exposure time was also adjusted as needed to achieve the desired image quality.

2.2.4.12. Northern Blot Analysis Utilizing Bio-Rad Image Lab 6.1

Analysis of Northern blots was conducted using Bio-Rad Image Lab software 6.1. The Image Lab 6.1 software was opened, and the image of the Northern blot to be analyzed was imported. The analysis tools in Image Lab were used to detect bands, define boundaries, subtract background noise. To determine the relative front, the software's lane profile feature was employed. By analyzing the migration distance of the bands in relation to the dye front and loading wells, the relative front was detected. This measurement was essential for calculating relative mobility, ensuring accurate comparison between samples. Finally, the bands were quantified according to the analysis requirements, with options for relative or absolute

quantification. Software tools for normalization, annotation, and manual quantification were employed as needed. The analyzed data, including band tables, was exported to Excel, and the image was saved in a format suitable for publication.

2.2.4.13. Blot Stripping and Storage for Subsequent Re-probing

The blot was stripped to allow re-probing with a different probe before it dried out. Approximately 50 mL of 0.2% SDS was heated in a microwave to near boiling and incubated with the blot in hybridization bottles for 10 minutes at room temperature with rotation. This step was repeated with boiling SDS. The blot was then rinsed with around 50 mL of 2x SSC followed by a rinse with water. To ensure complete removal of the probe, the blot was re-exposed on the Imager for at least as long as the original exposure time. If re-probing was not planned for the same day, the blot was wrapped in Saran wrap and stored at room temperature. While stripping may remove a small amount of RNA from the blot, it was possible to strip up to three times without issue.

2.3. Results

RNase MRP is involved in the generation of the two forms of 5.8S rRNA. Mutations in the MRP RNA have been shown to alter the 10:1(small: large) stoichiometry (Schmitt and Clayton 1992; Lindahl *et al*. 2009). I carried out analyses to investigate how the accumulation of the intronic region of CMK142T (which houses MRP) at 57 C (heat stress conditions) affects MRP expression and the stoichiometry of the two forms of 5.8S rRNA. I hypothesized that MRP accumulates in an inactive form under heat stress, which should result in a change in the 5.8S isoform ratio, so I used northern blotting to look for such a change. An rRNA cassette was constructed in SnapGene (a sequence viewing and analysis tool) to facilitate the study of ribosomal RNA (rRNA) processing in *Cyanidioschyzon merolae* (Figure 2.2). The constructed rRNA cassette was solely utilized to design specific probes targeting the rRNAs of interest for Northern blot analysis and does not contain any promoter sequence. The cassette was not meant to drive the expression of rRNA but solely for primer designs.

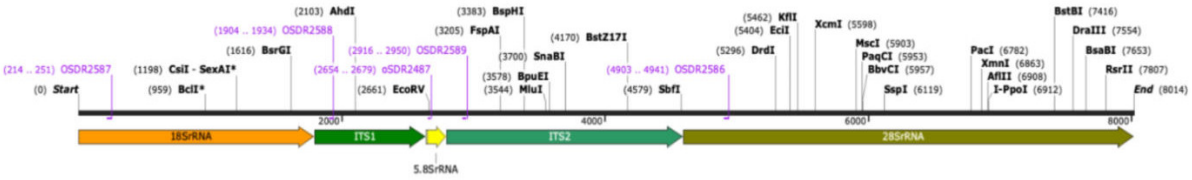

Figure 2.2. *C. merolae* rRNA Cassette. The rRNA sequences of *C. merolae* were identified and retrieved from the NCBI database using the appropriate accession numbers 5.8S rRNA (Accession Number: XR_002461615), 18S rRNA (Accession Number: XR_002461616), 28S rRNA (Accession Number: XR_002461614), ITS1 (Accession Number: AB158485), and ITS2 (Accession Number: AB158484).

After cultivating *C. merolae* and subjecting it to heat stress treatment, total RNA was extracted from the cells. The integrity of the RNA was then analyzed to ensure its suitability for downstream applications. As one of the major issues affecting the integrity of RNA is the ubiquitous presence of ribonucleases (RNases), RNA quality was quickly analyzed by adding

small amounts of commercial bleach to TBE buffer-based agarose gels prior to electrophoresis (described in Section 2.2.3). This RNA integrity check was to confirm that the RNA was of high quality, free from degradation, and appropriate for subsequent analyses such as Northern blotting. Figure 2.3 below demonstrates that the RNA extracted was of high quality and suitable for subsequent downstream analysis.

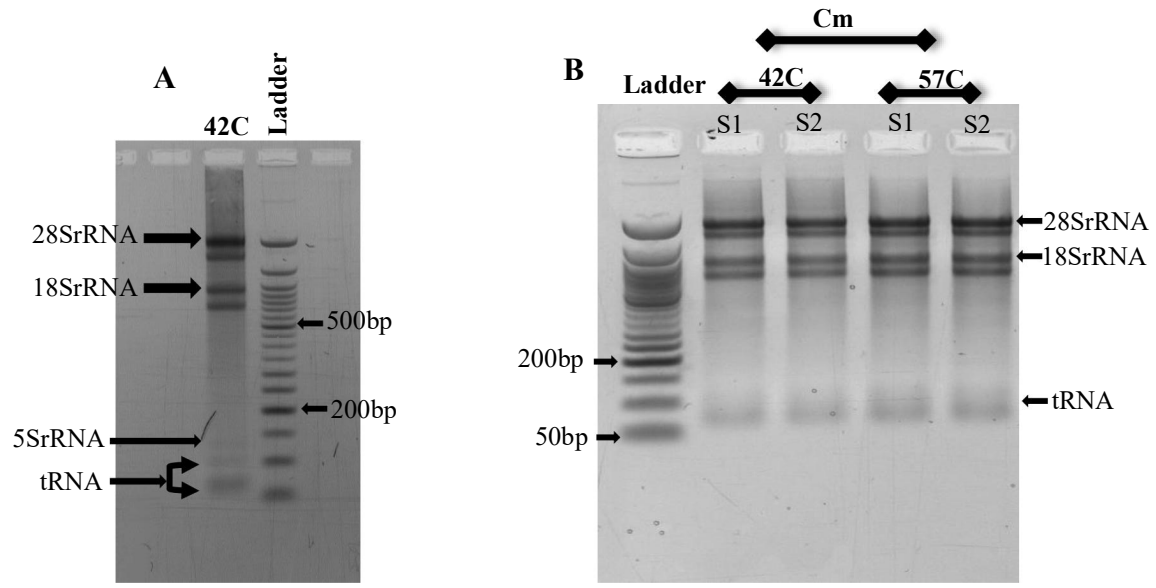

Figure 2.3. Isolation and analysis of total RNA from *Cyanidioschyzon merolae* Wild Type: RNA was isolated from Cm WT. Samples were examined by running 1xTBE, 2% Agarose Bleach gel **a)** Sample exposed to 42 C and **b)** Comparison of samples at two different temperatures 42 C and 57 C. 50bp DNA ladder was used as a size marker. The two samples in each temperature set in b, are technical replicates.

The total RNA samples were used for polyacrylamide Northern blotting to investigate: the expression of MRP under optimum temperature and heat stress, to determine whether *C. merolae* contains two distinct forms of 5.8S rRNA, and whether heat stress modulates RNase MRP function by altering the stoichiometric ratio of these 5.8S rRNA forms, as suggested in the literature (Figures 1.5a,1.5b,1.6a and 1.6b). The RNase MRP in *C. merolae* had only been bioinformatically identified in the intronic region of the CMK142T gene without experimental validation. To confirm the expression, I performed a northern blot on total RNA (Figure 2.4).

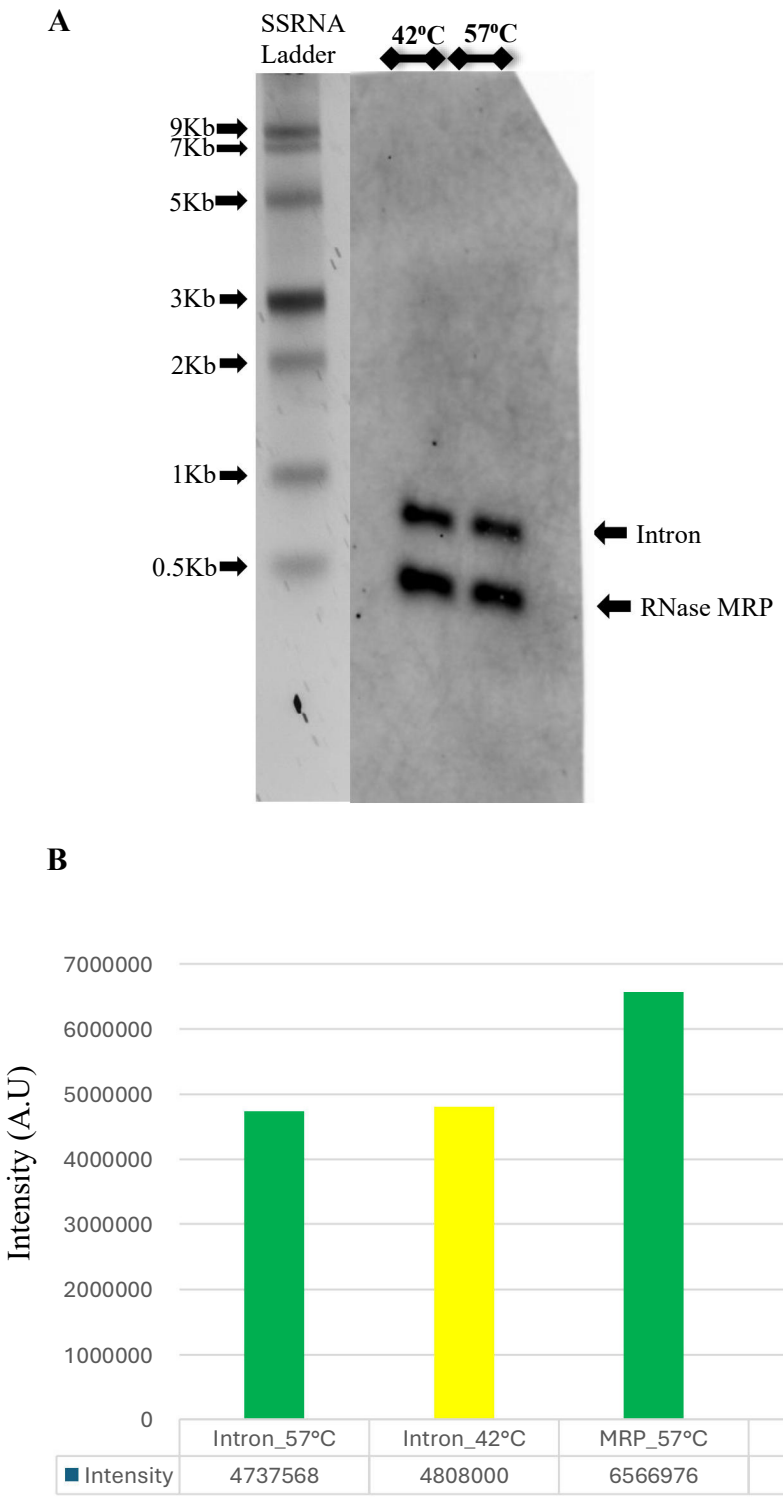

Figure 2.4. The RNA component of RNase MRP is stably expressed at 42 C and 57 C. A) RNA was isolated from *C. merolae* after growth and treatment at 42 C and 57 C temperatures and probed for MRP after running 1.5% formaldehyde-agarose gel for 6 hours at 50V and transferred to a nylon membrane. **B)** Quantification of MRP and Intron intensities using Bio-Rad Image Lab software 6.1.

Quantification of RNase MRP expression levels, based on band intensities at both temperatures (Figure 2.4a and b), confirmed the presence of RNase MRP in *C. merolae* but does not indicate the anticipated change in expression at 57 C. This result contrasts with the transcriptomic data, which indicated an increase in expression at 57 C (Figure 2.1), creating a discrepancy between the two findings.

Evidence from lab colleagues suggests that the transcriptomic data reflects adenylation of RNase MRP transcripts rather than their accumulation, and this may cause it to be targeted for degradation by the exosome, as polyadenylation in non-coding RNAs often signals turnover.

In light of the polyadenylation of MRP, I hypothesized that it becomes inactive under heat stress and would therefore lead to a change in the 5.8S isoform ratio. To investigate the presence of two forms of 5.8S rRNA and whether heat stress affects the stoichiometry of these two forms, I visualized total RNA on an ethidium bromide-stained gel (Figure 2.5). This analysis did not reveal any hint of the existence of two forms of 5.8SrRNA (see Figure 2.5 below).

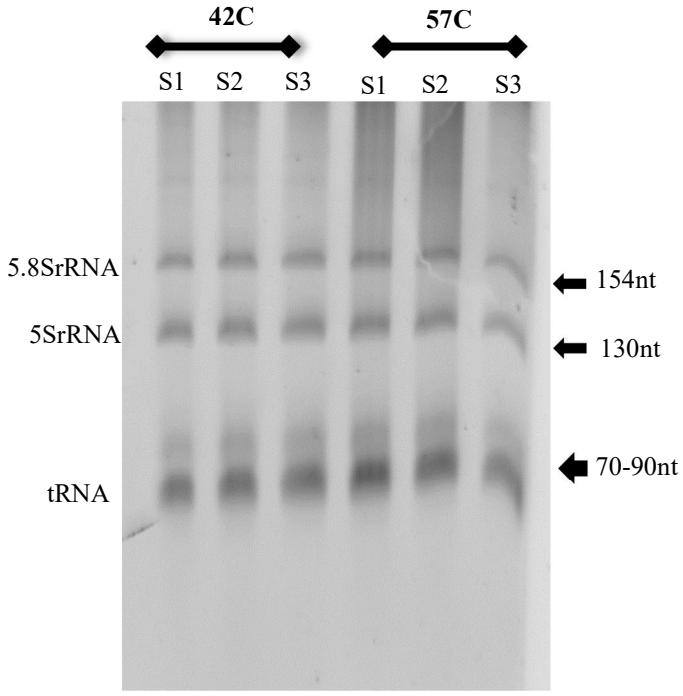

Figure 2.5. Detection of 5.8S rRNA in *C. merolae* using ethidium bromide-stained 6% PAGE. RNA was isolated from *C. merolae* after growth and treatment at 42 C and 57 C temperatures and examined by staining with ethidium bromide after running 6% PAGE. The three samples in each temperature set are technical replicates.

Since the initial results did not indicate the presence of two forms of 5.8S rRNA, I proceeded with a 6% PAGE Northern blot analysis run at different time intervals to evaluate the optimal migration time for different fragment sizes, balance resolution, and prevent the loss of smaller fragments or over-migration of larger ones (Figure 2.6).

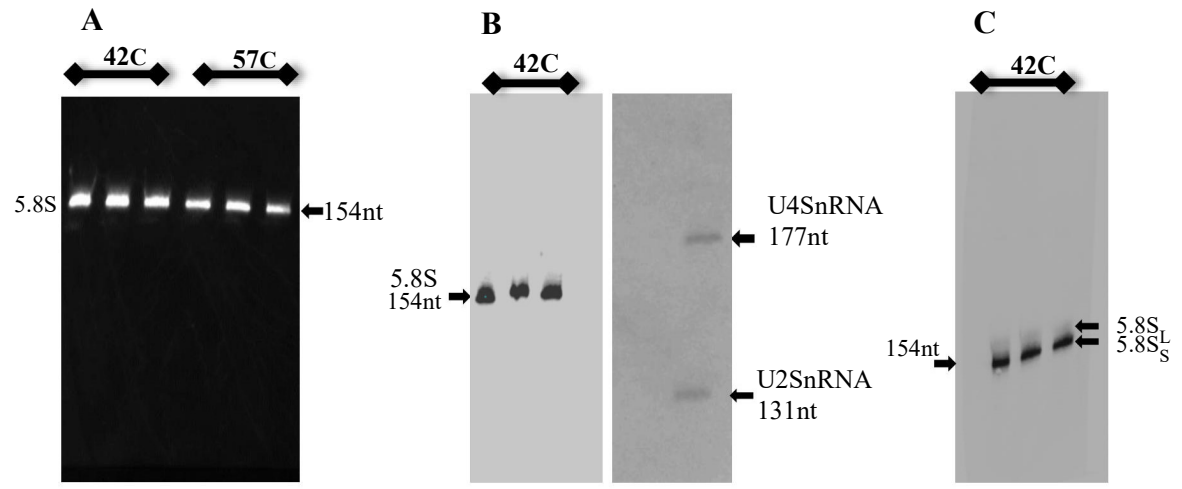

Figure 2.6. Northern analysis of 5.8S rRNA. Northern blots of total RNA separated on a 6% polyacrylamide gel for **(a)** 45 minutes**, (b)** 75 minutes, and **(c)** 90 minutes. Cells were treated at the indicated temperatures prior to RNA isolation. In **(b),** total RNA was probed for Cm U2 and U4 snRNAs for size markers. The three samples in each temperature set are technical replicates.

Panels b and c of Figure. 2.6 hints at the possibility of a long form of 5.8S in *C. merolae* confirming the exhibition of two forms of 5.8S rRNA, mirroring findings in *S. cerevisiae* and *D. melanogaster* wild-type cells (Figures 1.5c,1.6a, and 1.6b).

The third analysis utilized 8% PAGE with a 95-minute run, followed by probing for 5.8S rRNA after transferring the samples to a nylon membrane. This analysis confirmed the presence of two distinct forms of 5.8S rRNA but did not reveal any changes in the stoichiometry of these forms in *C. merolae* (Figure 2.7). These results suggest that the accumulation of the intronic region of CMK142T did not impact RNase MRP's expression or catalytic activity, as evidenced by the unchanged stoichiometry of the two 5.8S rRNA forms.

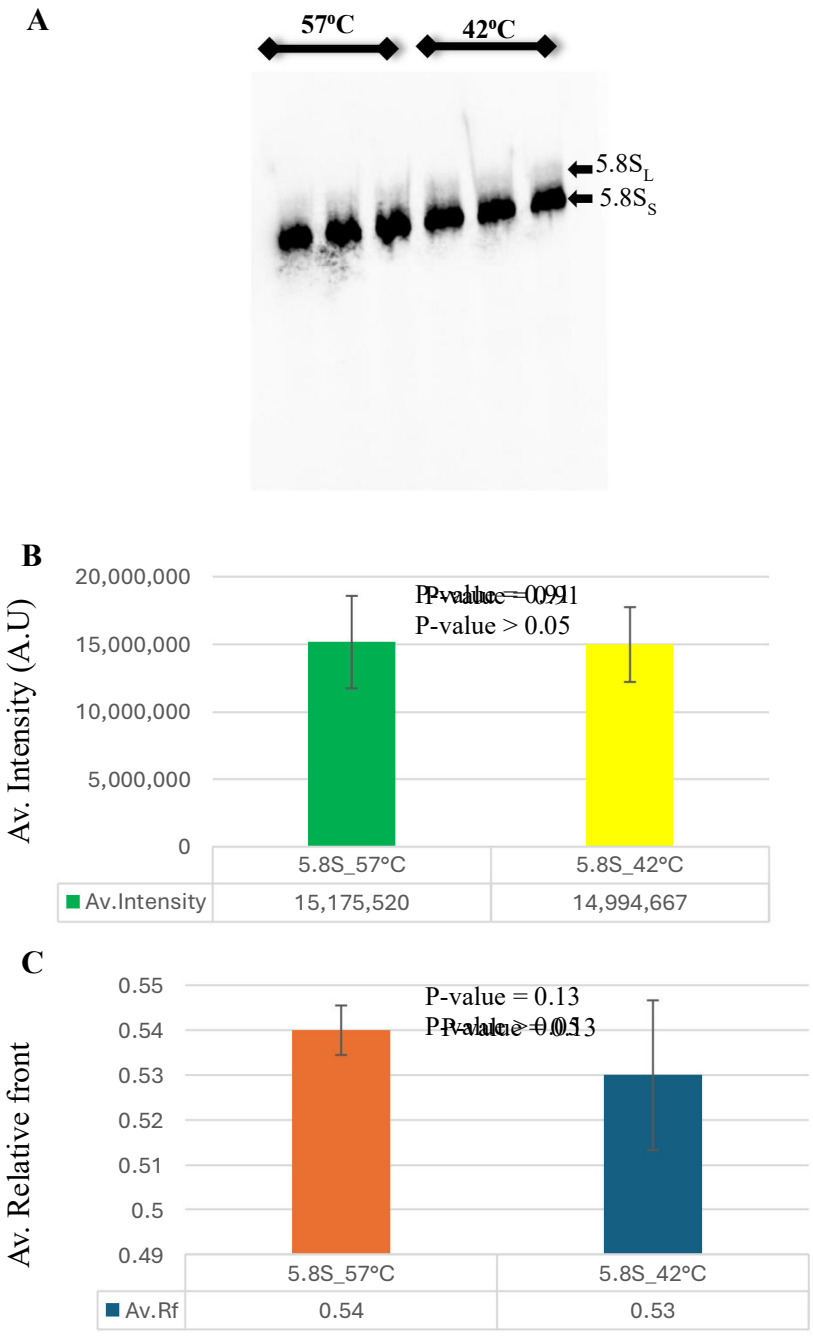

Figure 2.7. Heat Stress Effect on 5.8SrRNA Intensities using 8% PAGE. a) RNA was isolated from *C. merolae* after growth and treatment at 42 C and 57 C temperatures, probed for 5.8S rRNA after running 8% PAGE for 95 minutes, and transferred to a nylon membrane. **b)** band intensities and **c)** mobility (relative front) were quantified using Bio-Rad Image Lab software 6.1. The three samples in each temperature set are technical replicates.

Quantification of the intensities and relative front (the distance a specific RNA fragment migrates on the gel relative to the total distance traveled by the dye front) of the bands at these

two temperatures gave a P-value > 0.05 signifying that there is no statistical difference in the relative front and intensities of 5.8S rRNA either at 42C and 57C (Figure 2.7b and c).

2.4. Discussion

The previous observation indicated that the CMK142T intron is predicted to harbor the RNase MRP RNA, known from the literature to be involved in 5.8S rRNA processing and that the expression of this intron appears to increase dramatically under heat stress (Figure 2.1). I therefore, sought to confirm that the MRP RNA is expressed and to test whether the accumulation at 57 C reflects inactivation, which should be revealed in a change in the 5.8S isoform ratio as evidenced in *S. cerevisiae* and *D. melanogaster* (Schmitt and Clayton 1993; Schneider et al., 2010; Shadel et al., 2000). I successfully confirmed MRP expression, but surprisingly did not see the expected change in expression by Northern blotting. My labmates have evidence that the transcriptomic data reflects adenylation of MRP, rather than accumulation, causing it to be targeted for degradation by the exosome, as polyadenylation in non-coding RNAs often signals turnover. The result from the Northern blot implies that RNase MRP is stable even under heat stress in *C. merolae* (Figure 2.4). This stability of RNase MRP in *C. merolae* may reflect a broader evolutionary adaptation mechanism, allowing organisms to thrive in fluctuating thermal environments without detrimental effects on cellular processes (Lefort *et al*. 2014). Thus, RNase MRP's resilience under heat stress underscores its potential role in cellular homeostasis during environmental challenges. The data presented in this chapter also confirms the presence of two distinct forms of 5.8S rRNA but did not reveal any changes in the stoichiometry of these forms in *C. merolae* (Figures 2.6c and 2.7). Unlike in *S. cerevisiae* and *D. melanogaster*, the 5.8S isoforms were difficult to detect in my experiments, and I did not observe any change in their ratio. Another way to detect the two isoforms will be by primer

extension. However, these results suggest that the accumulation of the intronic region of CMK142T did not impact RNase MRP's expression or catalytic activity, as evidenced by the unchanged stoichiometry of the two 5.8S rRNA forms. This suggests that, unlike in *Arabidopsis thaliana*, where heat stress leads to rapid degradation of rRNA (Darriere *et al*., 2022), heat stress does not influence 5.8S rRNA processing in *C. merolae* (Figure 2.7). This difference highlights the potential for species-specific responses to thermal stress, indicating that the mechanisms governing rRNA stability and processing may vary significantly across different organisms. I conclude that either RNase MRP is not involved in 5.8S rRNA processing in *C. merolae*, or, more likely, heat does not inactivate MRP.

Chapter 3 - Heat Stress Inhibits rDNA Transcription, but 18S and 28S rRNA Processing Remains Unaltered as *C. merolae* Adheres to the Canonical rRNA Processing Pathway

3.1 Introduction

In this chapter, I detailed the experiments conducted to determine heat stress effect on rRNAs and assessed whether *Cyanidioschyzon merolae* follows the canonical rRNA processing pathway as observed in other eukaryotes. Northern blot analysis was employed to probe for processing intermediates in the rRNA transcript. Below is a schematic diagram generated with information from Li *et al*. (2021), depicting the expected bands in the canonical rRNA processing pathway and indicating the *C. merolae* probes used in this experiment.

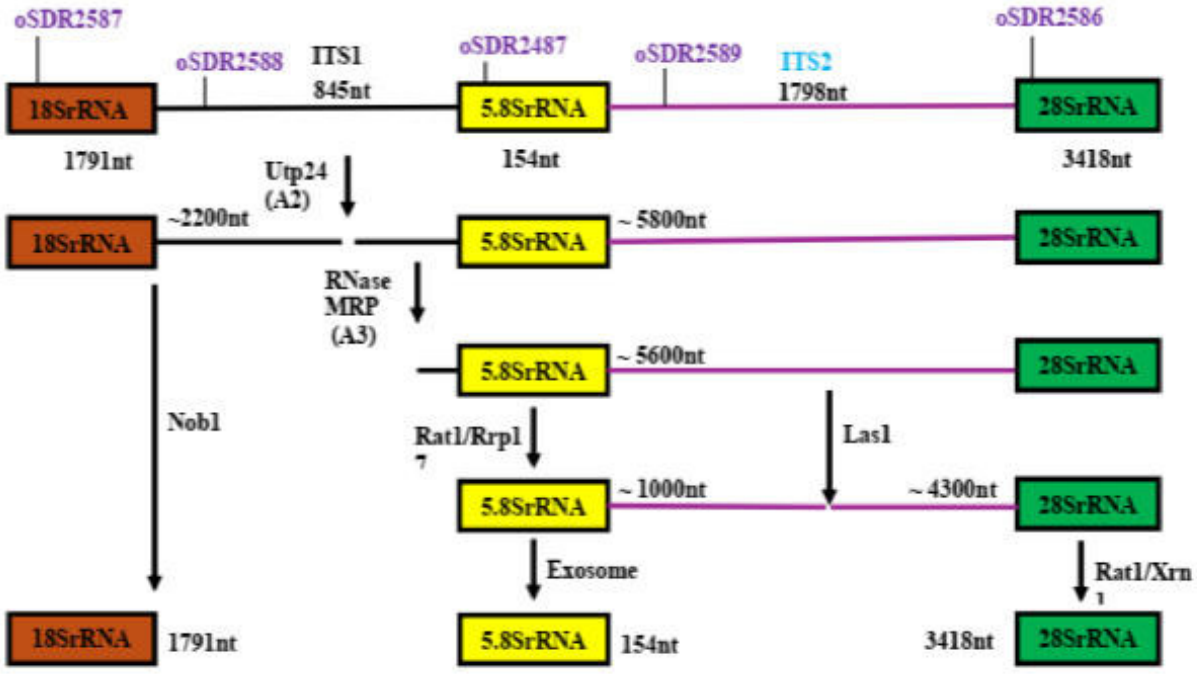

Figure 3.1. Canonical rRNA processing pathways. This figure depicts rRNA processing intermediates with names of relevant processing enzymes and their sites of action. Refer to Table 3.1 for the oligonucleotide sequences and the target positions on pre-rRNA to which they hybridize.

3.2 Materials and Methods

In this chapter, the materials and methods employed are the same as those outlined in Chapter 2, from sections 2.2.1 to 2.2.4.13, utilizing formaldehyde agarose Northern blotting and Capillary transfer techniques.

Table 3.1. Oligonucleotides used in Northern Blot Analysis

The oligonucleotides ordered from Integrated DNA Technologies are 5' biotinylated.

Oligonucleotide	Target	Sequence (5′ to 3′)
oSDR2487	Cm 5.8S rRNA	CGCTGCGAGAGCCTAGATATCCACCG
oSDR2586	Cm 28S rRNA	CGCTATCGGTCTCTCGCCGGTATTTAGCCTTAGGTGAAG
oSDR2587	Cm 18S rRNA	GTTACCATGAATCACCAGAGACCGCCGAGGCGGTTTGG
oSDR2588	Cm ITS1	ACCGCCGTCTTCCCACTGGGGAATAGCACAG
oSDR2589	Cm ITS2	ACGCATGCAGTCTGAGACAGACAGAACCTGCGCGC

3.3. Results and Discussion.

3.3.1 18S and 28SrRNAs Northern

Given that no change in the stoichiometry of 5.8S rRNA was observed in Chapter 2 and considering the possibility that RNase MRP may be involved in other rRNA processing steps, I extended the investigation to 18S rRNA, 28S rRNA, and other intermediates in the rRNA processing pathway. This decision was further motivated by the complex interplay between heat stress and rRNA processing observed in other organisms, such as *Arabidopsis thaliana*, where heat stress disrupts nucleolar structure, inhibits pre-rRNA processing, and alters ribosome profiles, leading to a rapid reduction in precursors for 18S, 5.8S, and 25S rRNAs (Darrière *et al*., 2022). To explore the effects of heat stress at 57 C on 18S and 28S rRNAs, I performed Northern blotting on total RNA (Figures 3.2 and 3.3).

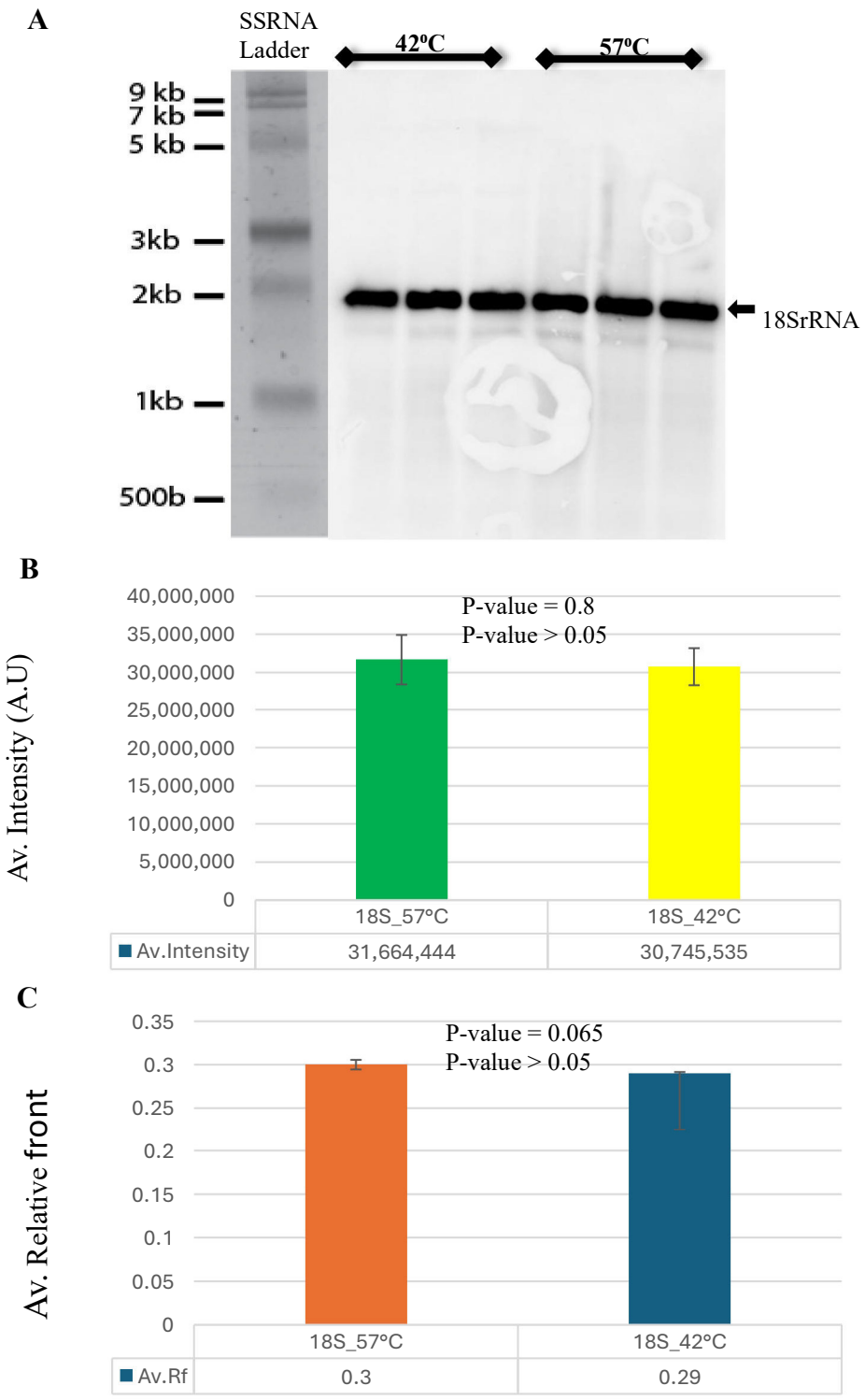

Figure 3.2. Heat stress does not impact 18S rRNA processing. a) RNA was isolated from *C. merolae* after growth and treatment at 42 C and 57 C temperatures, probed for 18S rRNA after running 1.5% formaldehyde-agarose gel for 6 hours at 50 V. **b)** band intensities and **c)** relative front (mobility) were quantified using Bio-Rad Image Lab software 6.1. The samples are technical replicates.

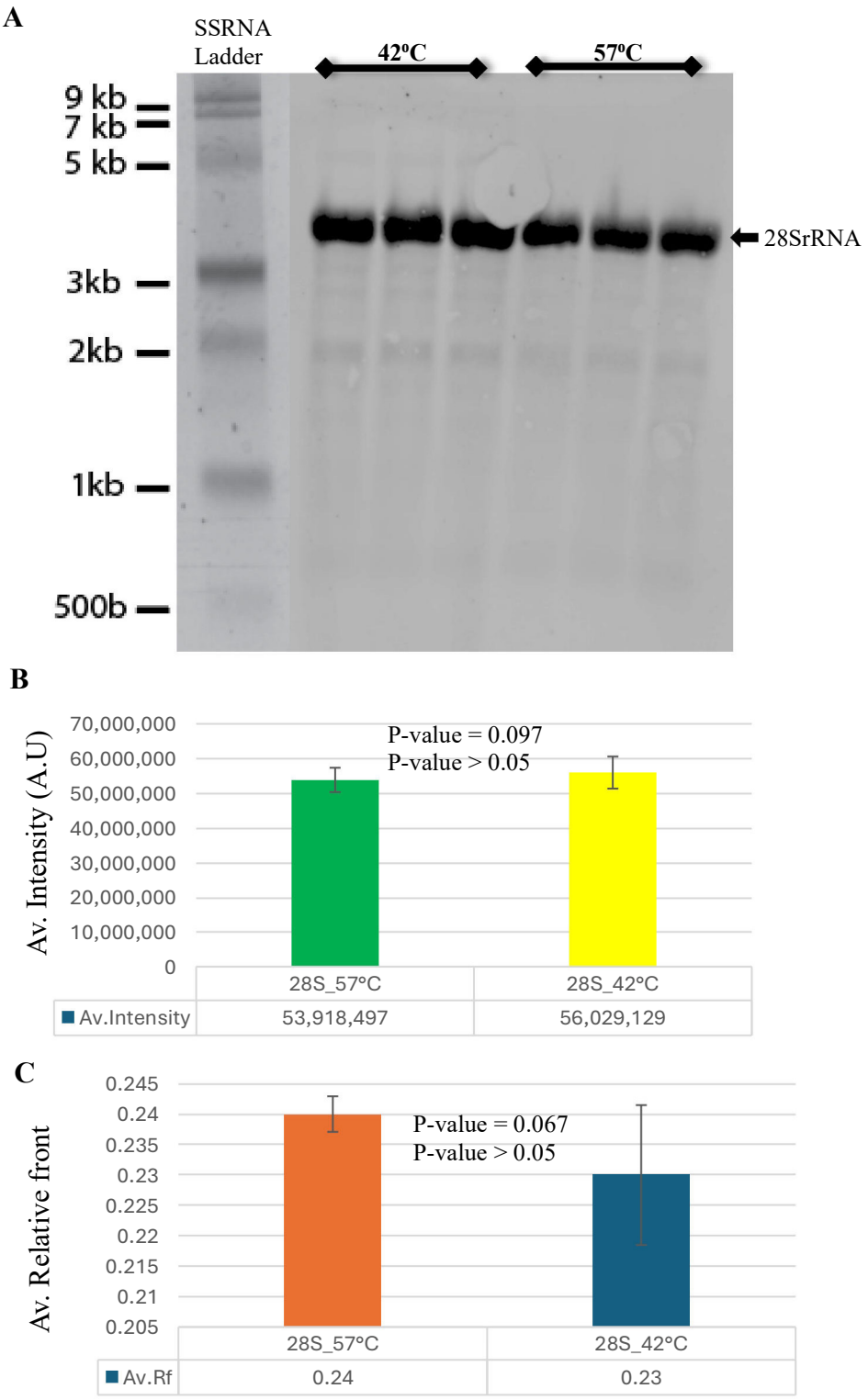

Figure 3.3. Heat stress does not impact 28S rRNA processing. a) RNA was isolated from *C. merolae* after growth and treatment at 42 C and 57 C temperatures, probed for 18S rRNA after running 1.5% formaldehyde-agarose gel for 6 hours at 50 V. **b)** band intensities and **c)** relative front (mobility) were quantified using Bio-Rad Image Lab software 6.1. The samples are technical replicates.

Figures 3.2 and 3.3 demonstrate that there are no detectable changes in the levels of 18S or 28S rRNA under heat stress conditions. However, since I previously observed no effects on 5.8S rRNA (as discussed in Chapter 2), I am unable to draw any conclusions regarding the potential role of RNase MRP in the processing of these rRNA forms. However, in contrast to findings in *Arabidopsis thaliana* where heat stress leads to the disruption of nucleolar structure, inhibition of pre-rRNA processing, and a rapid decline in detectable levels of 18S, 5.8S, and 25S rRNA precursors (Darrière *et al*., 2022), this data reveals that *C. merolae* exhibits a unique resilience under similar conditions. Specifically, exposure to 57 C does not affect the processing levels of 18S and 28S rRNA in *C. merolae*.

3.3.2 Detection of Pre-rRNA Intermediates

The canonical model for processing the primary Pol I transcript begins with the endonucleases Utp24 and Rnt1 cleaving the 5' ETS and 3' ETS, respectively, from the main portion of the pre-rRNA, forming the 32S intermediate (Figure 3.1) (Kufel *et al*., 1999; An *et al*., 2018). Utp24 then cleavages at the A2 site within ITS1, separating the rRNA sequences destined for the 40S and 60S ribosomal subunits. Further processing of ITS1 produces the 5' end of the 5.8S rRNA and the 3' end of the 18S rRNA. The 3' end of the 5.8S rRNA is generated by Las1 cleavage at the C2 site in ITS2, followed by exonucleolytic trimming by the exosome, with the downstream portion of ITS2 being removed by the exonucleases Rat1 and Xrn1 (Mitchell *et al*., 1997). Two pathways lead to forming the 5' end of the 5.8S rRNA. In the major pathway, the ribozyme RNase MRP cleaves ITS1 at the A3 site, after which exonucleases Rat1 and Rrp17 trim the resulting 5' end to create the “short” 5.8S rRNA (5.8SS).

To investigate potential heat stress effects on additional intermediates in the pre-rRNA processing pathway and to determine whether *C. merolae* follows the canonical rRNA

processing pathway, I utilized probing for these precursors (ITS1, ITS2, 5.8S, and 28S) on a 1.5% formaldehyde agarose gel and performed a Northern blot analysis.

3.3.2.1 Analysis of 5.8S and Processing Intermediates

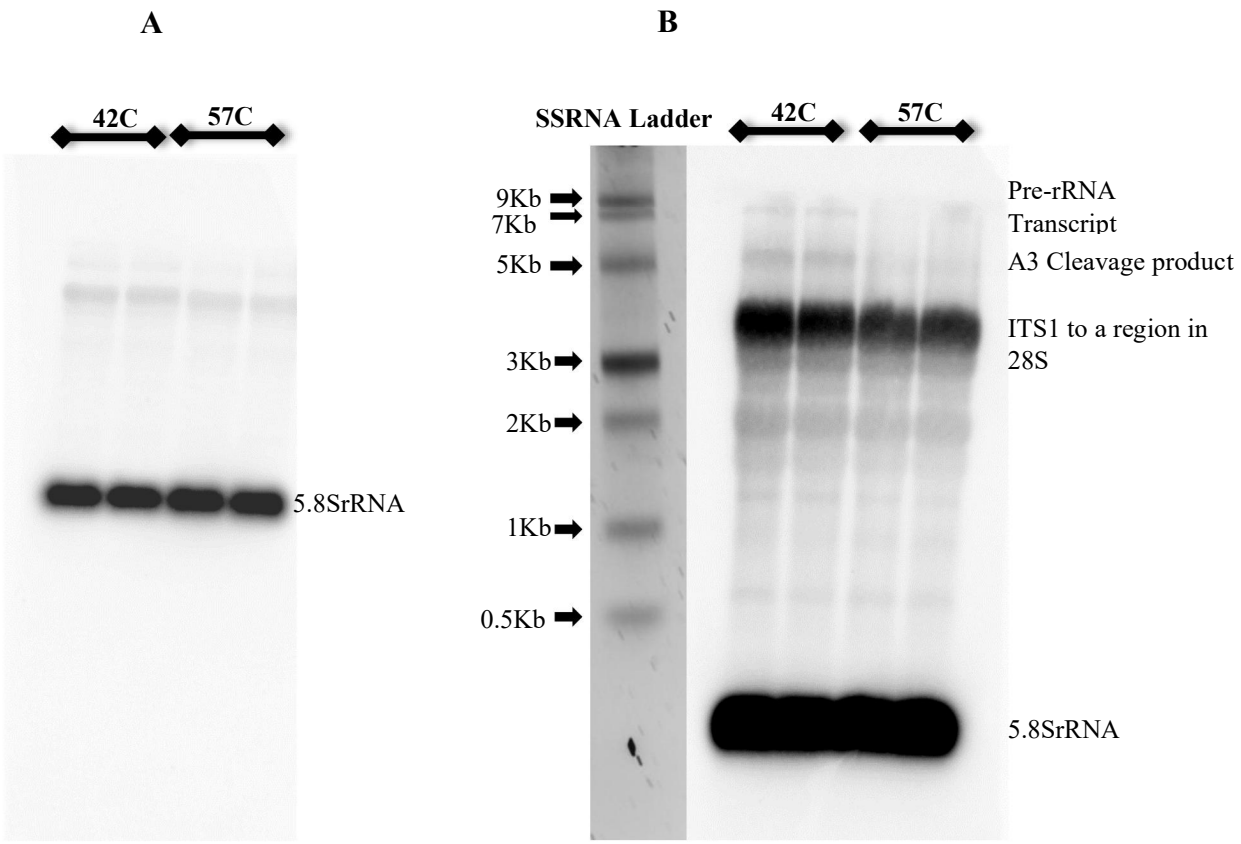

Figure 3.4. Detection of 5.8S rRNA on formaldehyde-agarose gel via Northern, illustrating intermediates associated with the Canonical rRNA Processing Pathway. RNA was isolated from *C. merolae* grown at both temperatures and probed for 5.8S rRNA under two conditions: **a)** 1.5% Formaldehyde-Agarose gel run for 3 hours with lower total RNA, and **b)** 1.5% formaldehyde-agarose gel run for 6 hours with higher total RNA to enhance the detection of intermediates. oSDR2487 probe was used. The samples are technical replicates.

The oSDR2487 probe is designed to hybridize specifically to the 5.8S rRNA region within the pre-rRNA transcript ($B1_L$ canonical processing site). Therefore, it is expected to detect the full-length pre-rRNA transcript, the A2/A3 cleavage intermediate, and the mature 5.8S rRNA species. Figure 3.4 indicates the presence of pre-rRNA and the A3 cleavage product, alongside

expected expression levels of 5.8S rRNA. However, a notable decrease in pre-rRNA prominence at 57 C was observed (Figure 3.4) suggesting reduced expression of pre-rRNA under heat stress conditions.

3.3.2.2 Analysis of ITS1 and Processing Intermediates

The next step is to investigate cleavage within the ITS1 region, which results in the separation of the 18S rRNA sequence from the 5.8S-ITS2-28S rRNA sequences (Figure 3.1). The 5.8S rRNA blot (Figure 3.4b), was stripped and reprobed with oSDR2588 within ITS1.

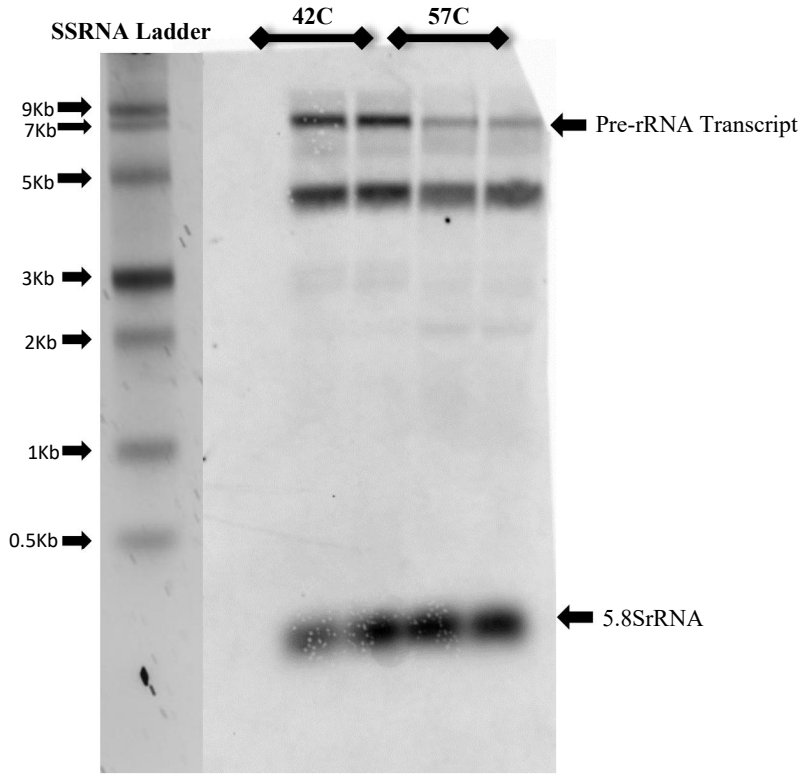

Figure 3.5. Detection of ITS1 on formaldehyde-agarose gel via Northern, revealing intermediates corresponding to the canonical rRNA Processing Pathway. RNA was isolated from *C. merolae* after growth at both temperatures and probed for 5.8S rRNA after running 1.5% formaldehyde agarose for 6 hours, this blot was stripped and re-probed for ITS1. oSDR2588 probe was used. The samples are technical replicates.

The oSDR2588 probe is designed to hybridize specifically to the ITS1 region within the pre-rRNA transcript. As such, it is expected to detect the full-length pre-rRNA transcript. The analysis reveals the detection of the pre-rRNA transcript. This also indicated a notable reduction in pre-rRNA levels under heat stress (Figure 3.5), corroborating the findings presented in Figure 3.4. This observation provides further evidence of rDNA transcription inhibition in response to heat stress conditions.

3.3.2.3 Analysis of ITS2 and Processing Intermediates

The ITS1 cleavage is then followed by a cleavage in ITS2, which results in the separation of the 5.8S and 28S rRNA sequences. Subsequent trimming of these intermediates generates the mature 5.8S and 28S rRNAs.

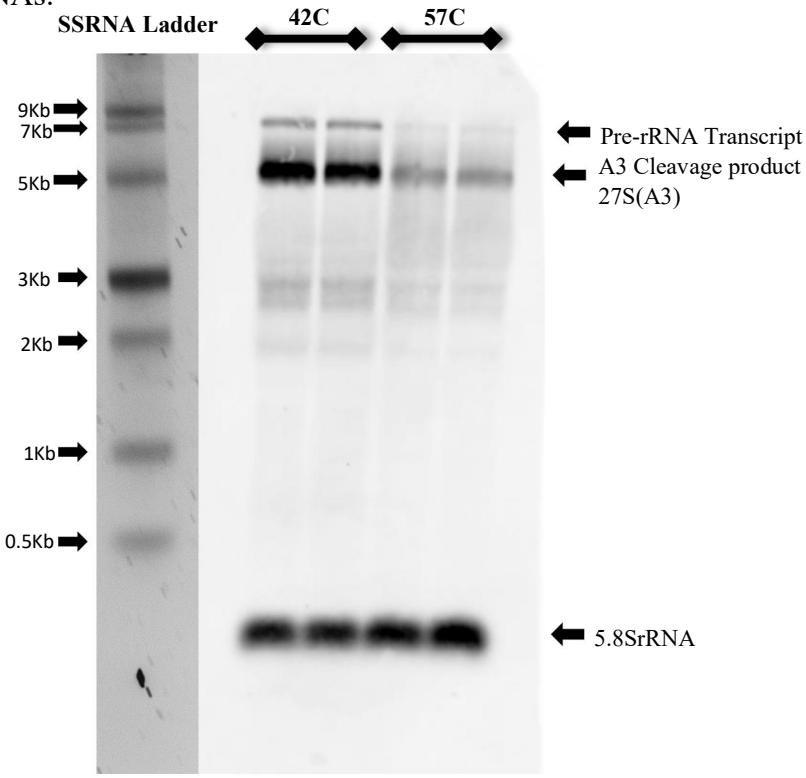

Figure 3.6. ITS2 detection on formaldehyde-agarose gel via Northern reveals intermediates corresponding to the Canonical rRNA Processing Pathway. RNA was isolated from *C. merolae* after growth at both temperatures and probed for 5.8S rRNA after running 1.5% formaldehyde agarose for 6 hours; this blot was stripped and re-probed for ITS2. oSDR2589 probe was used. The samples are technical replicates.

The oSDR2589 probe is designed to hybridize specifically to the ITS2 region within the pre-rRNA transcript. It is expected to detect the full-length pre-rRNA transcript as well as the A2/A3 cleavage intermediates generated during rRNA processing. The expected pre-rRNA transcript and A2/A3 cleavage intermediates were observed. However, the investigation of the internal transcribed spacer 2 (ITS2) region, similar to the findings observed in the 5.8S and ITS1 results, demonstrated a significant decrease in pre-rRNA levels under heat stress conditions (Figure 3.6). This consistent pattern across multiple rRNA processing components provides robust evidence supporting the inhibition of rDNA transcription during heat stress. The correlation between reduced pre-rRNA levels in the ITS2 region and the previously observed reductions in the 5.8S and ITS1 regions reinforces the notion that heat stress adversely affects rDNA transcription.

3.3.2.4 28S and Processing Intermediates

Lastly, a probe was designed to target the 5' end of 28S rRNA to detect other intermediates in the canonical pathway.

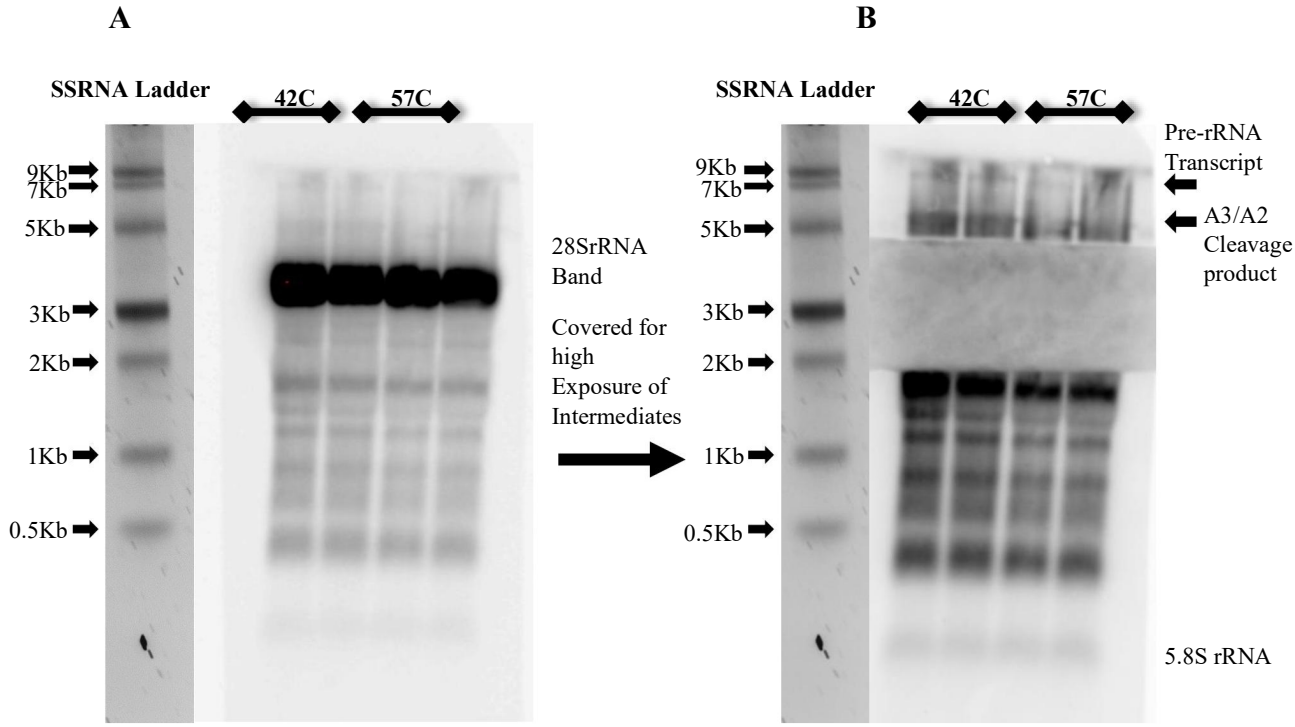

Figure 3.7. 28S rRNA detection on formaldehyde-agarose gel via Northern reveals intermediates corresponding to the Canonical rRNA Processing Pathway. a) RNA was isolated from *C. merolae* after growth at both temperatures and probed for 5.8SrRNA after running 1.5% formaldehyde agarose for 6 hours, this blot was stripped and re-probed for 28S rRNA**. b)** The 28S band was covered to ensure optimal exposure of other bands. oSDR2586 probe was used. The samples in each temperature set are technical replicates.

The oSDR2586 probe is designed to hybridize specifically to the 28S rRNA region within the pre-rRNA transcript. It is expected to detect the full-length pre-rRNA transcript, the A2/A3 cleavage intermediates, and the mature 28S rRNA. The expected bands were observed. The tabulated results of *C. merolae's* Canonical rRNA processing pathway Northerns and the bands observed are shown in Table 3.2 below.

Table 3.2. Observed Bands in Canonical rRNA Processing: Northern Blot Data Summary

	42 C					57 C				
OLIGO [a]	2587	2588	2487	2589	2586	2587	2588	2487	2589	2586
SIZES										
8kb pre-rRNA	✓ ++	✓ ++	✓ ++	✓ ++	✓ ++	✓ +	✓ +	✓ +	✓ +	✓ +
5.6kb A3 cleavage product	-	-	✓ ++	✓+++	✓ ++	-	-	✓ +	✓ +	✓ +
4.5kb pre-rRNA	-	✓+++	-	-	-	-	✓ +	-	-	-
28S rRNA	-	-	-	-	✓ +++	-	-	-	-	✓+++
18S rRNA	✓ +++	-	-	-	-	✓ +++	-	-	-	-
5.8S rRNA	-	-	✓+++	-	-	-	-	✓+++	-	-

a

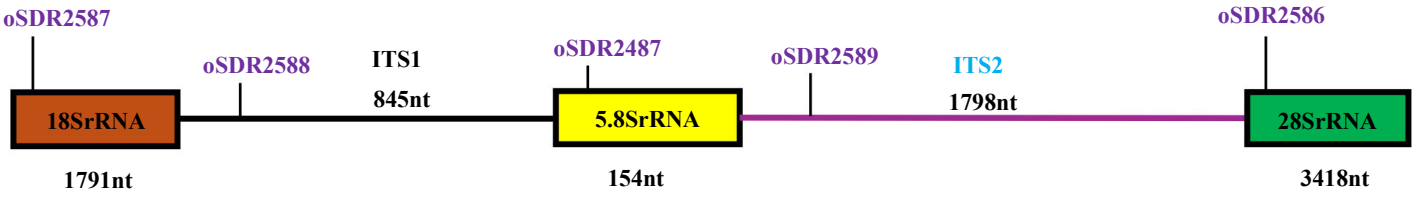

✓ = Detected + = Less Prominent ++ = Medium +++ = Prominent - = Not Detected

Figure 3.8 below presents the quantification of band intensities and the relative front of pre-rRNA intermediates seen at 42 C and 57 C (Figure 3.4 to Figure 3.7).

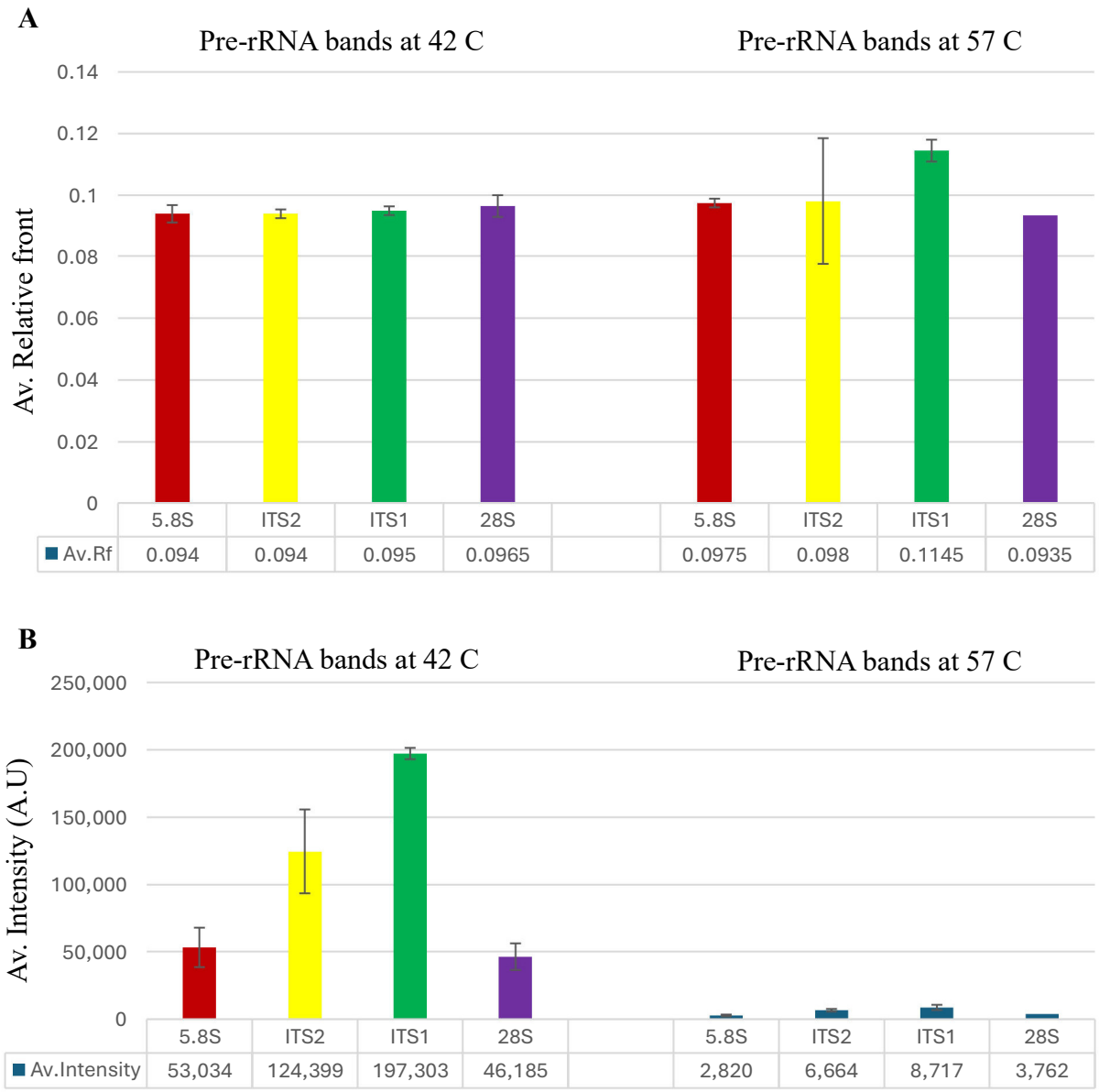

Figure 3.8: Pre-rRNA level reduced at 57 C: a) relative front (mobility) and **b)** band intensity of pre-rRNA levels reduced at 57 C. Bands were quantified using Bio-Rad Image Lab software 6.1.

To determine whether *Cyanidioschyzon merolae* follows the canonical rRNA processing pathway, Table 3.3 below, compares the expected bands for each probed intermediate in the canonical pathway with those observed in *C. merolae*. The presence of all expected bands in *C. merolae* supports the conclusion that this organism adheres to the canonical rRNA processing pathway.

Table 3.3. Canonical rRNA Processing Pathway: Expected vs. Observed Bands in *Cyanidioschyzon merolae*

Precursor Probes	Expected rRNA Canonical Processing Pathway Product	*C. merolae* Intermediate Product Observed
	8 kb pre-rRNA	✓
2487	5.6 kb A3 cleavage product	✓
	5.8S rRNA (154 b)	✓
2587	8 kb pre-rRNA	✓
	18S rRNA (1.7 kb)	✓
2586	8 kb pre-rRNA	✓
	5.6 kb A3 cleavage product	✓
	28S rRNA (3.4 kb)	✓
2589	8 kb pre-rRNA	✓
	5.6 kb A3 cleavage product	✓
2588	8 kb pre-rRNA	✓

✓ = Detected

3.4. Discussion.

The stability of 5.8S rRNA (Figure 2.7, chapter 2), 18S rRNA, and 28S rRNA levels (Figures 3.2 and 3.3 respectively) under heat stress in *C. merolae* contrasts with the observed inhibition of rRNA maturation in *A. thaliana (*Darrière *et al*., 2022), mammals (Ghosha and Jacob 1996;

Coccia *et al*., 2017) and the altered ribosome profiles seen in other eukaryotes. The unaltered levels of mature 5.8S, 28S, and 18S rRNAs in *C. merolae* under heat stress despite a reduction in pre-rRNA levels (Figures 3.5 and 3.6), suggest the presence of a sophisticated regulatory mechanism that ensures ribosome function is maintained under extreme conditions. This mechanism prioritizes the stability of mature rRNAs to maintain ribosome function. This could involve post-transcriptional stabilization or modification of mature rRNAs, protecting them from degradation during stress. Alternatively, if no such regulation exists, heat stress could impair pre-rRNA processing, leading to a reduction in both precursor and mature rRNA levels, potentially disrupting ribosome biogenesis. The maintenance of mature rRNAs under stress indicates a sophisticated mechanism ensuring ribosomal function under extreme conditions.

This finding implies that *C. merolae* may possess distinct adaptive mechanisms that ensure the maintenance of ribosome biogenesis even under extreme environmental stress, highlighting the evolutionary diversity in stress response pathways across species. One possible explanation is that mature rRNAs, once synthesized, exhibit high stability and resistance to degradation, allowing their levels to remain constant even when rDNA transcription is inhibited. Alternatively, *C. merolae* may possess an efficient rRNA processing machinery that optimizes the conversion of available pre-rRNA into mature rRNAs, compensating for the diminished precursor synthesis. The organism may also regulate rRNA turnover by slowing the degradation of mature rRNAs during stress, thereby preserving essential ribosomal components. These adaptive mechanisms, potentially involving specialized pathways that protect and stabilize rRNAs, highlight the resilience of *C. merolae* in maintaining cellular functions despite environmental challenges. This contrasts with organisms such as *Arabidopsis thaliana*, where heat stress leads to a rapid decline in rRNA levels, illustrating the evolutionary diversity in stress

response strategies. Furthermore, the reduction in pre-rRNA levels at 57 C, suggesting that rDNA transcription is inhibited in *C. merolae* under heat stress may be attributed to an effect on RNA polymerase I or a regulatory element involved in rDNA transcription. These findings align with observations in *Arabidopsis thaliana*, where heat stress impedes pre-rRNA processing (Darriere *et al*., 2022), and in mammals, where a brief heat shock inhibits both pre-rRNA transcription and its subsequent processing into mature rRNAs (Ghosha and Jacob, 1996). Additionally, it is well-established that heat stress inhibits rDNA transcription in animal cells (Ghosha and Jacob, 1996; Coccia *et al*., 2017).

Further research is needed to elucidate the molecular basis of this stability, which could offer insights into the broader mechanisms of stress tolerance in extremophiles.

Chapter 4 - In Silico Prediction of *C. merolae's* MRP RNA: Secondary Structure, Conserved Regions, and Protein Constituents of the RNase MRP Complex

4.1 Introduction

The RNase MRP complex is an essential ribonucleoprotein enzyme involved in the processing of precursor rRNA, particularly in the generation of the mature 5.8S rRNA in eukaryotes. Its RNA component is essential for its catalytic activity, while its associated proteins are necessary for structural stability and proper function. Studies in well-characterized organisms such as *Saccharomyces cerevisiae*, *Homo sapiens*, *Drosophila melanogaster*, and *Chlamydomonas reinhardtii* have revealed conserved secondary structures within the RNase MRP RNA component and a common set of protein constituents. In the case of *S. cerevisiae*, conserved regions, and domains were identified through structural probing experiments, while the structure of *D. melanogaster* MRP RNA and other organisms were derived through comparative genomics involving *S. cerevisiae* and *Homo sapiens*. These features highlight the evolutionary conservation and functional importance of the complex. However, *Cyanidioschyzon merolae*, a red alga with a highly streamlined genome, offers a unique opportunity to investigate how these structural and functional elements have been conserved or diverged over evolutionary time.

In this chapter, I address two key questions: Does the RNase MRP RNA in *C. merolae* possess conserved secondary structural regions comparable to those found in other eukaryotic organisms? Second, does the RNase MRP complex in *C. merolae* retain the same protein constituents, or has it lost some of these proteins as part of its evolutionary adaptation? By answering these questions, this analysis will not only enhance our understanding of the structural and functional conservation of RNase MRP in *C. merolae* but also provide insights into its evolutionary divergence.

Predicting the secondary structure of RNase MRP RNA is important for identifying conserved regions that may be functionally important. Conservation of structure often correlates with

conservation of function, and by comparing *C. merolae* to *S. cerevisiae, Drosophila*, humans, and other organisms, we can infer which regions of the RNA are essential for catalytic activity. Additionally, the identification of these regions opens the possibility of mirroring mutational analysis experiments performed in *S. cerevisiae*. If similar regions of the RNase MRP RNA are conserved in *C. merolae*, mutations performed in these regions in *S. cerevisiae* may provide valuable functional insights that could be translated to *C. merolae*.

Furthermore, the identification of the protein constituents of RNase MRP in *C. merolae* is of particular interest because this organism's reduced genomic content suggests potential evolutionary streamlining. In other eukaryotes, RNase MRP is composed of several conserved proteins that are necessary for its assembly and function. Understanding whether C. merolae has retained all these proteins or has lost some provides important clues to how the RNase MRP complex may have adapted to function with fewer components in this minimalistic organism.

This analysis also connects to other chapters of this thesis, particularly the investigation into how RNase MRP functions under heat stress and its role in the processing of 5.8S rRNA. By first determining whether *C. merolae* retains key conserved structural and protein elements of RNase MRP, we can then assess whether these elements are involved in the observed resilience of the complex under stress conditions. Thus, in this chapter, I built a secondary structure model based on sequence alignments with MRP from other organisms using RNA folding software and manual examination of base pairing potential to lay a foundation for the broader study of RNase MRP function in *C. merolae*, both in normal conditions and under heat stress, linking structure to function and evolutionary adaptation.

4.2 Materials and Methods

4.2.1 Genome and Protein Sequences

RNase MRP protein sequences were retrieved from NCBI - The National Centre for Biotechnology Information at the National Library of Medicine and the Universal Protein knowledgebase (http://www.ncbi.nlm.nih.gov/gene/), Swiss-Prot (http://www.expasy.ch/sprot/), and UniProt (http://www.expasy.uniprot.org/). The *C. merolae* genome sequence was obtained from the NCBI GenBank database. Comparative genomic analysis was conducted with other model organisms, including *Saccharomyces cerevisiae* (baker's yeast), *Homo sapiens* (humans), *Drosophila melanogaster* (fruit fly), *Caenorhabditis elegans* (nematode), and *Chlamydomonas reinhardtii* (green alga). The genome and protein sequences of these organisms were also retrieved from NCBI, UniProt, and Ensembl databases to facilitate comparative analysis. These sequences were used as references for identifying homologous regions and conserved domains.

4.2.2 Alignment of *Cyanidioschyzon merolae* MRP RNA with Other Organisms

The MRP RNA sequence of *C. merolae* was retrieved from the NCBI GenBank database. To compare this sequence with those from other organisms, homologous MRP RNA sequences were obtained from RNAcentral and Rfam databases. Organisms used for this comparative analysis included *Saccharomyces cerevisiae* (baker's yeast), *Homo sapiens* (humans), *Drosophila melanogaster* (fruit fly), *Caenorhabditis elegans* (nematode), and *Chlamydomonas reinhardtii* (green alga). In addition, the following organism-specific databases were used; the *Saccharomyces* Genome Database (Cherry et al., 1997) and the Drosophila Genome Project (Christie et al., 2003). Multiple sequence alignments were performed using Clustal Omega v3.13.8 (Sievers and Higgins, 2013) and MUSCLE v3.8.31 (Sievers et al., 2010), allowing for

the identification of conserved nucleotides and secondary structure elements across different species. Pairwise sequence alignments were also conducted using EMBOSS Needle (http://www.ebi.ac.uk/Tools/psa/emboss_needle/) for more detailed comparisons, highlighting conserved base-pairing interactions relevant to the secondary structure of MRP RNA. The results of these alignments were used to infer evolutionary relationships and to validate the structural predictions made for *C. merolae* MRP RNA.

4.2.3 Identification of Protein Homologs

To identify homologs of the known protein constituents of RNase MRP in *Cyanidioschyzon merolae*, Position-Specific Iterative BLAST (PSI-BLAST) searches (Altschul and Koonin, 1998) was used. All known protein subunits of RNase MRP were used as queries in these searches, with an E-value threshold of 0.001 set for inclusion in subsequent PSI-BLAST iterations. In some cases, multiple PSI-BLAST searches were performed with different query sequences to maximize the identification of potential homologs. The primary database searched was the NCBI GenBank protein set (Benson et al., 2006). For proteins not present in this database, sequences were retrieved from individual genome projects or identified through TBLASTN searches of genome sequences. These novel sequences were subsequently included in the database used for PSI-BLAST searches to ensure comprehensive coverage. Additionally, in some instances, further homologs were identified using Pfam models, which provided supplementary sequence data and enhanced the search's robustness.

4.2.4 Validation of RNase MRP Protein Homologs via Reciprocal BLAST Searches

To identify homologs of RNase MRP protein constituents in *C. merolae*, I employed a reciprocal BLAST search strategy based on the approach described by (Ward and Moreno-Hagelsieb 2014). Initially, forward BLASTP searches were conducted using known RNase MRP proteins from organisms such as *Saccharomyces cerevisiae* (yeast), *Homo sapiens* (humans), *Drosophila melanogaster* (fruit fly), *Caenorhabditis elegans* (nematode), and *Chlamydomonas reinhardtii* (green alga) as queries to identify putative orthologs in *C. merolae*. These searches were performed using the NCBI BLAST tool (Altschul and Koonin, 1998) with a BLOSUM62 matrix and an E-value threshold of 0.001 to ensure significant matches. To validate the identified homologs and resolve ambiguous or unexpected results, reciprocal BLASTP searches were carried out. In this approach, the identified *C. merolae* proteins were used as queries against the protein databases of the original species from which the RNase MRP subunits were first identified. The same E-value threshold of 0.001 was applied in these reciprocal searches. A *C. merolae* protein was confirmed as a true homolog if the reciprocal BLAST search returned the original query protein or a closely related homolog as the top hit with an E-value smaller than 10^-10. If the top hit did not correspond to the original query protein, all candidate *C. merolae* proteins with an E-value threshold of less than 10^-2 were further analyzed against the original organism's proteome. Additionally, the domain structure of uncertain candidates was examined using NCBI's DELTA-BLAST tool to distinguish true orthologs from false positives. This comprehensive approach increased the likelihood that the identified proteins were indeed functional homologs of the known RNase MRP components in *C. merolae*.

4.3. Results

In this section, I address the question of whether the RNase MRP RNA in *Cyanidioschyzon merolae* retains conserved structural regions and protein constituents found in other eukaryotic organisms. To explore this, I used comparative computational analysis to predict the secondary structure of the RNase MRP RNA, alongside bioinformatic tools to identify the corresponding protein components compared with known RNase MRP structures in organisms such as *Saccharomyces cerevisiae*, *Homo sapiens*, *Drosophila melanogaster*, and *Chlamydomonas reinhardtii*. The secondary structure predictions revealed conserved regions that align with functional domains in other species, suggesting that *C. merolae* has maintained functional aspects of RNase MRP. Similarly, the analysis of protein constituents showed a streamlined set of core proteins, consistent with the organism's reduced genome but still sufficient for maintaining RNase MRP activity. The following sections will detail these structural predictions and protein identifications, and their implications for understanding the evolutionary conservation and divergence of RNase MRP in *C. merolae*.

4.3.1 Conserved Regions and Predicted Secondary Structure of RNase MRP RNA

To identify conserved regions, nucleotides, and structural elements within *C. merolae* MRP RNA that correspond to these experimentally validated and evolutionarily conserved structures (Figures 1.5A and 1.6C), I performed a comparative genomics analysis. This approach allowed for the alignment of *C. merolae* RNase MRP RNA with the conserved and structurally probed RNase MRP RNA sequences from *S. cerevisiae, D. melanogaster,* and other model organisms, facilitating the identification of evolutionarily conserved features within the *C. merolae* RNase MRP RNA structure.

Figure 4.1 below illustrates the alignment of *C. merolae* RNase MRP RNA with *D. melanogaster* RNase MRP RNA, highlighting the conserved regions that underpin the prediction of structural motifs within the RNase MRP RNA. The sequence alignment reveals a 46.4% similarity between the RNase MRP RNAs of these two organisms. Consistent with existing literature (Piccinelli et al., 2005), the alignment shows the conservation of the ubiquitous P1, P2, and P3 helices, as well as the CR-I, CR-IV, and CR-V regions. The P4 helix is again formed by pairing of elements from the CR-I and CR-V regions.

Figure 4.2 also illustrates the alignment of *C. merolae* RNase MRP RNA with *Chlamydomonas reinhardtii* RNase MRP RNA, highlighting the conserved regions that serve as a foundation for predicting structural motifs within the RNase MRP RNA. The sequence alignment reveals a 39.7% similarity between the RNase MRP RNAs of these two organisms.

Furthermore, Figures 4.3 and 4.4 illustrates the alignment of *C. merolae* RNase MRP RNA with *Saccharomyces cerevisiae* and *Homo sapiens* RNase MRP RNA, highlighting the conserved regions that serve as a basis for predicting structural motifs within the RNase MRP RNA. The sequence alignment reveals a 39.5% and 40.1% similarity between *C. merolae* against *Sc* and *Hm* RNase MRP RNAs respectively. The alignment shows the conservation of the Domain 1 region (the CR-I, CR-IV, and CR-V regions). The P4 helix is formed by pairing elements from the CR-I and CR-V regions.

Lastly, figure 4.5, the predicted secondary structure, was built using manual model building to manipulate the secondary structure with the predicted conserved regions and I utilized other bioinformatic tools (Mfold and sfold) to make it domain 2 region.

```
Aligned sequences: 2
# 1: Drosophila Melanogaster (Dm)
# 2: Cyanidioschyzon Merolae (Cm)
# Matrix: EDNAFULL
# Gap penalty: 10.0
# Extend penalty: 0.5
# Length: 515
# Identity:     239/515 (46.4%)
# Similarity:   239/515 (46.4%)
# Gaps:         206/515 (40.0%)
# Score: 444.5
#=======================================
                          P1 Helices
EMBOSS_001         1 GCCGGTTTGAGTCTTCCATGCTTGTCTCTCG--------GGGCCACAAA-     41 Dm
                       .||...||.|||.|.|.||  ||..||||        |.||.||..|
EMBOSS_001         1 --GGGGAAGACTCTGCTAAGC--GTTCCTCGTTATCAGAGCGCTACGTAC     46 Cm
EMBOSS_001        42 -----ACG---AGTTCCTGG---------TAA------CTC------AA-     61 Dm
                         |||   .|.||||||         |||      |||      ||
EMBOSS_001        47 GGTTTACGGGAGGGTCCTGGATTAGCCCCTAAACCAGGCTCGGTGCGAAC     96 Cm
                                                       P3    P4(CR-I)
EMBOSS_001        62 ---------CTGAT--AATGCC-----------CTGGGCGAAAGTCCCC     88 Dm
                             |||||  .|||||            |||||.||||||||||
EMBOSS_001        97 AGGTGCGCCCTGATTCGATGCCAGCCGTTTGGCTCTGGGTGAAAGTCCCC    146 Cm
EMBOSS_001        89 GGGC-CTAGGATAGAAAGTATCAAGGT-GTAA--AAAG-TGTGC---ACA    130 Dm
                     ||.| .||||..|||.|||.||  ||| ||||  |||| ||.||   .||
EMBOSS_001       147 GGACAGTAGGTCAGAGAGTGTC--GGTGGTAAGCAAAGCTGGGCGTTTCA    194 Cm
EMBOSS_001       131 AAACACCCACCACCCCTG-TGGTGGGTGGTGCA-------TTCGCCTATA    172 Dm
                     ...|.|.|| |||..||| |.|.||| ..||||       ..|.||.|||
EMBOSS_001       195 GGTCGCGCA-CACTTCTGCTCGCGGG-ACTGCAACCACAGAACCCCAATA    242 Cm
EMBOSS_001       173 ----------TTCTGCG-------GAATTTCGCCTGGCGTATGGATGAAG    205 Dm
                             |.|||||       |||..||||.||.|| |||| ||.||
EMBOSS_001       243 AGAGCGGGAGTGCTGCGCGACAGTGAACGTCGCTTGTCG-ATGG-TGCAG    290 Cm
EMBOSS_001       206 AGGATTTTATCC--GAA------------------TCCTTACGCGCCA-G    234 Dm
                     .|         |  |||                  |.|||.|||.||| |
EMBOSS_001       291 CG---------CTGGAACCTGCTGCCGCGTTGGGGTGCTTGCGCCCCATG    331 Cm
                                                  CR-IV     P2
EMBOSS_001       235 GTTGTCTGCGGAAATCTGCCAGAGT-AATCTTAGATATGG-ACGAG----    278 Dm
                     .|||.|.||||.|..||||   |.| ||||  ||..|||| |||||
EMBOSS_001       332 TTTGGCAGCGGCAGCCTGC---ACTGAATC--AGCAATGGAACGAGCGAG    376 Cm
EMBOSS_001       279 -----------TTGGTAGGACTCGGCGGGTGGTGTTCACACACTTTCTCG    317 Dm
                             ||..| |||  |||||                  .||||
EMBOSS_001       377 AGCGACCGTCCTTCAT-GGA--CGGCG------------------ACTCG    405 Cm
                                           CR-V
EMBOSS_001       318 TCTGAGAAACCGCCTACACAGAATGGGGCTTACATTGGGAAACTCGGACG    367 Dm
                       |||            |||.||||||||          ||||.|.|.
EMBOSS_001       406 --TGA------------ACACAATGGGGCTT----------ACTCTGGCA    431 Cm
EMBOSS_001       368 GCGCACTCCCTTTTT    382 Dm
                     |.|..||||||
EMBOSS_001       432 GTGTGCTCCCT----    442 Cm
```

Figure 4.1: Sequence alignment of *C. merolae* RNase MRP RNA with *Drosophila melanogaster* RNase MRP RNA. Conserved regions within Domain 1 of the MRP structure are highlighted. *Drosophila* conserved sequences are highlighted in yellow and Cm in red. The names of the conserved regions are labeled in green.

```
# Aligned sequences: 2
# 1: Chlamydomonas reinhardtii (Cr)
# 2: Cyanidioschyzon merolae (Cm)
# Matrix: EDNAFULL
# Gap penalty: 10.0
# Extend penalty: 0.5
# Length: 474
# Identity:     159/474 (33.5%)
# Similarity:   188/474 (39.7%)
# Gaps:         239/474 (50.4%)
# Score: 356.5
EMBOSS_001         1 ------------GCGCAGUG-----------CGGAGGGCCACCU-CGGUG     26 Cr
                       ||..||.|           |.|||.||.||.: |||:
EMBOSS_001         1 GGGGAAGACTCTGCTAAGCGTTCCTCGTTATCAGAGCGCTACGTACGGT-     49 Cm
EMBOSS_001        27 UCACUUACGGCAGGAGUCGAGGGGCUGCUGCUUUGAGCGCGGCC-----C     71 Cr
                      ::||||        |||||  :.|:|..:: |||    ||     |
EMBOSS_001        50 ----TTACGG--------GAGGG--TCCTGGATT-AGC----CCCTAAAC     80 Cm
                                                              P3
EMBOSS_001        72 CCGGCUGGGCGC-------UGCAUCCAUGUAUU-GA-GCACAUC------    106 Cr
                     |.|||:.||.||       :|| .||.:| |:: || || ||.|
EMBOSS_001        81 CAGGCTCGGTGCGAACAGGTGC-GCCCTG-ATTCGATGC-CAGCCGTTTG    127 Cm
                           P4(CR-I)                    P8
EMBOSS_001       107 -----GGGCGAAAGUCCCCGGGCGACGGGGCAGAGAGUGCC-------AG    144 Cr
                          |||.|||||:||||||.|....||.|||||||:|.|        ||
EMBOSS_001       128 GCTCTGGGTGAAAGTCCCCGGACAGTAGGTCAGAGAGTGTCGGTGGTAAG    177 Cm
EMBOSS_001       145 C-------------------------------------------CCGCAAG    152 Cr
                     |                                           |.||||.
EMBOSS_001       178 CAAAGCTGGGCGTTTCAGGTCGCGCACACTTCTGCTCGCGGGACTGCAAC    227 Cm
EMBOSS_001       153 GGCAGGACCCC-------------------CGCG--------CGUCGUUU    175 Cr
                     ..|||.|||||                    ||||        ||:||.::
EMBOSS_001       228 CACAGAACCCCAATAAGAGCGGGAGTGCTGCGCGACAGTGAACGTCGCTT    277 Cm
EMBOSS_001       176 UUACGA-----------------------CCGCG--GGGCAGCUCGCCAU    200 Cr
                     .: |||                      |||||  |||..||:.||
EMBOSS_001       278 GT-CGATGGTGCAGCGCTGGAACCTGCTGCCGCGTTGGGGTGCTTGC---    323 Cm
EMBOSS_001       201 AGCAACA-GUUAUGUGGC------------CAGUG-----GGGAUACAAC    232 Cr
                      ||..|| |::   :|||            ||.:|     |..|:..|||
EMBOSS_001       324 -GCCCCATGTT---TGGCAGCGGCAGCCTGCACTGAATCAGCAATGGAAC    369 Cm
                                                                CR-V
EMBOSS_001       233 ---------CCACC------------------------AACACAACGGGG    249 Cr
                             |.|||                         |||||||.||||
EMBOSS_001       370 GAGCGAGAGCGACCGTCCTTCATGGACGGCGACTCGTGAACACAATGGGG    419 Cm
EMBOSS_001       250 CUUACUCCCGCACUGACG------    267 Cr
                     |::||:|..|||.:| .|
EMBOSS_001       420 CTTACTCTGGCAGTG-TGCTCCCT    442 Cm
```

Figure 4.2: Sequence alignment of *C. merolae* RNase MRP RNA with *Chlamydomonas reinhardtii* RNase MRP RNA. P3, P4(CR-I and CR-V), and P8 regions 1 of the MRP structure are highlighted. *Chlamydomonas* conserved sequences are highlighted in yellow and Cm in red. The names of the regions are labeled in green.

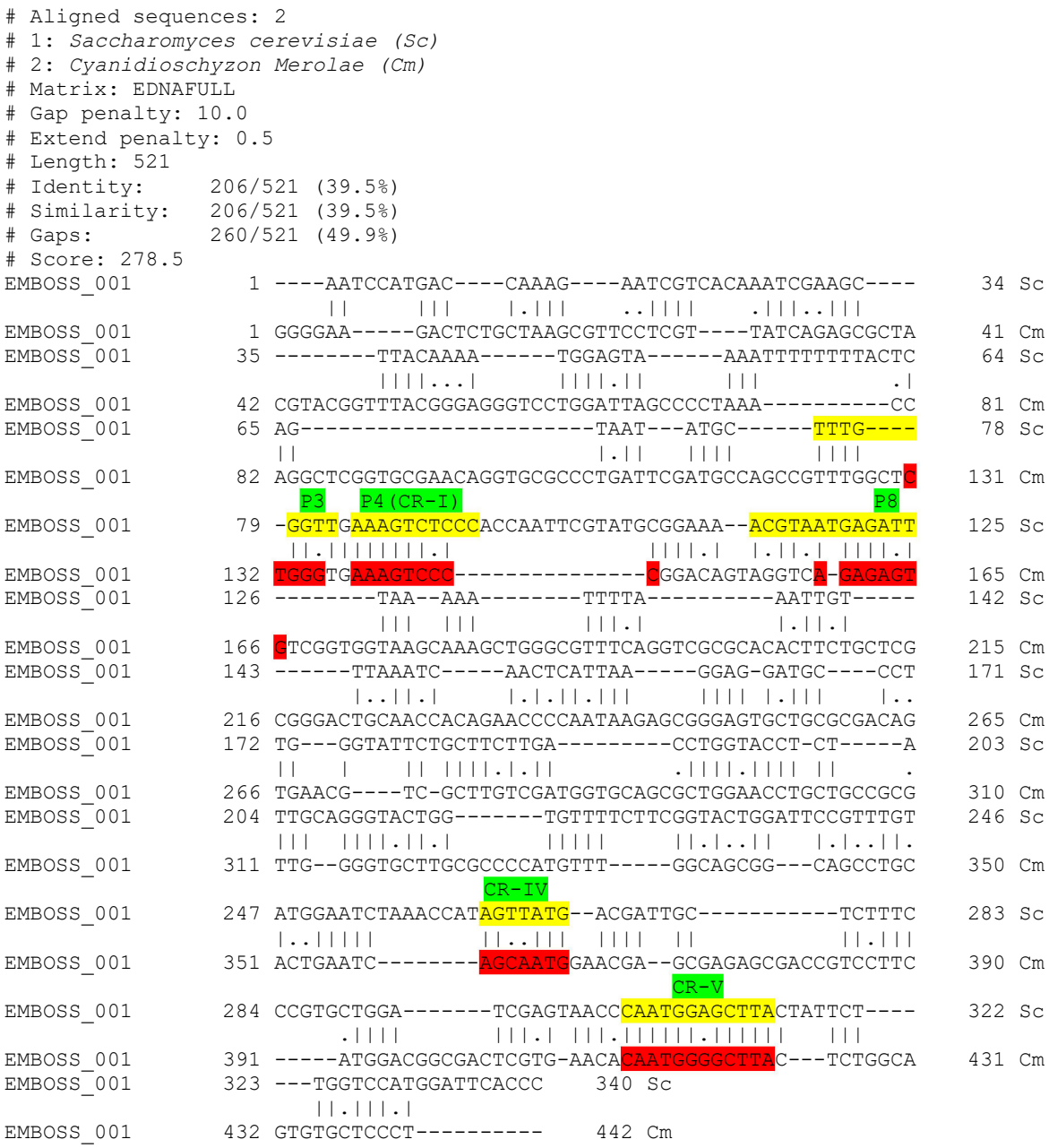

Figure 4.3: Sequence alignment of *C. merolae* RNase MRP RNA with *Saccharomyces cerevisiae* RNase MRP RNA. The alignment highlights conserved regions that provide a foundation for predicting structural motifs within the RNase MRP RNA. The sequence similarity between the RNase MRP RNAs of these two organisms is 39.5%. Conserved regions within Domain 1, including CR-I, CR-IV, and CR-V, are evident. The P4 helix is observed to form through pairing elements from the CR-I and CR-V regions.

```
# Aligned sequences: 2
# 1: Homo sapiens (Hm)
# 2: Cyanidioschyzon Merolae (Cm)
# Matrix: EDNAFULL
# Gap penalty: 10.0
# Extend penalty: 0.5
# Length: 469
# Identity:     192/469 (40.9%)
# Similarity:   192/469 (40.9%)
# Gaps:         226/469 (48.2%)
# Score: 335.0
EMBOSS_001         1 ---------------------------------------------TGGTT      5 Hm
                                                                  .||||
EMBOSS_001         1 GGGGAAGACTCTGCTAAGCGTTCCTCGTTATCAGAGCGCTACGTACGGTT     50 Cm
                           P2 helices
EMBOSS_001         6 CGTGCTGAAGG--CCTGTAT-----CCT-----AGGCT--------ACA-     34 Hm
                       |.|.|.|||  ||||.||     |||     |||||        |||
EMBOSS_001        51 --TACGGGAGGGTCCTGGATTAGCCCCTAAACCAGGCTCGGTGCGAACAG     98 Cm
                                                        P3    P4(CR-I)
EMBOSS_001        35 -----CACTGAGGACTCTGTTCCTCCCCTTTCCGC-CTAGGGGAAAGTCC     78 Hm
                         |.||   ||.||..|.||..||.||| .|| ||.||.||||||||
EMBOSS_001        99 GTGCGCCCT---GATTCGATGCCAGCCGTTT-GGCTCTGGGTGAAAGTCC    144 Cm
EMBOSS_001        79 CCGGAC-CTCGGGCAGAGAGTGCCACGTGCATACGCA--------CGT--    117 Hm
                     |||||| .|.||.|||||||||.| .||| .||.|||        |||
EMBOSS_001       145 CCGGACAGTAGGTCAGAGAGTGTC-GGTG-GTAAGCAAAGCTGGGCGTTT    192 Cm
EMBOSS_001       118 -AG-------ACA-TTCCCCGCTTCCC---ACT----CCAAAGTCCGCCA    151 Hm
                      ||       ||| |||..|   ||.|   |||    |||.||..|.|||
EMBOSS_001       193 CAGGTCGCGCACACTTCTGC---TCGCGGGACTGCAACCACAGAACCCCA    239 Cm
EMBOSS_001       152 AGAAG-------------------------CGTATCCCGCT--------G    168 Hm
                     |.|||                        |||    ||||        |
EMBOSS_001       240 ATAAGAGCGGGAGTGCTGCGCGACAGTGAACGT----CGCTTGTCGATGG    285 Cm
EMBOSS_001       169 AGCGGCG-----------TGGCGCG--GGGGCGTCATCCGTCAGCTCCCT    205 Hm
                     .||.|||           ||.||||  ||||.| |.|.||       ||.
EMBOSS_001       286 TGCAGCGCTGGAACCTGCTGCCGCGTTGGGGTG-CTTGCG-------CCC    327 Cm
                                                    P2
EMBOSS_001       206 CTAGTTACGCA--GGCAG--TGC---GTGTC----------CGCGC---A    235 Hm
                     |..|||..|||  |||||  |||   |..||          ||.||   |
EMBOSS_001       328 CATGTTTGGCAGCGGCAGCCTGCACTGAATCAGCAATGGAACGAGCGAGA    377 Cm
                                                          CR-V
EMBOSS_001       236 CCAACC-------------------------ACAC---GGGGCTCATTCT    257 Hm
                     .|.|||                          ||||   ||||||.|.|||
EMBOSS_001       378 GCGACCGTCCTTCATGGACGGCGACTCGTGAACACAATGGGGCTTACTCT    427 Cm
EMBOSS_001       258 --CAGCGCGGCTGTT----    270 Hm
                       |||.|    ||.|
EMBOSS_001       428 GGCAGTG----TGCTCCCT    442 Cm
```

Figure 4.4: Sequence alignment of *C. merolae* RNase MRP RNA with *Homo sapiens* RNase MRP RNA. The alignment highlights conserved regions that serve as a basis for predicting structural motifs within the RNase MRP RNA. The sequence similarity between the RNase MRP RNAs of these two organisms is 40.1%. Conserved regions within Domain 1, including CR-I, CR-IV, and CR-V, are evident. The P4 helix is formed by pairing elements from the CR-I and CR-V regions.

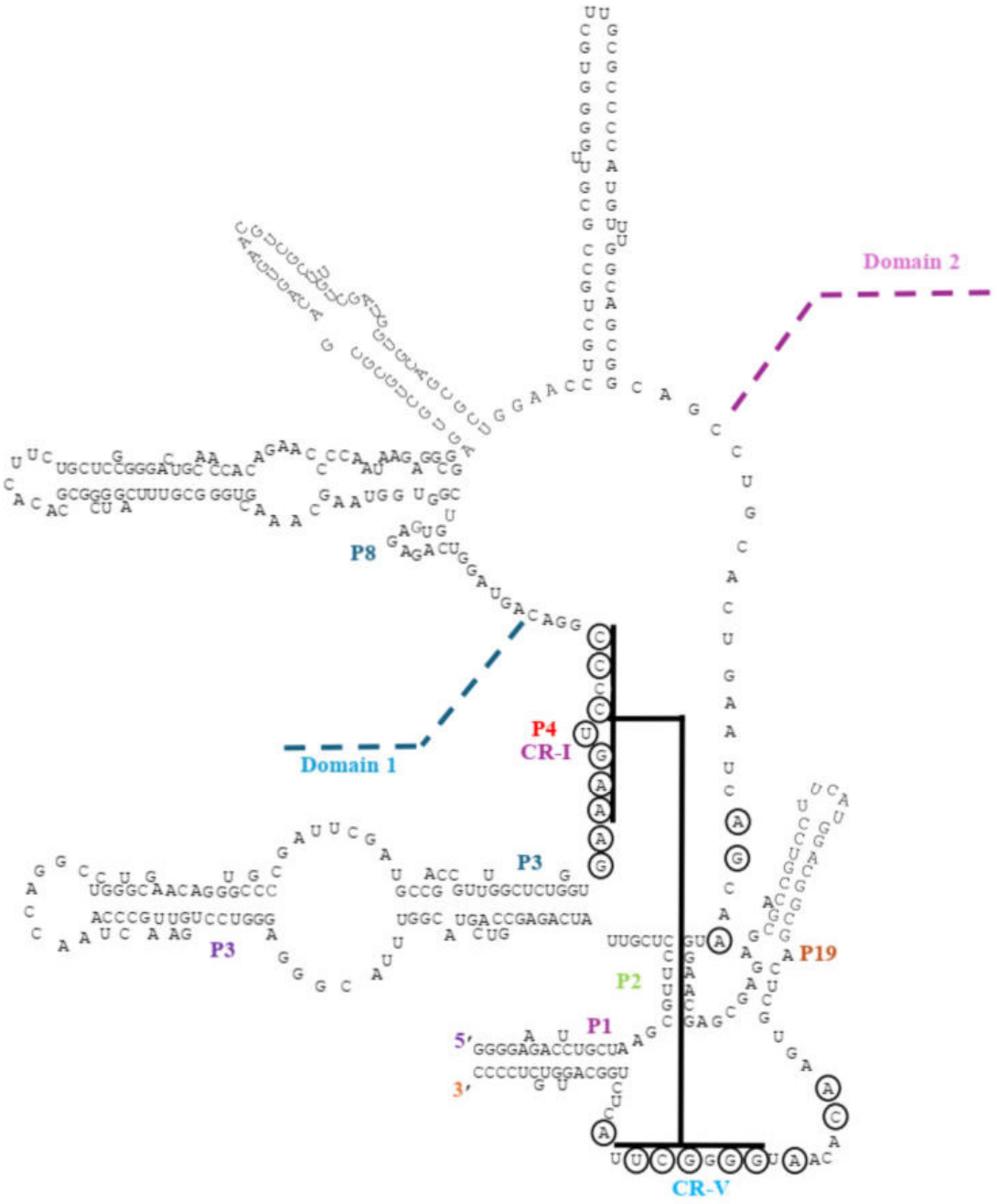

Figure 4.5: Predicted secondary structure of *C. merolae* RNase MRP RNA. The structure was generated based on sequence alignments with RNase MRP RNAs from *Drosophila melanogaster*, *Saccharomyces cerevisiae*, and *Chlamydomonas reinhardtii*. Conserved regions, including the P1, P2, and P3 helices, as well as the CR-I, CR-IV, and CR-V regions, are highlighted. The P4 helix, formed by the pairing of elements from the CR-I and CR-V regions, is also depicted.

4.3.2 Identification of Protein Constituents of the RNase MRP Complex

Having predicted the structure of *C. merolae* RNase MRP RNA, I sought a more complete picture of the *C. merolae* MRP particle by identifying the corresponding protein constituents of RNase MRP. I used PSI-BLAST and reciprocal BLAST searches to identify homologs of the known protein subunits of RNase MRP from various organisms. I predicted the protein constituents of the *C. merolae* RNase MRP complex based on what has been found in *Saccharomyces cerevisiae*, *Homo sapiens*, *Chlamydomonas reinhardtii,* and *Drosophila melanogaster* as shown below (Table 4.1).

Table 4.1: Predicted Protein Constituents of RNase MRP in *Cyanidioschyzon merolae* Identified Through Comparative Genomic Analysis.

***S. cerevisiae* MRP Proteins**	***S. cerevisiae* Protein Length (aa)**	***C.merolae* Gene**	**Best Hit (BH)**	***C.merolae* Protein Length (aa)**	**Query Cover (QC) - %**	**% ID**	**E-value**	**Reciprocal Best Hit (RBH)**
POP1	875	CMR143C	+	920	23	30	2e-08	+
POP3	195	-	-	-	-	-	-	-
POP4	279	CMG096C	+	282	46	26	3e-08	+
POP5	173	CMO008C	+	194	54	25	0.018	+
POP6	158	-	-	-	-	-	-	-
POP7	140	-	-	-	-	-	-	-
POP8	133	-	-	-	-	-	-	-
SNM1	198	-	-	-	-	-	-	-
RMP1	201	-	-	-	-	-	-	-
RPP1/p30	293	CMM152C	+	298	67	26	2e-09	+
RPR2	144	CMI187C	+	163	70	20	3e-18	+

aa = Amino acids + = Present - = Absent e = 10^

In comparing the RNase MRP protein constituents between *Saccharomyces cerevisiae* and *Cyanidioschyzon merolae*, I observed that only five of the eleven proteins in *S. cerevisiae* have homologs in *C. merolae*. These homologous proteins vary in their degree of conservation based

on amino acid length, query coverage (QC), E-value, and percentage identity. POP1, although showing similar amino acid lengths (920 in *C. merolae* vs. 875 in *S. cerevisiae*), POP1 has relatively low query coverage (23%), an E-value of 2×10^{-8}, and a percentage identity of 30%. This suggests that while the overall length is comparable, the protein is less conserved in terms of sequence similarity, indicating functional divergence. POP4 has a query coverage of 46%, an E-value of 3×10^{-8}, and a percentage identity of 26%. With nearly identical lengths (282 vs. 279 amino acids), this suggests moderate conservation, but the lower percentage identity indicates some sequence variability. POP5, with 54% query coverage, an E-value of 0.018, and a percentage identity of 25%, shows moderate conservation, though the length of the protein in *C. merolae* (194) is slightly longer than in *S. cerevisiae* (173). The higher E-value and lower identity indicate that POP5 may have diverged more than others. RPP1, showing 67% query coverage, an E-value of 2×10^{-9}, and a percentage identity of 26%, is highly conserved in terms of length (298 vs. 293), with relatively higher conservation overall compared to POP5. RPR2 is the most conserved protein of the five, with 70% query coverage, the lowest E-value (3×10^{-18}), and a percentage identity of 20%. Despite the lower identity percentage, the close similarity in length (163 vs. 144) and the high query coverage indicate that RPR2 retains a highly conserved structure. In conclusion, RPR2 and RPP1 are the most conserved based on query coverage, E-value, and amino acid length, with RPR2 showing particularly strong structural conservation. POP1, despite its similar length, has the lowest conservation based on sequence similarity and query coverage, making it the least conserved of the group.

4.4. Discussion

I was surprised to observe the presence of stably-expressed, non-coding RNAs in the introns of *C. merolae*, and particularly their apparent accumulation in response to heat stress. To investigate their function, I sought to investigate the identity of that from the gene CMK142T.

The comparative genomic and computational analyses carried out in this study reveal the conservation of RNase MRP RNA and proteins in *C. merolae*. By aligning the predicted secondary structure of C. *merolae* RNase MRP RNA with those from other well-characterized organisms, including *Saccharomyces cerevisiae*, *Homo sapiens*, *Drosophila melanogaster*, and *Chlamydomonas reinhardtii*, I observed that key structural motifs, particularly those within Domain 1, are conserved across these species (Figure 4.1 to Figure 4.4).

The sequence alignments of *C. merolae* RNase MRP RNA with those of *Drosophila melanogaster*, *Saccharomyces cerevisiae*, and *Chlamydomonas reinhardtii*, is evidence that certain structural motifs and conserved regions are maintained across these diverse species. The alignment results consistently demonstrate the preservation of key elements, such as the P1, P2, and P3 helices, as well as the CR-I, CR-IV, and CR-V regions, which are integral to the RNase MRP RNA's function. These conserved motifs not only highlight the evolutionary significance of these regions but also provide insights into the structural stability and functional integrity of the RNase MRP complex across different organisms.

The consistent observation of these conserved regions across multiple species justifies the prediction of the secondary structure of *C. merolae* RNase MRP RNA (Figure 4.5). The predicted structure, grounded in both computational models and comparative genomic data, aims to reflect the conserved structural motifs identified in these alignments. This suggests that the

catalytic core and the RNA processing function of RNase MRP have been maintained through evolution, which is indicative of their essential role in cellular processes.

However, the identification of protein constituents reveals a notable divergence in the complexity of the RNase MRP complex in *C. merolae*. While the well-studied RNase MRP in *S. cerevisiae* comprises 11 protein subunits (Piccinelli *et al*., 2005; Rosenblad et al., 2006; Lopez *et al*. 2009), the complex in *C. merolae* appears to be composed of only five (5) proteins. This reduction in protein constituents may reflect adaptations specific to *C. merolae*, possibly due to its minimalistic genome and the specialized environment in which it thrives. The retention of the core proteins POP1, POP4, POP5, RPP1, and RPR2 highlights their likely important roles in the assembly and function of the RNase MRP complex in this red alga.

These findings underscore the balance between conservation and adaptation within the RNase MRP complex, emphasizing the potential for functional diversity even among conserved molecular machines. Further experimental validation of these computational predictions is necessary to elucidate the precise roles of these protein subunits and to understand how the reduced complexity of RNase MRP in *C. merolae* affects its functionality.

Chapter 5 - Mutational analysis of the RNA component of *C. merolae* RNase MRP Reveals a Shift in the Stoichiometry of the Two Forms of 5.8S rRNA

5.1 Introduction

I conducted a mutational analysis of the RNA component of *C. merolae* RNase MRP to elucidate its function and impact on rRNA processing. To achieve this, I employed two distinct methodologies: direct gene replacement and plasmid shuffling. In the former, I directly replaced the WT MRP with a mutant MRP via homologous recombination while the latter involved generating an MRP deletion strain covered by a counter-selectable plasmid with WT MRP. Upon transforming a second plasmid with a mutant MRP, the WT can be "shuffled" out by counter-selection.

In *Saccharomyces cerevisiae*, the RNase MRP RNA, encoded by the essential gene *NME1*, had been extensively mutagenized to provide insights into its structure and functions. Researchers employed a gene shuffle technique to create yeast strains expressing 26 independent mutations in the *NME1* gene. These strains were characterized based on their growth at various temperatures, their ability to utilize different carbon sources, the stability of RNase MRP RNA, and the efficiency of 5.8S rRNA processing (Shadel *et al*., 2000). This detailed analysis revealed that 11 mutations were lethal, six exhibited temperature-sensitive lethality, and several mutants displayed a preference for non-fermentable carbon sources (Table 5.1). Importantly, the severity of growth defects in these mutants correlated directly with the extent of disruption in 5.8S rRNA processing (Figure 5.1), thereby identifying the essential regions of RNase MRP RNA for its nuclear function. My investigation in *C. merolae* mirrors the approach used in yeast, offering a perspective on the conserved roles of RNase MRP across species. Specifically, I tried three mutations but was able to examine the effects of two mutations (highlighted in green in Table 5.1) of the RNA component of *C. merolae* RNase MRP on the stoichiometry of the two forms of 5.8S rRNA and assessed the overall stability of RNase MRP RNA. By juxtaposing our results

with those obtained in yeast, we aim to demonstrate that *C. merolae* MRP has a similar function to yeast MRP in regulating the balance of the two forms of 5.8S rRNA.

Table 5.1. Summary of *NME1* Mutagenesis Data

Name	Change	1 Growth phenotype (°C) (dextrose/glycerol)				2 $5.8S_S$/ $5.8S_L$ ra	3 RNA stability
		17	20	30	37		
NME1	none	4	4	4	4	10/1	4
No phenotype							
nme1-14	Δ4–8	4	4	4	4	10/1	4
nme1-16	Δ194–205	4	4	4	4	10/1	4
nme1-17	Δ186–210	3	4	4	4	10/1	4
nme1-19	Δ170–173	4	4	4	4	10/1	4
nme1-4	Δ328–335	4	4	4	4	10/1	4
nme1-5	U90G, C91A	4	4	4	4	10/1	4
nme1-3.2	Δ2–6	3	3	4	4	10/1	3
nme1-3/4	Δ2–6, Δ328–335	3	3	4	4	10/1	4
Lethal phenotype							
nme1-1	Δ124–148	0	0	0	0	10/1	4
nme1-6	Δ174–215	0	0	0	0	10/1	2
nme1-7	Δ36–68	0	0	0	0	10/1	1
nme1-10	Δ98–111	0	0	0	0	10/1	2
nme1-13	UCC 90→92 AUG	0	0	0	0	10/1	
nme1-20	Δ2–6, Δ170–173	0	0	0	0	10/1	
nme1-Δ20	Δ97–147	0	0	0	0	10/1	4
nme1-33	Δ304–339 + 80 bp 3′	0	0	0	0	10/1	4
nme1-53	Δ150–174	0	0	0	0	10/1	2
nme1-145	Δ310–311	0	0	0	0	10/1	
nme1-147	Δ310–313	0	0	0	0	10/1	
Conditional phenotypes							
nme1-2	Δ237–252	4	4	4	0/1	1/8	4
nme1-P6	G122A	3	2	1	0	1/10	4
nme1-8	CCATGA 4→9 GACGTC	2	2	3	0	10/1	2
nme1-mtProc	Δ55–66 VAATAATATTCTT	1	3	3	3	10/1	4
nme1-3.1	Δ2–6, C279G	2/2	2/2	4/4	3/0	3/2	1
nme1-11	Δ45–64	0/1	1	3	2	1/1	4
nme1-12	Δ277–298	0/2	0/2	0/2	0/1	1/10	4

The table summarizes the mutagenesis data for individual NME1 mutants, with each mutant listed on the left. The specific base changes are identified, with numbering corresponding to the position within the NME1 transcript (Schmitt and Clayton, 1992). [1]Growth phenotypes are scored on a scale from 0 to 4, where 0 indicates no growth and 4 represents wild-type growth. When two numbers are provided, they reflect growth on dextrose alone or dextrose and glycerol. [2] The ratios of 5.8S rRNA were measured from ethidium bromide-stained gels and represent steady-state levels. [3] RNA stability is also quantified on a scale from 0 to 4, with 0 indicating no detectable RNA and 4 corresponding to wild-type RNA levels (Shadel et al., 2000).

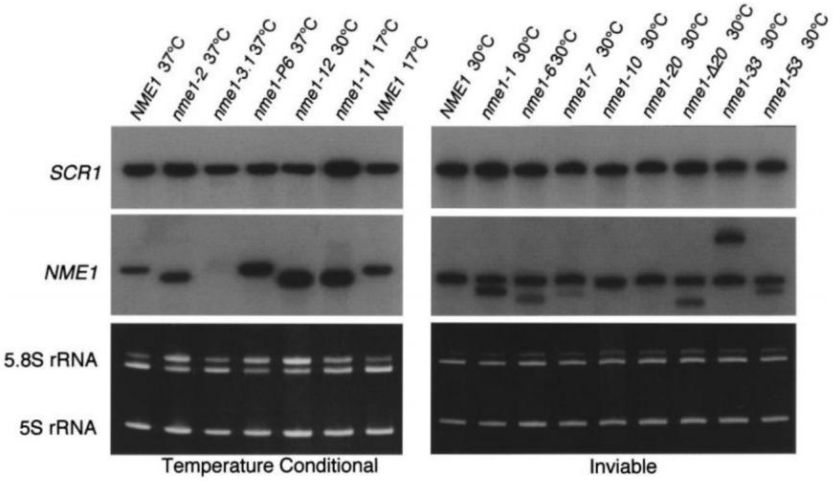

Figure 5.1. *NME1* mutation results in altered 5.8S rRNA isoform ratio. (top) present Northern blot analyses for the indicated *NME1* mutants, using an *NME1* probe to detect MRP RNA and an *SCR1* probe as a control for RNA loading levels. (bottom) display ethidium bromide-stained agarose gels, highlighting the 5.8S rRNA profiles for each mutant. For temperature-sensitive mutants, RNA was harvested after shifting to the non-permissive temperature. Inviable mutants were maintained with a wild-type copy of the *NME1* gene (Shadel et al.,2000).

5.2 Materials and Methods.

5.2.1 Construction of Plasmid for Mutagenesis

To generate a plasmid for mutagenesis, I employed a systematic approach involving sequential restriction digests, gel electrophoresis, oligonucleotide duplex formation, ligation, and cloning. This procedure was executed in two distinct phases (Figures 5.2 and 5.3).

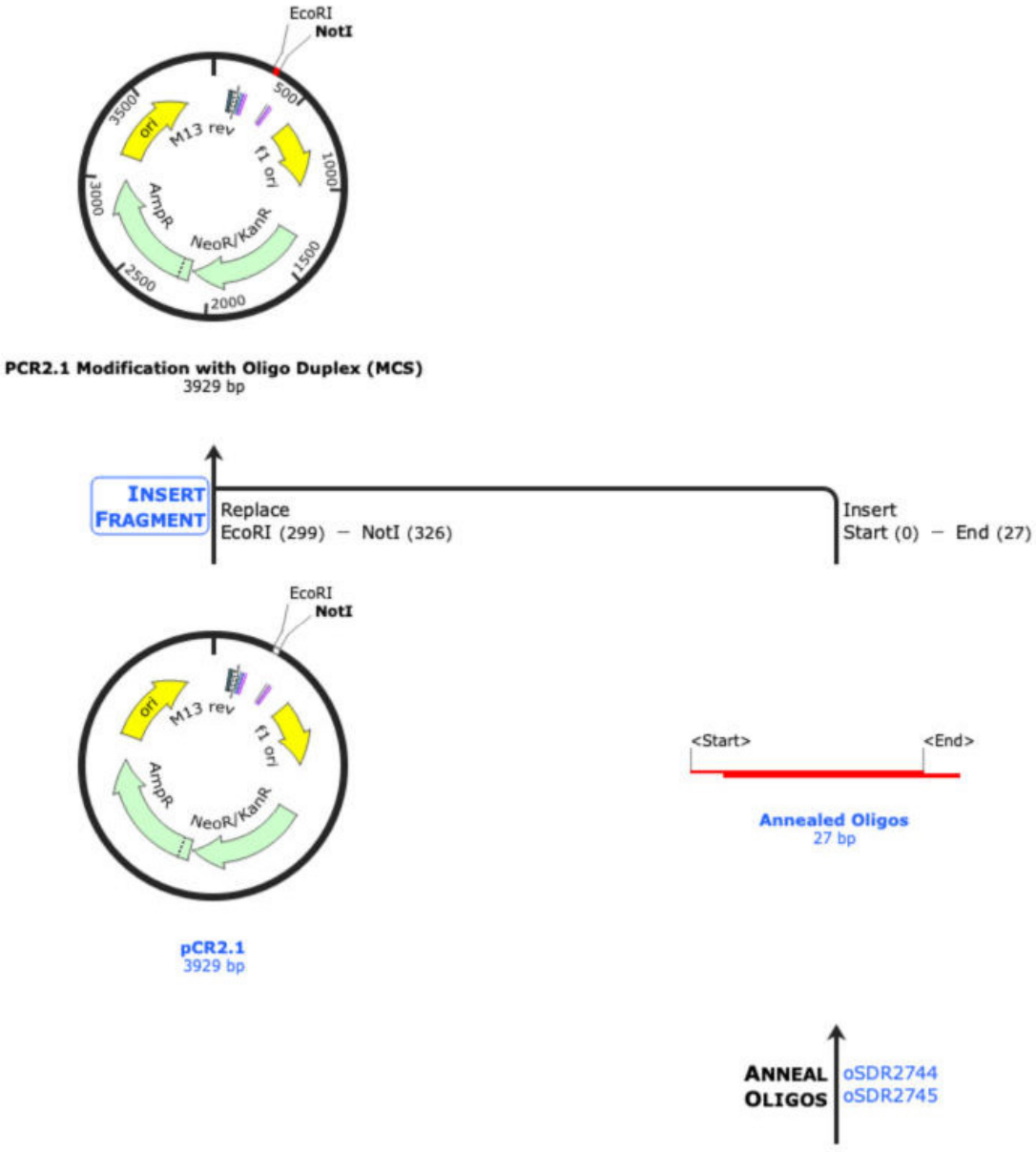

Figure 5.2. Modification of PCR2.1 with Multiple Cloning Sites. Arrows indicate the directionality of the workflow, starting from the bottom of the figure.

To obtain a backbone vector for subsequent procedures, a restriction digest was performed. The reaction mixture included 3,000 ng of the pCR2.1 plasmid, 1X CutSmart Buffer (New England Biolabs), and the restriction enzymes EcoRI and NotI, totaling 30 µL. This mixture was incubated at 37 C for 60 minutes. The backbone fragment of interest from the digested pCR2.1 was purified using the E.Z.N.A. Gel Extraction Kit (Omega Bio-tek).

To prepare the oligonucleotide duplex, 50 pmoles of each oligo, oSDR2744 and oSDR2745 (see Table 5.2), were combined from 5 µL of 10 µM solutions of each oligo. The mixture was supplemented with 0.5 µL of 1 M KCl and subjected to a heat denaturation step at 65 C for 5 minutes. Following heating, the mixture was allowed to cool gradually to room temperature for 20 minutes. The resulting oligonucleotide duplex, with a concentration of 5 µM, was then diluted 1:100 in water to achieve a final concentration of 50 nM, equivalent to 50 fmol/µL.

To introduce a customized multiple cloning site (MCS) into the prepared backbone vector, a ligation reaction was conducted. The reaction mixture comprised 1X T4 DNA Ligase Buffer (New England Biolabs), 1X T4 DNA Ligase, 73 ng of the pCR2.1 backbone fragment, and 50 fmol of the MCS duplex in a total volume of 10 µL. The mixture was incubated at room temperature for 15 minutes. Subsequently, half of the ligation reaction was added to 50 µL of DH5α competent *E. coli* cells that had been thawed on ice. The cells were then incubated on ice for 30 minutes, heat-shocked at 42 C for 45 seconds, and returned to ice for 2 minutes. The cells were then mixed with 150 µL of LB medium, plated onto LB-agar plates containing carbenicillin, and incubated overnight at 37 C.

Following incubation, four colonies were selected for inoculation into LB medium containing 100 µg/mL ampicillin for overnight growth in a shaker at 300 rpm and 37 C. Plasmid DNA was

isolated from each bacterial culture using the E.Z.N.A. Plasmid DNA Mini Kit I (Omega Bio-tek). To verify the presence of the insert, I performed an RE digest using PmeI and AgeI.

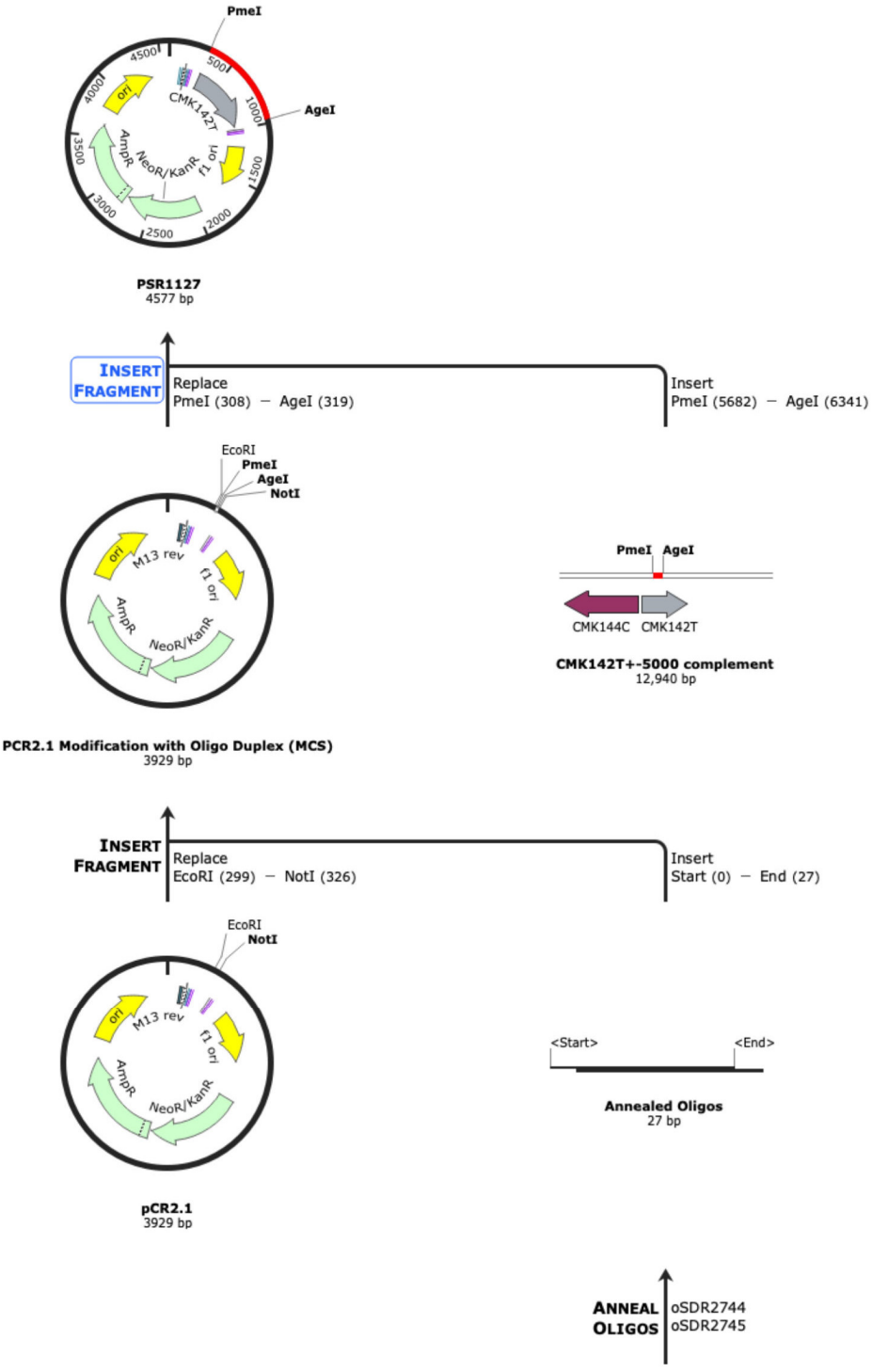

Figure 5.3. ***Introduction of CMK142 Region into the Modified pCR 2.1 Vector for Mutagenesis***. Arrows indicate the directionality of the workflow, starting from the bottom of the figure.

To generate the CMK142 insert DNA, PCR amplification was conducted using Q5 High-Fidelity DNA Polymerase (New England Biolabs). The reaction mixture included 1X Q5 Reaction Buffer, 200 µM dNTPs, 0.5 µM each of primers oSDR2307 and FUB94 (Table 5.2), 5 ng of *Cyanidioschyzon merolae* wild-type genomic DNA as the template, and 1 U of Q5 High-Fidelity DNA Polymerase, with a final volume of 50 µL. Thermocycling conditions were as follows: an initial denaturation at 98 C for 30 seconds, followed by 35 cycles of denaturation at 98 C for 5 seconds, annealing at 66 C for 20 seconds, and extension at 72 C for 30 seconds, with a final extension at 72 C for 2 minutes.

Restriction digests of both the purified insert DNA (200ng) and the modified pCR2.1 vector (designated PSR1126, 2 µg) were performed with PmeI-HF and AgeI-HF, and purified using the E.Z.N.A. Gel Extraction Kit (Omega Bio-tek). The K142 insert was ligated into the vector

and confirmed by RE digest using Pme1 and Age1.

5.2.2 Construction of Knockout Plasmid

To generate a knockout plasmid via molecular cloning to knock out the endogenous CMK142T in an attempt to establish a plasmid shuffling system in *C. merolae*, I employed a systematic approach involving sequential restriction digests, gel electrophoresis, ligation, and cloning. This procedure was executed in two distinct phases (Figures 5.4 and 5.5).

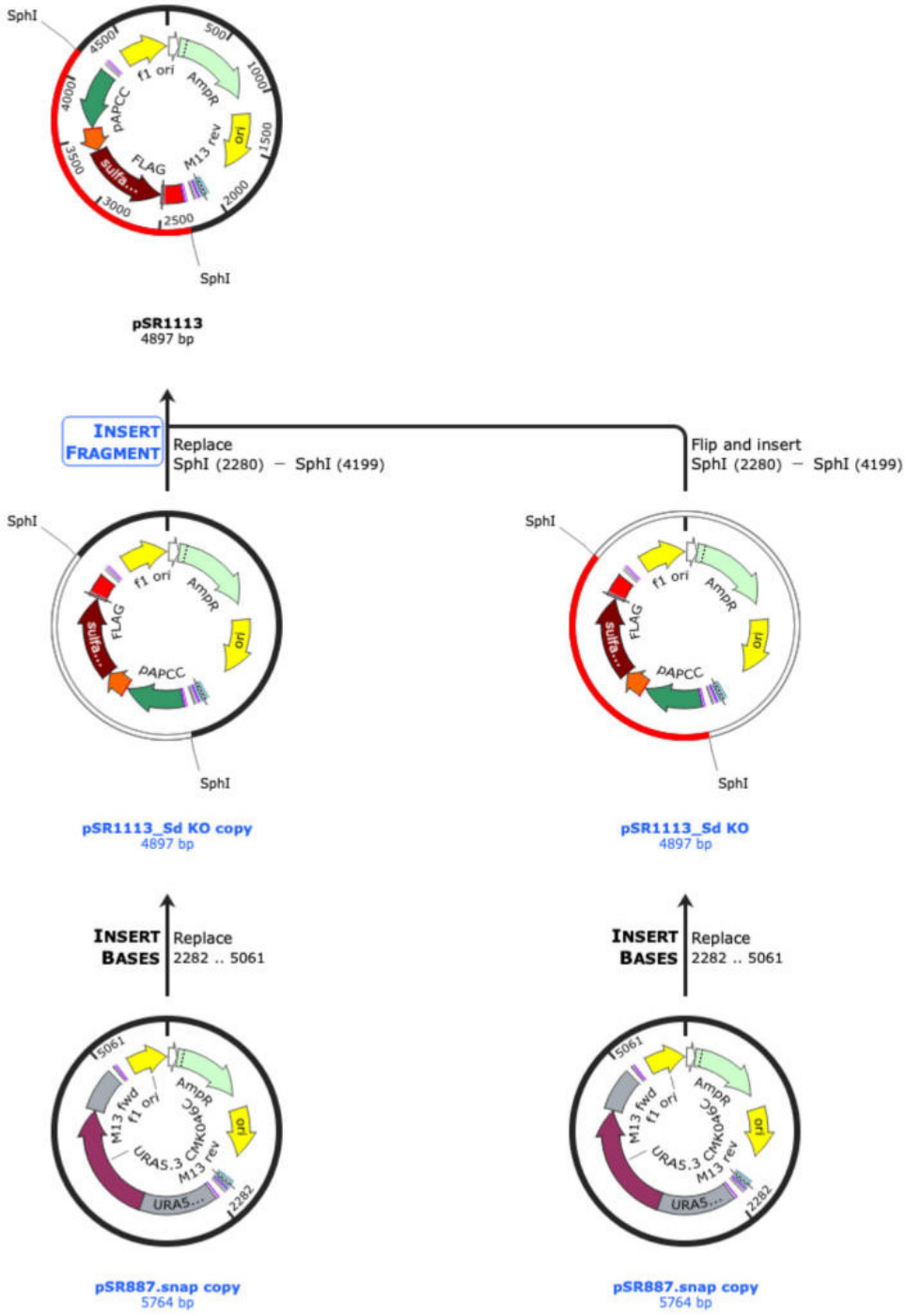

Figure 5.4. Construction of PSR1113 Vector with a Sulfadiazine Marker. Arrows indicate the directionality of the workflow, starting from the bottom of the figure.

To obtain a backbone vector for subsequent steps, a restriction digest was carried out, the reaction mixture comprised 1X CutSmart Buffer (New England Biolabs), 2,000 ng of PSR887, SphI-HF, in a final volume of 30 µL. The digestion was incubated at 37 C for 1 hour. This was done to remove the URA5.3 marker in PSR887.

To generate the sulfadiazine marker, PCR amplification was conducted using Q5 High-Fidelity DNA Polymerase (New England Biolabs) as described in section 5.2.1 using 0.5 µM each of primers oSDR2743 and oSDR2744 (Table 5.2), and 5 ng of PSR1052 as the template. Thermocycling conditions were the same as described in 5.2.1, annealing at 65 C for 20 seconds, and extension at 72 C for 39 seconds. Dephosphorylation of the restriction-digested pSR887 backbone plasmid was performed in a reaction mixture that contained 1X Shrimp Alkaline Phosphatase Buffer (Promega), 405 ng of linearized pSR887, and 1 U of Shrimp Alkaline Phosphatase in a total volume of 50 µl that was incubated at 37 C for 15 min followed by inactivation of the enzyme at 65 C for 15 min. The insert DNA was ligated into the SAP-treated PSR887 vector, transformed 50 µL of DH5α competent *E. coli* cells as described in section 5.2.1, and confirmed by RE digest using BamH1 and Spe1.

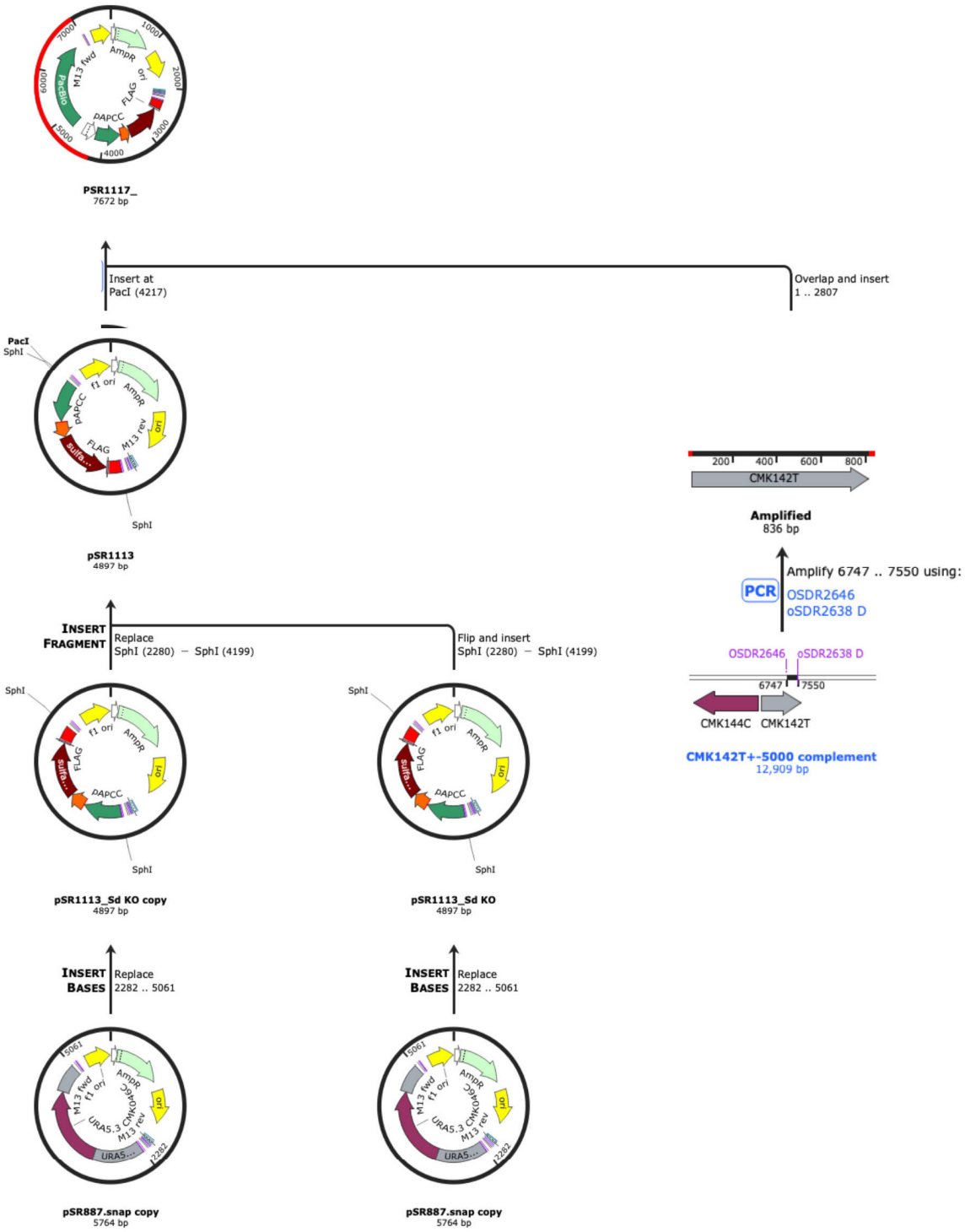

Figure 5.5. Introducing CMK142 Homology Arms into PSR1113. Arrows indicate the directionality of the workflow, starting from the bottom of the figure.

For the preparation of the LIC vector, 500 ng of vector DNA; PSR1113 (250 fmol) was digested with either 0.5 µL of PacI in a 10 µL reaction containing 1X CutSmart Buffer at 37 C for 3 hours, or with 0.5 µL of SwaI in a 10 µL reaction containing 1X NEB Buffer 3.1 at 25 C for 3 hours. Following digestion, the reaction was heat-inactivated at 65 C for 20 minutes. Half of the digested product was treated with T4 DNA polymerase (NEB) for 30 minutes at 22 C in a mixture containing 0.5 µL of 10X CutSmart Buffer, 0.5 µL of 100 mM DTT, 0.5 µL of 50 mM dCTP (for PacI) or dGTP (for SwaI), 0.4 µL of T4 DNA polymerase, and 3.1 µL of water. The enzyme was then inactivated by heating at 75 C for 20 minutes. PCR amplification was conducted using Q5 High-Fidelity DNA Polymerase (New England Biolabs) to generate the insert DNA. The reaction mixture included 1X Q5 Reaction Buffer, 200 µM dNTPs, 0.5 µM of each set of primers oSDR2646/oSDR2638(PacI) and oSDR2647 and oSDR2648 (SwaI) (Table 5.2), 1 ng of *C. merolae* Wild-type genomic DNA as the template, and 1 U of Q5 High-Fidelity DNA Polymerase, in a final volume of 50 µL. Thermocycling conditions were the same as described in section 5.2.1, annealing at 65 C for 20 seconds, and extension at 72 C for 30 seconds (PacI) and 10 seconds (Swa1).

For the LIC PCR preparation, a 250 fmol aliquot of the PCR product was treated with T4 DNA polymerase under the same conditions as the vector digestion.

For the LIC reaction, 1 µL of the treated vector (25 ng, 10 fmol) was combined with 1 µL of the treated PCR product (25 fmol) and incubated at room temperature for 5 minutes, transformed 50 µL of DH5α competent *E. coli* cells as described in section 5.2.1 and confirmed by RE digest using BamH1 and Spe1.

5.2.3 Construction of Transient and Integrable Plasmids

The construction of transient and integrable plasmids was achieved through the generation of three distinct plasmids, each serving a specific purpose. Two transient plasmids were developed, each incorporating a different selectable marker - URA5.3 and Chloramphenicol Acetyl Transferase (CAT) - to facilitate the plasmid shuffling technique. Additionally, one integrable plasmid was constructed to carry the targeted mutations required for the direct replacement method. This process was executed in three distinct phases.

For Phase I and II (Figures 5.6 and 5.7 respectively), preparation of the Pac1 LIC vector was performed as described in Section 5.2.2. PCR amplification was conducted using Q5 High-Fidelity DNA Polymerase (New England Biolabs), with 0.5 µM of each primer (oSDR2645 and oSDR2637; Table 5.2) and 1 ng of *Cyanidioschyzon merolae* wild-type genomic DNA as the template, as outlined in Section 5.2.1.

The thermocycling conditions were the same as described in Section 5.2.1, except for the annealing temperature of 68 C for 20 seconds and an extension step at 72 C for 56 seconds.

The LIC reaction was then performed as outlined in Section 5.2.2. The LIC product was used to transform *DH5α* competent *E. coli* cells as detailed in Section 5.2.1 and confirmed by RE digest using XbaI for the URA plasmid and BamH1 for the CAT plasmid.

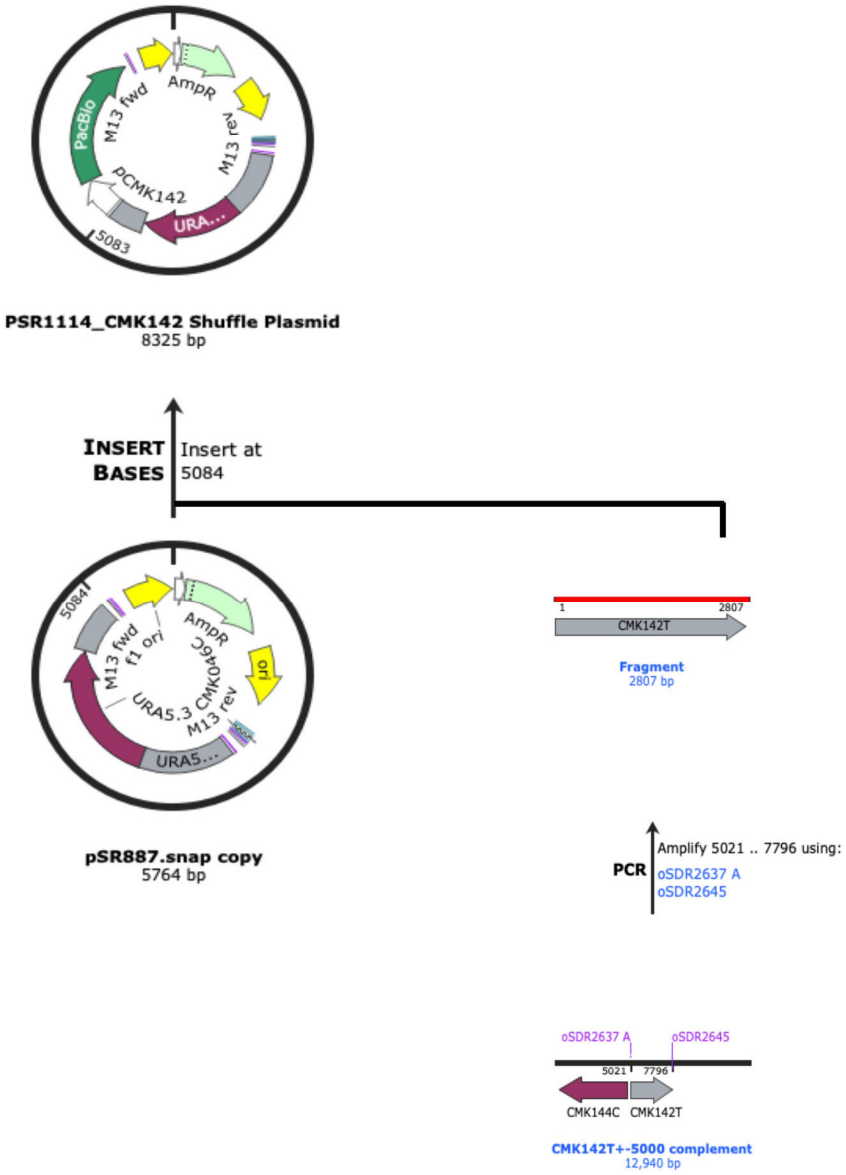

Figure 5.6 Introducing CMK142 region into the PacI site of PSR887. Arrows indicate the directionality of the workflow, starting from the bottom of the figure.

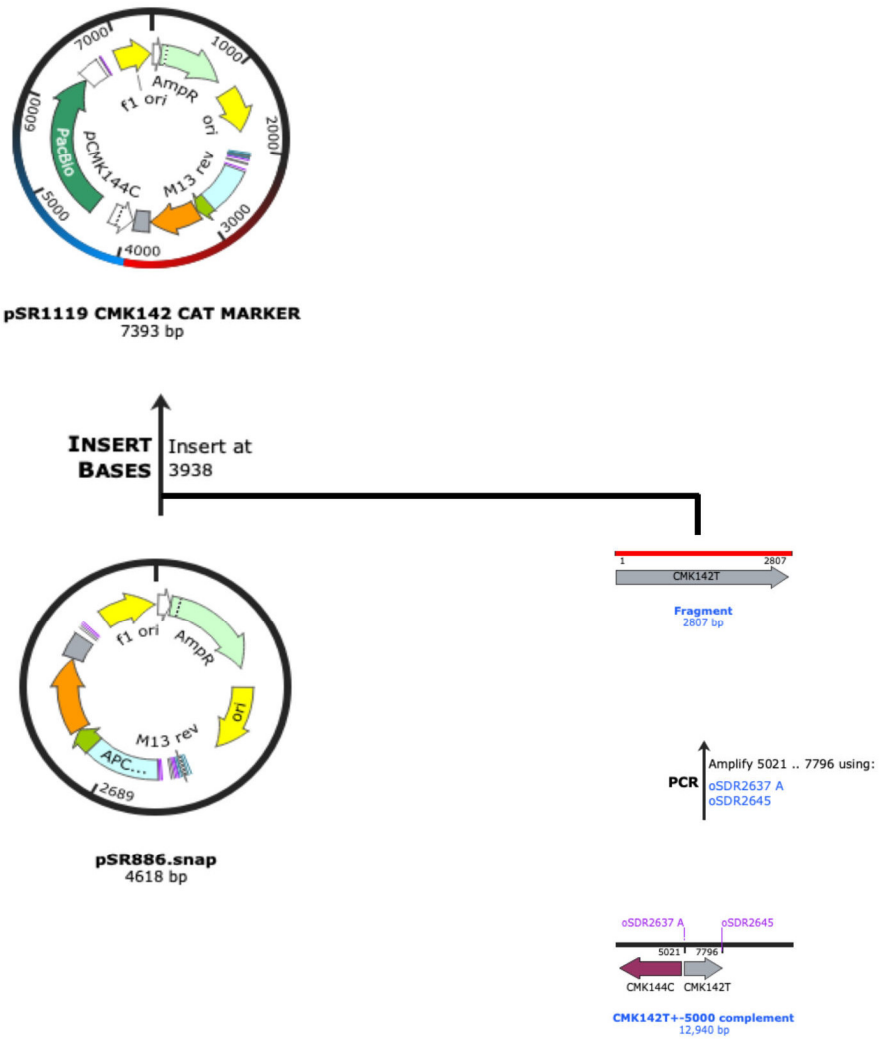

Figure 5.7 Introducing CMK142 region into the PacI site of PSR886. Arrows indicate the directionality of the workflow, starting from the bottom of the figure.

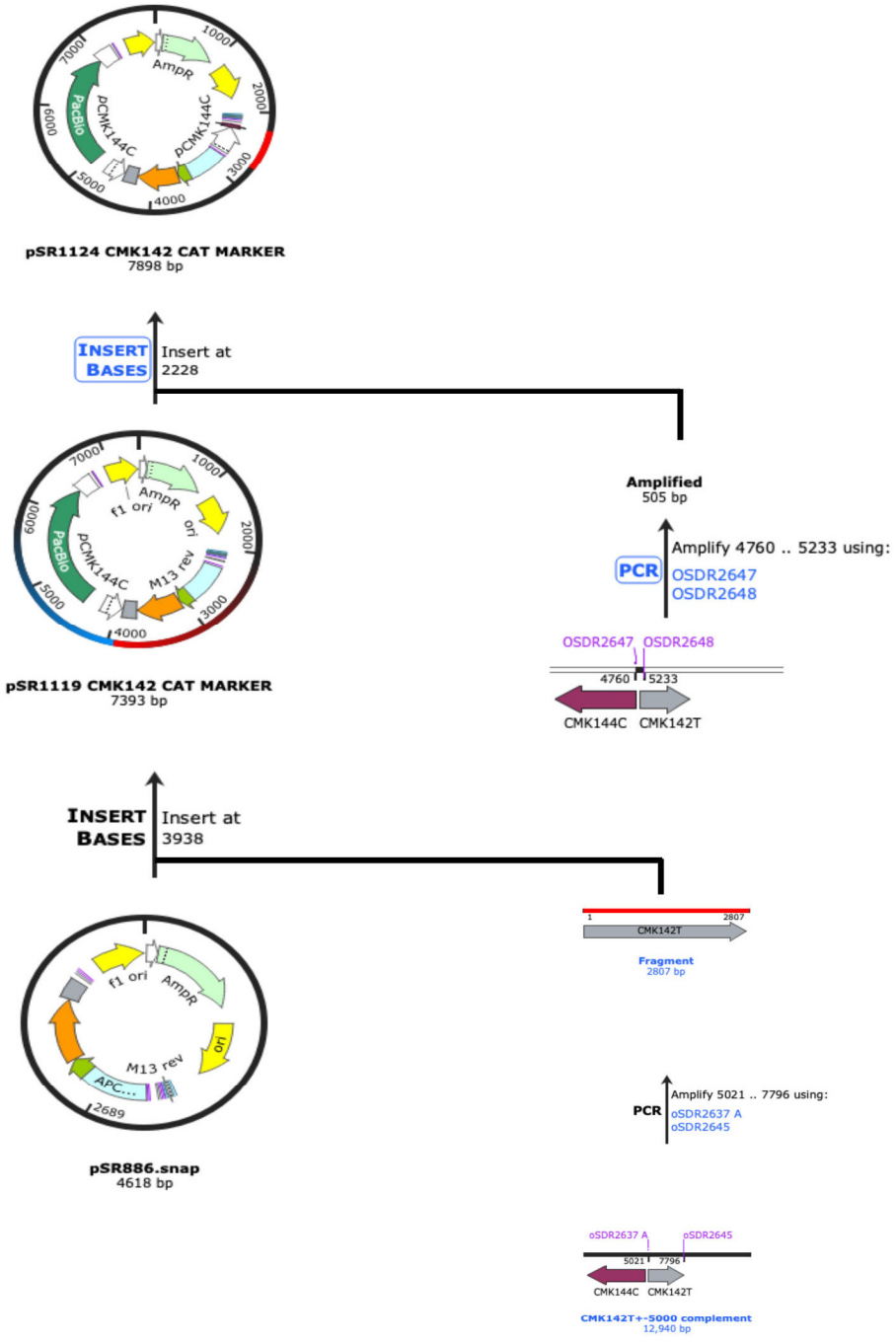

Figure 5.8 Introducing a second homology arm into the SwaI site of PSR1119. Arrows indicate the directionality of the workflow, starting from the bottom of the figure.

Swa1 preparation of the LIC vector (500 ng of vector DNA; PSR1119 250 fmol from phase II) was performed as described in Section 5.2.2. PCR amplification was conducted using Q5 High-

Fidelity DNA Polymerase (New England Biolabs), with 0.5 µM of each primer (oSDR2647 and oSDR2648; Table 5.2) and 1 ng of *Cyanidioschyzon merolae* wild-type genomic DNA as the template, as outlined in Section 5.2.1. The thermocycling conditions were the same as described in Section 5.2.1, except for the annealing temperature of 68 C for 20 seconds and an extension step at 72 C for 56 seconds. The LIC reaction was then performed as outlined in Section 5.2.2. The LIC product was used to transform *DH5α* competent *E. coli* cells as detailed in Section 5.2.1 and confirmed by RE Digest using XbaI for the URA plasmid and BamH1 for CAT.

5.2.4 Making of Mutant Plasmids

For the mutational analysis of the RNase MRP RNA component in *Cyanidioschyzon merolae*, I employed the "Around-the-Horn" site-directed mutagenesis technique. The primers for each set of mutations were phosphorylated using T4 polynucleotide kinase (PNK) in a reaction mix containing 10X Kinase buffer, $MgSO_4$, ATP, and PNK, followed by incubation at 37 C for 45 minutes. The reaction mixture contained 1X Q5 Reaction Buffer, 200 µM dNTPs, 0.5 µM of each set of primers oSDR2649/oSDR2650, oSDR2651/oSDR2652 and oSDR2653/oSDR2654 (Table 5.2) for Δ343 – 356, Δ372 - 405 and G162A respectively, 5 ng of PSR1127 as the template, and 1 U of Q5 High-Fidelity DNA Polymerase, in a final volume of 50 µL. Thermocycling conditions were as follows: an initial denaturation at 98 C for 30 seconds, followed by 35 cycles of denaturation at 98 C for 5 seconds, annealing at 63 C for 20 seconds, and extension at 72 C for 2.17 minutes, with a final extension at 72 C for 2 minutes. The PCR product was treated with DpnI to digest the template plasmid, and the desired PCR product was purified with the E.Z.N.A. Cycle Pure Kit (Omega Bio-tek). A ligation reaction was conducted. The reaction mixture comprised 1X T4 DNA Ligase Buffer (New England Biolabs), 1X T4 DNA Ligase (Blunt), and 91 ng of DpnI-treated PCR Product in a total volume of 10 µL. The

mixture was incubated at room temperature for 15 minutes, transformed 50 µL of DH5α competent *E. coli* cells, and inoculated on an LB medium as described in section 5.2.1.

Whether or not my plasmid contained the mutations was initially determined by performing a colony PCR on both the wild-type (PSR1127) and the mutants, assessing whether the size of the PCR products corresponded to the expected mutant size or the size of the unedited PSR1127 plasmid. PCR was performed using *Taq* DNA Polymerase with Standard *Taq* Buffer (New England Biolabs) and a DNA Engine Dyad Peltier Thermal Cycler (Bio-Rad Laboratories). Each reaction mixture contained 1X Standard *Taq* Reaction Buffer, 200 µM dNTPs, 0.5 µM of each primer (FuB 146 and FuB147 in Table 5.2), 2ng of template DNA (either wild-type PSR1127 or mutants), and 1 U of *Taq* DNA Polymerase in a total volume of 20 µl. Thermocycling conditions consisted of an initial denaturation at 95 C for 5 min, 35 cycles of denaturation at 95 C for 20 sec, annealing at 58 C for 20 sec, and extension at 68 C for 1 min, followed by a final extension at 68 C for 5 min. The PCR products were run alongside a 100 bp DNA Ladder (New England Biolabs) on a 2% agarose gel containing ethidium bromide at 150 V for 60 minutes and visualized using a Gel Doc imaging system. After initial confirmation of successful mutations, samples were sent to sequence at the Eurofins SimpleSeq Facility using the primer oSDR1445 (Table 5.2).

5.2.5 Inserting Mutated Regions from PSR1127 into Integrable Plasmids

Following sequencing and validation of the mutations in PSR1127, the resulting mutated region of interest was excised and inserted into integrable plasmids for transformation into *C. merolae.* Each restriction digest reaction mixture contained 1X CutSmart Buffer (New England Biolabs), 3,000 ng of plasmid DNA (either mutated PSR1127/PSR1127b or PSR1124), and PmeI-HF and AgeI-HF in a total volume of 30 µl. The reactions were incubated at 37 C for 60 minutes. After digestion, the 7,239-bp backbone from PSR1124 and the respective insert from the digested mutant plasmids (636-bp from PSR1127 and 669-bp from PSR1127b) were purified using the E.Z.N.A. Gel Extraction Kit (Omega Bio-tek). Ligation reaction and transformation of DH5α competent *E. coli* cells was performed as described in section 5.2.1 using 80 ng of vector DNA, and 68 ng of the inserts in a total volume of 10 µL. BamHI RE digest was used to verify plasmids (Figures 5.9 and 5.10).

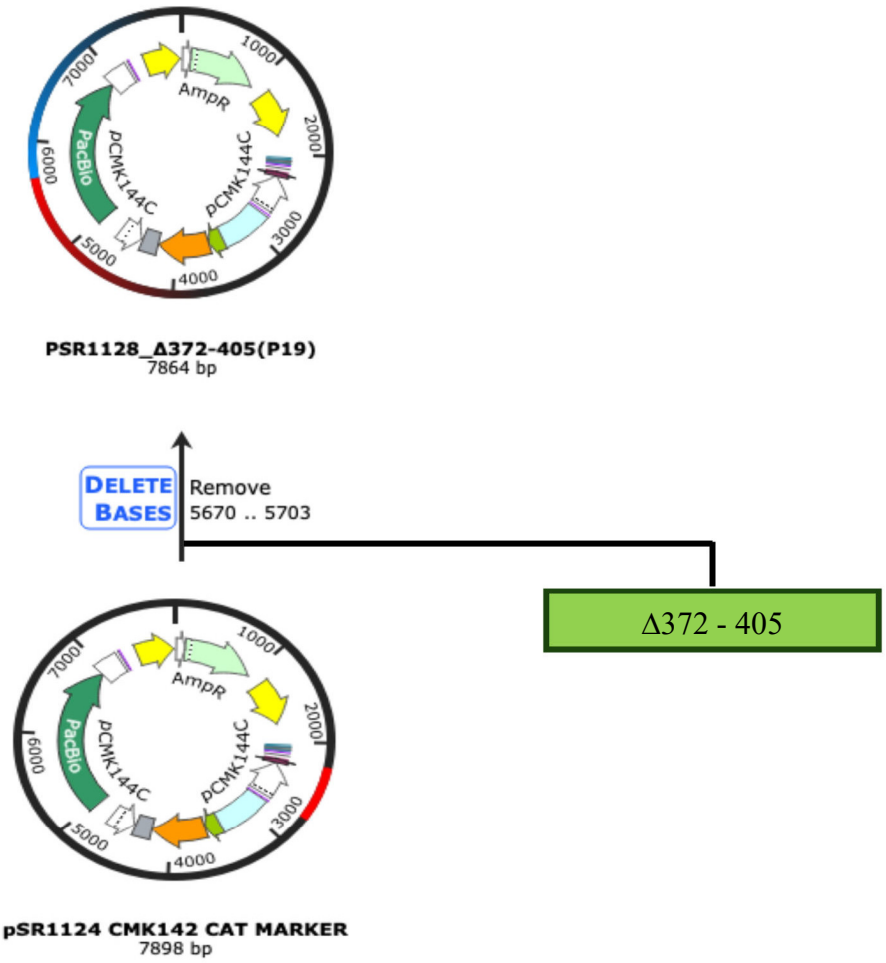

Figure 5.9 Introducing a Δ372 - 405 *mutant into* PSR1124 to generate PSR1128. Arrows indicate the directionality of the workflow, starting from the bottom of the figure.

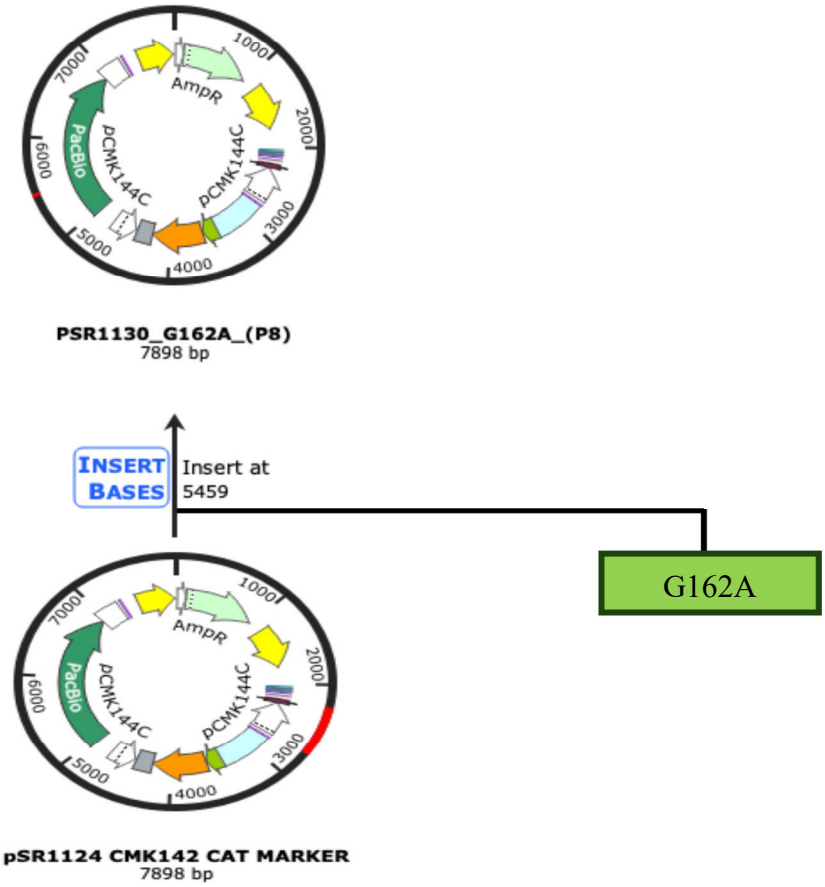

Figure 5.10 Introducing a G162A *mutant into* PSR1124 to generate PSR1130. Arrows indicate the directionality of the workflow, starting from the bottom of the figure.

To generate the original linear DNA vector for the transformation of *Cyanidioschyzon merolae*, PCR was carried out using Q5 High-Fidelity DNA Polymerase (New England Biolabs) and a DNA Engine Dyad Peltier Thermal Cycler (Bio-Rad Laboratories). Each PCR mixture contained 1X Q5 Reaction Buffer, 200 µM dNTPs, 0.5 µM of each primer (oSDR2647 and oSDR2645), 5 ng of plasmid template DNA (pSR1128; figure 5.11 or pSR1130; figure 5.12), and 1 U of Q5 High-Fidelity DNA Polymerase in a total volume of 50 µL.

The thermocycling conditions were as follows: initial denaturation at 98 C for 30 seconds, followed by 35 cycles of denaturation at 98 C for 5 seconds, annealing at 72 C for 20 seconds, and extension at 72 C for 1 minute and 45 seconds. A final extension step was performed at 72 C for 2 minutes. A portion of the PCR product was run alongside a 1 kb DNA Ladder (New England Biolabs) on a 0.7% agarose gel containing ethidium bromide and visualized using a Gel Doc imaging system. The remaining PCR products were purified using the E.Z.N.A. Cycle Pure Kit (Omega Bio-tek), and concentrations were measured using a NanoDrop spectrophotometer.

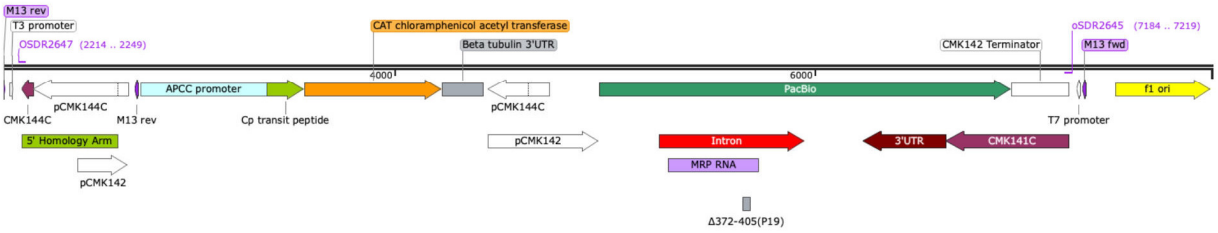

Figure 5.11 Linear transformation product amplified from PSR1128.

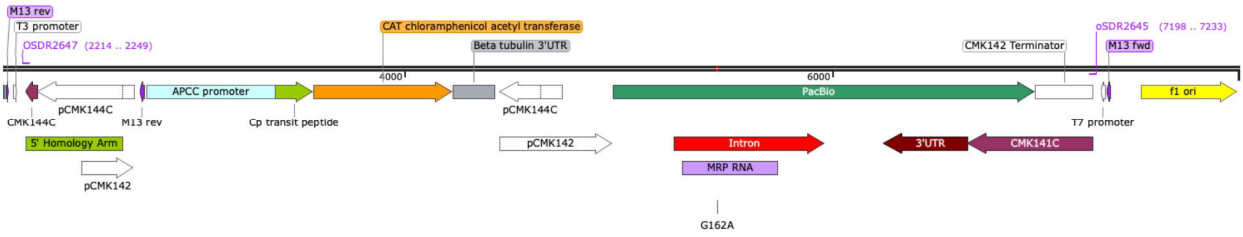

Figure 5.12 Linear transformation product amplified from PSR1130.

Table 5.2. Oligonucleotides used in the construction and sequencing of Plasmid Shuffling or Direct Replacement vectors. Primers oSDR2637, oSDR2638, oSDR2307, oSDR1445, FUB94, Fub146 and FUB147 were designed by Dr. Martha Stark.

Oligonucleotides	Directionality	Sequence (5′ to 3′)
oSDR2643	Forward	GCATGC CGACGAGAACGTATAAGGAGTG
oSDR2644	Reverse	GCATGC ACACTTTTTGCCTGCACAAGTT
oSDR2645	Reverse	ATG TTA AGT GGA TTA C GCAGGTTTTGAACGAGGTGG
oSDR2646	Forward	AGTTGAAGTATGTTACTCGTCTGTGTTTCTCTCGTGG
oSDR2647	Forward	CTTATCTCAATATTTGCAGGAGAAGACACCGCTACG
oSDR2648	Reverse	AACAATCACCAATTTGGTCATGGTGTGGTGAAACGC
oSDR2649	Forward	TCAGCAATGGAACGAGCG
oSDR2650	Reverse	CCGCTGCCAAACATGG
oSDR2651	Forward	GTGAACACAATGGGGCTTAC
oSDR2652	Reverse	GCTCGTTCCATTGCTGATTC
oSDR2653	Forward	AAGTGTCGGTGGTAAGCAAAG
oSDR2654	Reverse	TCTGACCTACTGTCCGG
oSDR2637	Forward	AGTTGA AGT ATGTTACACTAGAGACGCTTCCGTGAC
oSDR2638	Reverse	ATGTTAAGTGGATTACACCCGATTACCTTGCGTCA
oSDR2744	Forward	AATTCGTTTAAACGATATCACCGGTGC
oSDR2745	Reverse	GGCCGCACCGGTGATATCGTTTAAACG
oSDR2307	Forward	TCGGACGTGGTTAGTTGACG
oSDR1445	Reverse	GTAATACGACTCACTATAGGGCG
FUB94	Reverse	GCGATCCTGAATCTGGTCAA
FUB146	Forward	AATAAGAGCGGGAGTGCTG
FUB 147	Reverse	CCAGAGTAAGCCCCATTGTG

5.2.6 Transformation of *C. merolae*

The protocols for cultivating and transforming *Cyanidioschyzon merolae* were adapted from Kobayashi *et al*. (2010). The standard growth conditions for *C. merolae* included using either liquid MA2G media [40 mM $(NH_4)_2SO_4$, 8 mM KH_2PO_4, 4 mM $MgSO_4$, 1 mM $CaCl_2$, 184 µM H_3BO_3, 100 µM $FeCl_3$, 80 µM Na_2EDTA, 36 µM $MnCl_2$, 6.4 µM Na_2MoO_4, 3.08 µM $ZnCl_2$, 1.2 µM $CuCl_2$, 0.68 µM $CoCl_2$, 50 mM glycerol] or solid 0.75X MA2G media [with all components reduced by 25% except for glycerol, and 4.62 mg/mL Gelzan (Caisson Labs) as a gelling agent] for plating. Cultures were incubated at 42C with 2% CO_2 under continuous illumination at 90 µmol photons$\cdot m^{-2}\cdot s^{-1}$.

Three days before transformation, wild-type *C. merolae* cells were diluted in MA2G media to achieve an actively dividing culture with an $OD_{750} < 3.0$ by the day before transformation. On the day before transformation, the cells were further diluted to an $OD_{750} = 0.25\text{-}0.40$, allowing the culture to reach a target $OD_{750} = 0.8\text{-}1.0$ within one day. In preparation, two plates containing solid 0.75X MA2G media, supplemented with 250 µg/mL chloramphenicol, were poured and left to dry overnight at room temperature, then stored upside down in a plastic sleeve at 4 C.

On the day of transformation, 40 mL of cells were centrifuged at 2,000 × g for 10 minutes, washed in 1 mL of warm MA-I buffer [20 mM $(NH_4)_2SO_4$, 2 mM $MgSO_4$, 92 µM H_3BO_3, 18 µM $MnCl_2$, 3.2 µM Na_2MoO_4, 1.54 µM $ZnCl_2$, 0.6 µM $CuCl_2$, 0.34 µM $CoCl_2$], centrifuged at 2,000 × g for 12 seconds, and resuspended in a total volume of 200 µL of warm MA-I buffer. Each 25-µL aliquot of this cell suspension contained approximately $5.00\text{-}6.25 \times 10^6$ cells. For each transformation, 25 µL of cells were mixed with 100 µL of MA-I buffer containing the nucleic acids to be delivered and 60 µg of sonicated salmon sperm DNA, followed by the addition of 125 µL of 60% w/v PEG 4000 in MA-I buffer. After the immediate addition of 1 mL of warm

MA2G, the entire transformation reaction was diluted to a final volume of 50 mL of warm MA2G in a graduated glass cylinder.

Three transformations were performed: the first served as a negative control with no DNA, the second contained 5 µg of PSR1128, and the third included 5 µg of PSR1130. One day post-transformation, plates were spotted with 15-µL aliquots of 20% v/v cornstarch in MA2GC (MA2G conditioned media). The cells were centrifuged at 2,000 × g for 10 minutes, resuspended in 300 µL of MA2GC, subjected to a series of serial dilutions, and 10-µL aliquots of cells were dispensed onto each cornstarch spot. The plates were incubated under standard conditions until colonies formed.

For cells transformed with the sulfadiazine (Sd) resistance marker both transient and integrated, the selection process began one day post-transformation by culturing the cells in liquid MA2G media containing 5 µg/mL and 7.5 µg/mL Sd. Following a 10-day incubation, when a noticeable difference between the transformed cells and the control was observed, the Sd concentration was increased to 10 µg/mL to enhance selection pressure. Four to six days after this increase, a clear distinction between the control and transformed cells was evident. Subsequently, the transformed cells were plated on 0.75X MA2G agar plates and incubated under standard growth conditions until colonies formed.

For CAT transient transformations, to maintain the transformed plasmid under constant selection pressure, I initiated the process 24 hours post-transformation by centrifuging the cells at 2,000 × g for 10 minutes. The cell pellet was resuspended in 1 mL of MA2G media supplemented with 150 µg/mL chloramphenicol (Cp). The resuspended cells were transferred to a 6-well plate containing 6 mL of the same media and incubated under standard conditions. To maintain selective pressure, 150 µg/mL chloramphenicol was added directly to the cultures every three

days, without media replacement. By day 6, both the control and experimental cultures appeared yellow-green, indicating stress; however, by day 9, the experimental culture had transitioned to a dark green color, while the control culture remained yellow-green.

5.2.7 Analysis of Colonies

Colonies were picked and inoculated into 16 µL of MA2G medium in a 96-well plate for high-resolution screening by PCR using Taq polymerase. The colony PCR was performed using *Taq* DNA Polymerase with Standard *Taq* Buffer (New England Biolabs) and a DNA Engine Dyad Peltier Thermal Cycler (Bio-Rad Laboratories). Each reaction mixture contained 1X Standard *Taq* Reaction Buffer, 200 µM dNTPs, 0.5 µM of each primer (oSDR2607/ oSDR2637 and oSDR2259/ oSDR2645 in Table 5.3), 1 µl of template DNA (either wild-type genomic DNA or colony suspension), and 1 U of *Taq* DNA Polymerase in a total volume of 20 µl. Thermocycling conditions consisted of an initial denaturation at 95 C for 5 min, 35 cycles of denaturation at 95 C for 20 sec, annealing at 56 C for 20 sec, and extension at 68 C for 1 min and 31 sec, followed by a final extension at 68 C for 5 min. The PCR products were run alongside a 100 bp DNA Ladder (New England Biolabs) on a 0.7% agarose gel containing ethidium bromide at 150 V for 1 hour and visualized using a Gel Doc imaging system. The remainder of the resuspended colonies were transferred to 200 µL of MA2G medium supplemented with chloramphenicol. To minimize evaporation, 100 µL of water was added between the wells surrounding the cell suspensions, and the plate was wrapped in grafting tape. The cultures were incubated for approximately three days until small green cell clumps formed at the bottom of the wells. Positive cultures were subsequently transferred to 2 mL of MA2G medium with chloramphenicol in a 24-well plate and grown for an additional four days. Once the cultures appeared green, genomic DNA was isolated from 0.25 mL of the culture using Quick Edward's Genomic DNA

preparation method (1-2 OD units of cells were harvested by centrifugation. The cell pellet was resuspended in 200 µL of Edwards Buffer and vortexed for 5 seconds; a reduced volume of 100 µL was used for smaller pellets. Isopropanol (200 µL) was then added, mixed by inversion, and centrifuged at 13,000 x g for 5 minutes. The supernatant was decanted, and the pellet was air-dried for less than 2 minutes by inverting the tube on a paper towel. The DNA pellet was resuspended in 100 µL of water, or 50 µL for smaller pellets, using a pipette. Insoluble material was removed by centrifugation at 13,000 x g for 1 minute. The DNA solution was diluted 1:10, and 1 µL was used for PCR; performed as described earlier, with a wild-type control included).

Table 5.3. Primers Used to Verify Successful Genomic Integration.

Oligonucleotides	Directionality	Sequence (5′ to 3′)
oSDR1831	Reverse	AACCTAACTCTCCGTCGCTA
oSDR2259	Forward	AGTTGAAGTATGTTACAAGCTCACAGGCAAAACAG
oSDR2263	Forward	TTCTAAATCGCTTCCAGCCG
oSDR2264	Reverse	GTTTTTGCCTGGTCCCTACA
OSDR2607	Forward	GTTCGGCATCCTGAACCTGA

5.2.8 Northern Blot Analysis

Northern blot analysis was performed as described earlier in section 2.1.2 to 2.1.4.12.

5.3. Results

5.3.1 Plasmid Construction

To investigate the function of RNase MRP in 5.8S rRNA processing, I conducted mutational analysis on its RNA component. The aim was to assess whether mutations that disrupt the stoichiometry of the two forms of 5.8S rRNA in *S. cerevisiae* also do so in *C. merolae*, thereby confirming its conserved role in 5.8S rRNA biogenesis. For these experiments, I generated the plasmids described in the materials and method section with their respective diagram of the cloning steps. I initiated the construction of plasmids for mutagenesis by inserting an oligonucleotide duplex, which harbored two multiple cloning sites (MCS), into the PCR 2.1 backbone. The pCR 2.1 vector was initially linearized by digestion with EcoRI and NotI (Figure 5.13) to create compatible ends for the MCS insertion, facilitating downstream cloning steps.

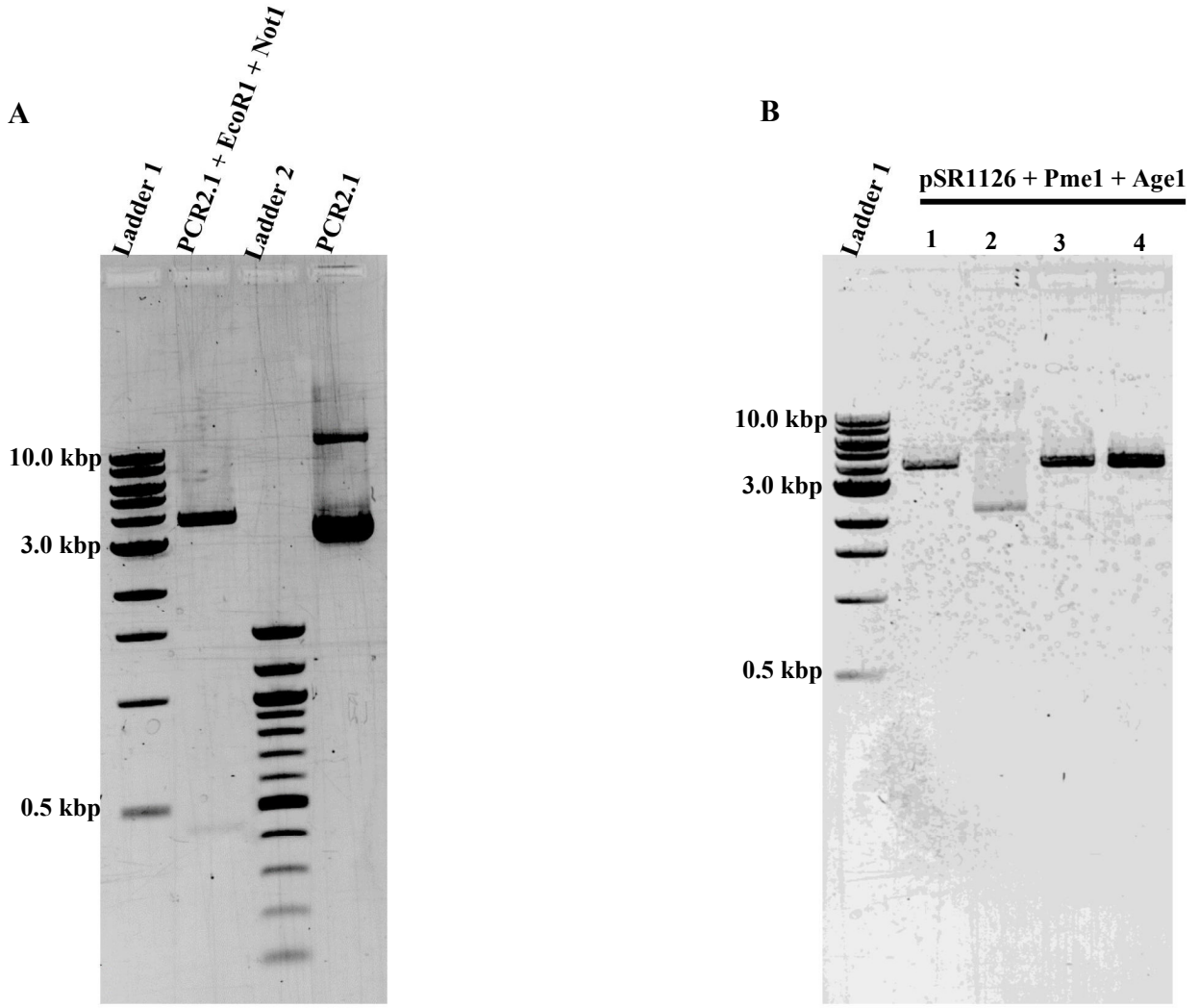

Figure 5.13. Restriction digest analysis of pCR2.1 and pSR1126. A 0.7% agarose gel stained with ethidium bromide displaying the results of restriction digests: **(a)** pCR2.1 digested with EcoRI and NotI, producing the expected 3,886 bp backbone fragment along with a ~500 bp fragment that was subsequently discarded; and **(b)** pSR1126 digested with PmeI and AgeI, resulting in the desired 3,913 bp product. The size markers used were the 1 kb DNA ladder (Ladder 1) and the 100 bp DNA ladder (Ladder 2) for reference.

The DNA insert was derived from CMK142 and ligated into the PmeI and AgeI multiple cloning sites of pSR1126, resulting in the construction of pSR1127. The successful integration of the insert was confirmed by restriction digest analysis of pSR1127 using PmeI and AgeI (Figure 5.14).

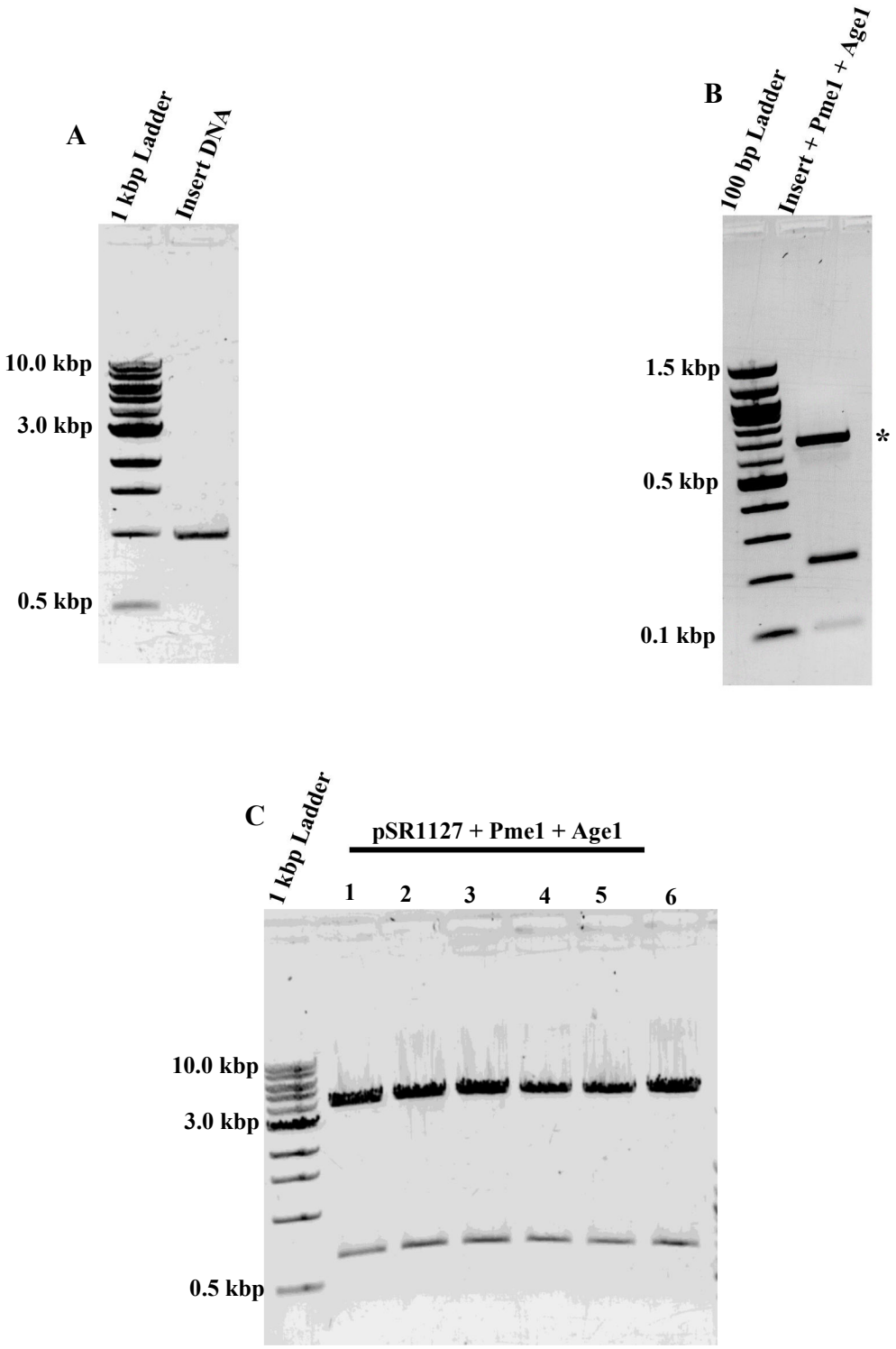

Figure 5.14. Restriction Digest Analysis of Insert DNA and pSR1127. A 0.7% agarose gel stained with ethidium bromide displaying **(a)** Insert DNA of expected size of 990 bp and the results of restriction digests: **(b)** Insert DNA digested with PmeI and AgeI, producing the expected 670 bp fragment denoted with * **(c)** pSR1127 digested with PmeI and AgeI with 1,2,3,4,5,6 displaying the desired 3,913 bp and 670 bp products. The size markers used were the 1 kb DNA ladder or the 100 bp DNA ladder for reference.

To construct a plasmid containing the sulfadiazine resistance marker, pSR887, which originally carried a URA5.3 marker, was digested with SphI and XhoI to excise the URA5.3 marker, leaving the backbone for subsequent cloning. The sulfadiazine marker insert was generated from pSR1052, and ligation was then performed to join the backbone, and the sulfadiazine marker insert; pSR1113. The successful integration of the insert was confirmed by restriction digest analysis of pSR1113 using two sets of restriction enzymes (BamH1/XhoI and BamH1/Spe1) to also confirm insert directionality (Figure 5.15).

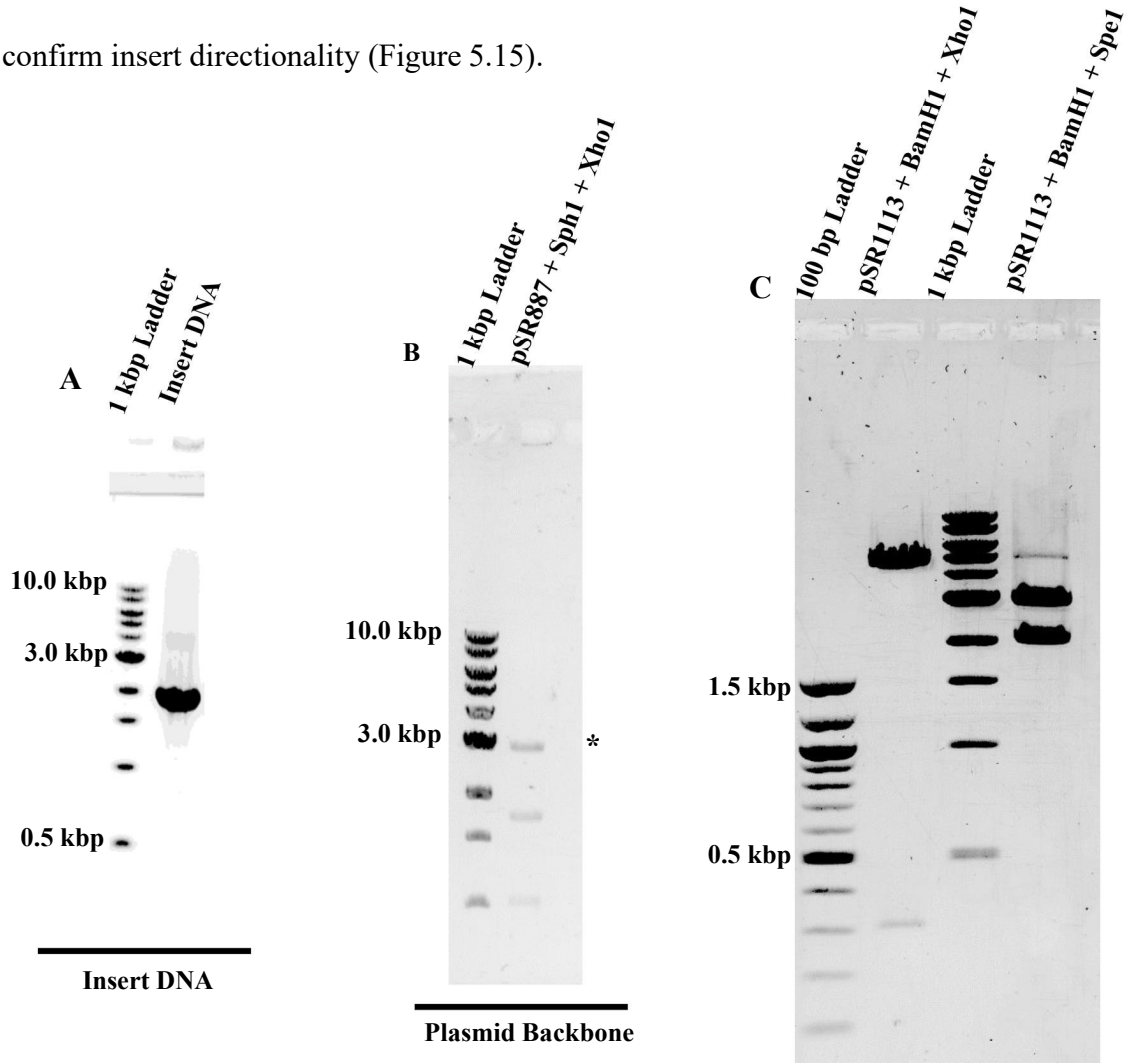

Figure 5.15. Construction and restriction digest analysis of pSR1113. A 0.7% agarose gel stained with ethidium bromide displaying **(a)** Insert DNA of expected size of 1, 913 bp and the results of restriction digests: **(b)** pSR887 digested with SphI and XhoI, producing the expected 2,978 bp backbone fragment **(c)** pSR1113 digested with BamHI and XhoI displaying the expected 4,590 bp and 302 bp bands and BamH1 and Spe1 displaying the desired 2,867 bp and 2,025 bp products. The size markers used were the 1 kb DNA ladder or the 100 bp DNA ladder for reference.

The knockout plasmid, pSR1117, designed for the disruption of the endogenous *CMK142* gene to establish a plasmid shuffling system in *Cyanidioschyzon merolae*, was constructed through ligation-independent cloning (LIC). DNA fragments derived from *CMK142* were inserted into the SwaI and PacI sites of the pSR1113 vector. The insertion into the SwaI site was validated by restriction digest analysis using BamHI and XhoI (Figure 5.16).

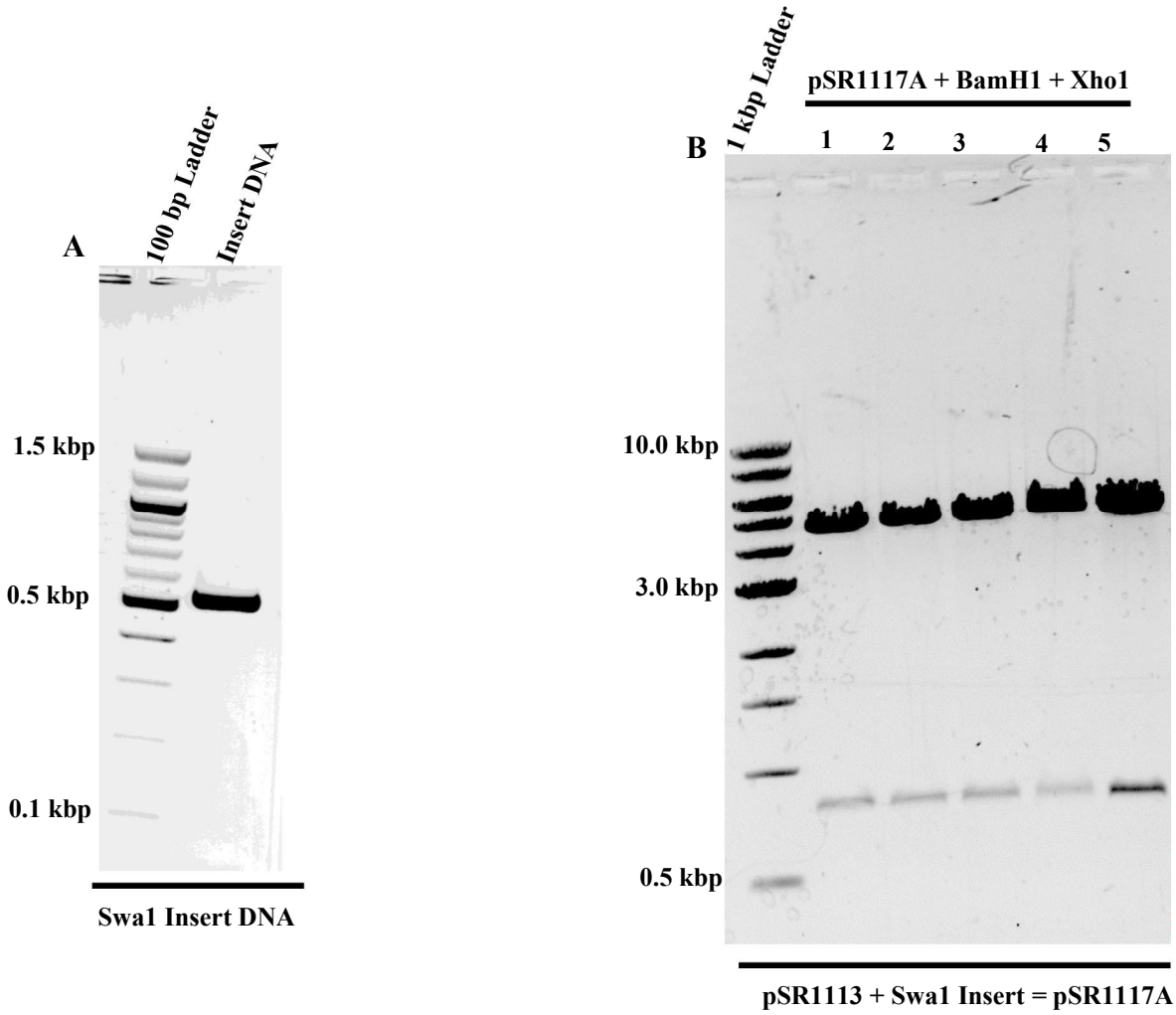

Figure 5.16. Insertion of CMK142-derived DNA fragment into the SwaI site of the pSR1113 vector. A 0.7% agarose gel stained with ethidium bromide displaying **(a)** Insert DNA of expected size of 505 bp and **(b)** The insert cloned into the Swa1 site of pSR1113 and digested with BamHI and XhoI, producing the expected 4,590 bp and 755 bp fragments. The size markers used were the 1 kb DNA ladder and the 100 bp DNA ladder for reference.

The plasmid pSR1117A, containing the validated SwaI insert, was subsequently used as a template for the insertion of the 3' homology arm derived from the *CMK142* gene into the PacI site, resulting in the construction of the final knockout plasmid, pSR1117. Successful integration of the fragment at the PacI site was confirmed by restriction digest analysis using BamHI and XhoI (Figure 5.17).

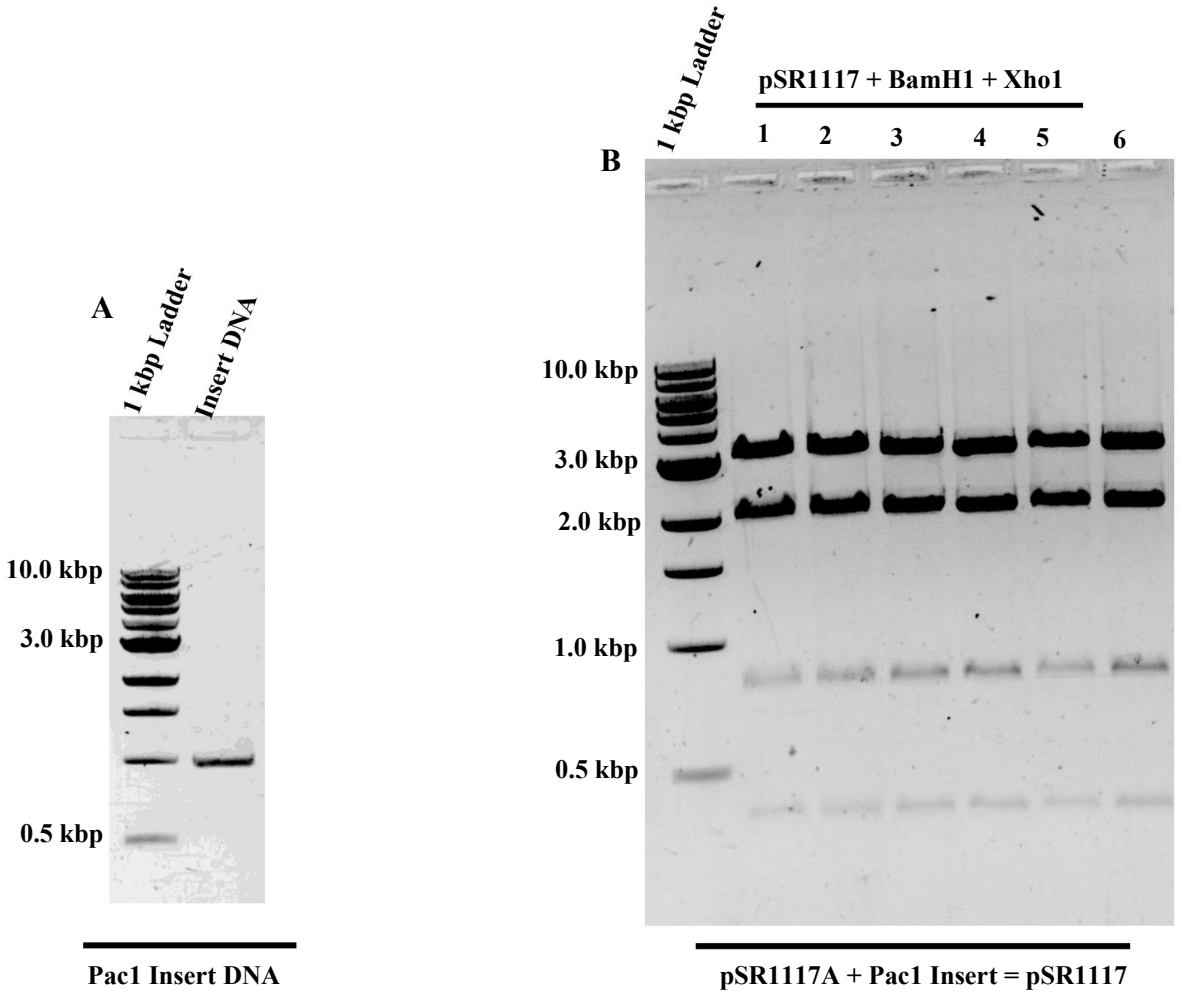

Figure 5.17. Construction and Restriction Digest Analysis of pSR1117. A 0.7% agarose gel stained with ethidium bromide displaying **(a)** Insert DNA of expected size of 1,037 bp and **(b)** The insert cloned into the Pac1 site of pSR1117A to generate pSR1117. The final plasmid is digested with BamHI and XhoI, with samples 1 to 6 producing the expected 3,019 bp, 2,010 bp, 745 bp, and 368 bp fragments. The size marker used was the 1 kb DNA ladder for reference.

To generate two shuttle plasmids with distinct selectable markers (URA5.3 and CAT), insert DNA was generated from CMK142 containing our MRP RNA locus and cloned into the PacI sites of pSR887 (harboring the URA5.3 selectable marker) and pSR886 (harboring the CAT selectable marker) Figure 5.18.

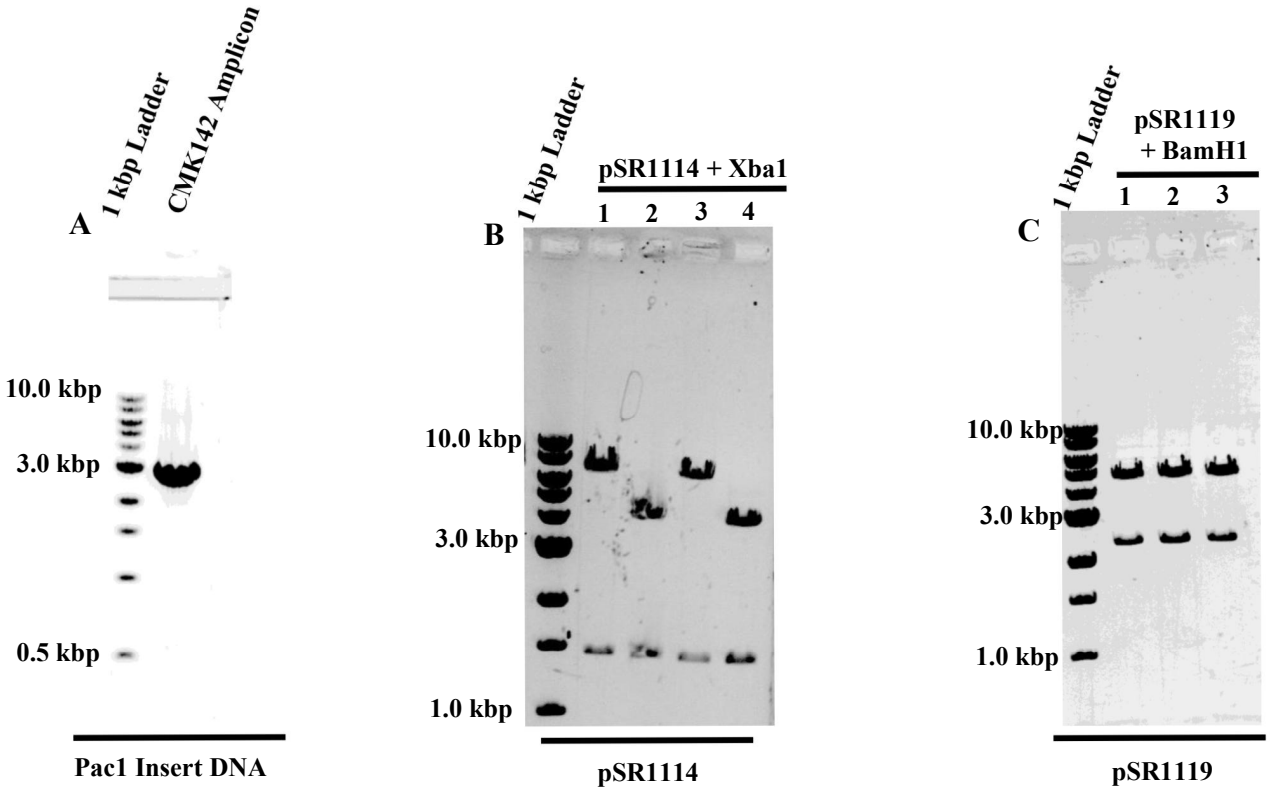

Figure 5.18. Construction and Restriction Digest of two shuffle plasmids with distinct selectable markers. A 0.7% agarose gel stained with ethidium bromide displaying **(a)** Insert DNA of expected size of 2,776 bp that was cloned into Pac1 sites of pSR887 and pSR886 via ligation independent cloning to generate pSR1114 and pSR1119 respectively **(b)** Restriction digest of pSR1114 with XbaI, producing the expected 7,067 bp and 1,472 bp fragments and **(c)** Restriction digest of pSR1119 with BamHI displaying the expected 4,966 bp and 2,427 bp fragments. The size marker used was the 1 kb DNA ladder for reference.

To generate an integrable CAT amplicon capable of incorporating mutant *MRP* and replacing the endogenous *MRP* at the *CMK142* locus, I constructed a CAT integrable plasmid. This was achieved by inserting a 5' homology arm into the SwaI site of pSR1119 using ligation-independent cloning (Figure 5.19).

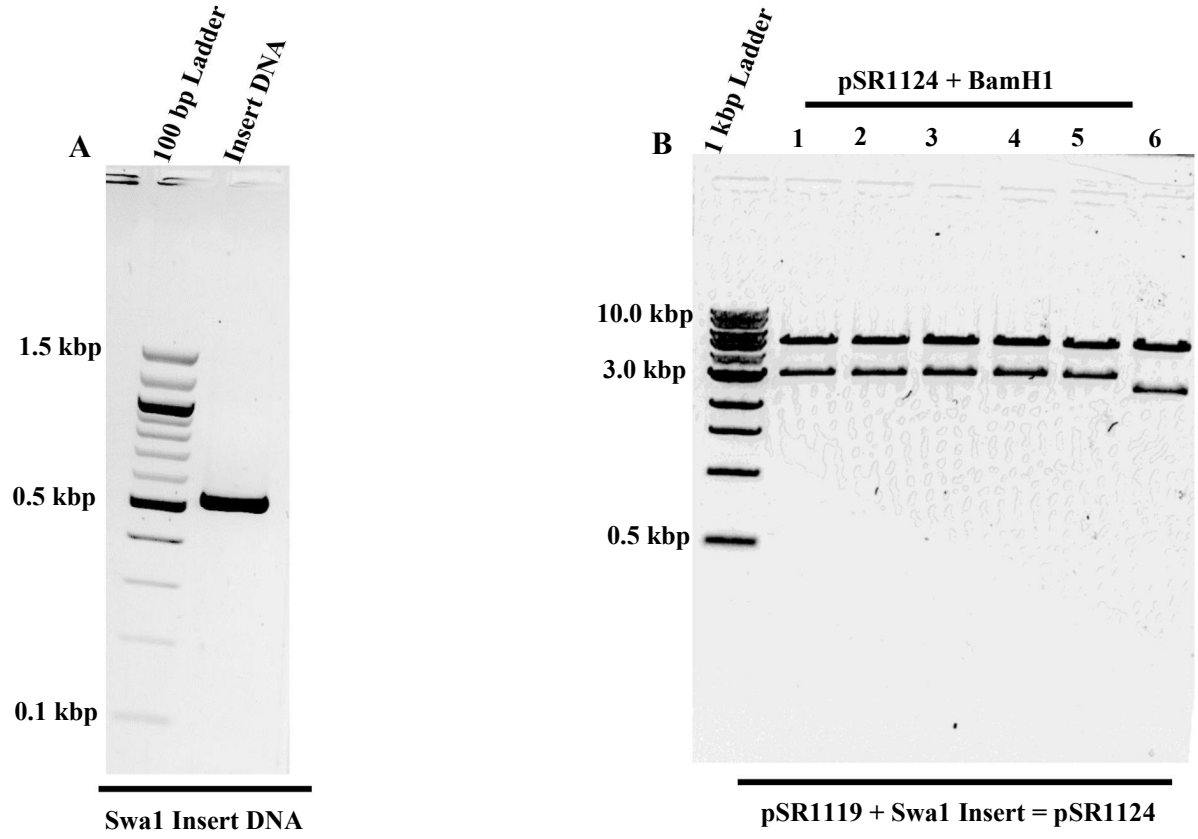

Figure 5.19. Construction and Restriction Digest of pSR1124. A 0.7% agarose gel stained with ethidium bromide displaying **(a)** Insert DNA of expected size of 505 bp that was cloned into Swa1 sites of pSR1119 to generate pSR1124 **(b)** Restriction digest of pSR1124 with BamHI, displaying the expected 4,966 bp and 2,932 bp fragments. The size markers used were the 1 kb DNA ladder and the 100 bp DNA ladder for reference.

To generate mutant plasmids using "Around-the-Horn" site-directed mutagenesis, as described in Materials and Methods section 5.1.4, phosphorylated primers were employed in a PCR reaction using pSR1127 as the template to introduce the desired mutations. Figures 5.20 and 5.21 display the mutation sites on the predicted RNase MRP RNA secondary structure in *Cyanidioschyzon merolae* and the corresponding PCR results from the mutagenesis, respectively.

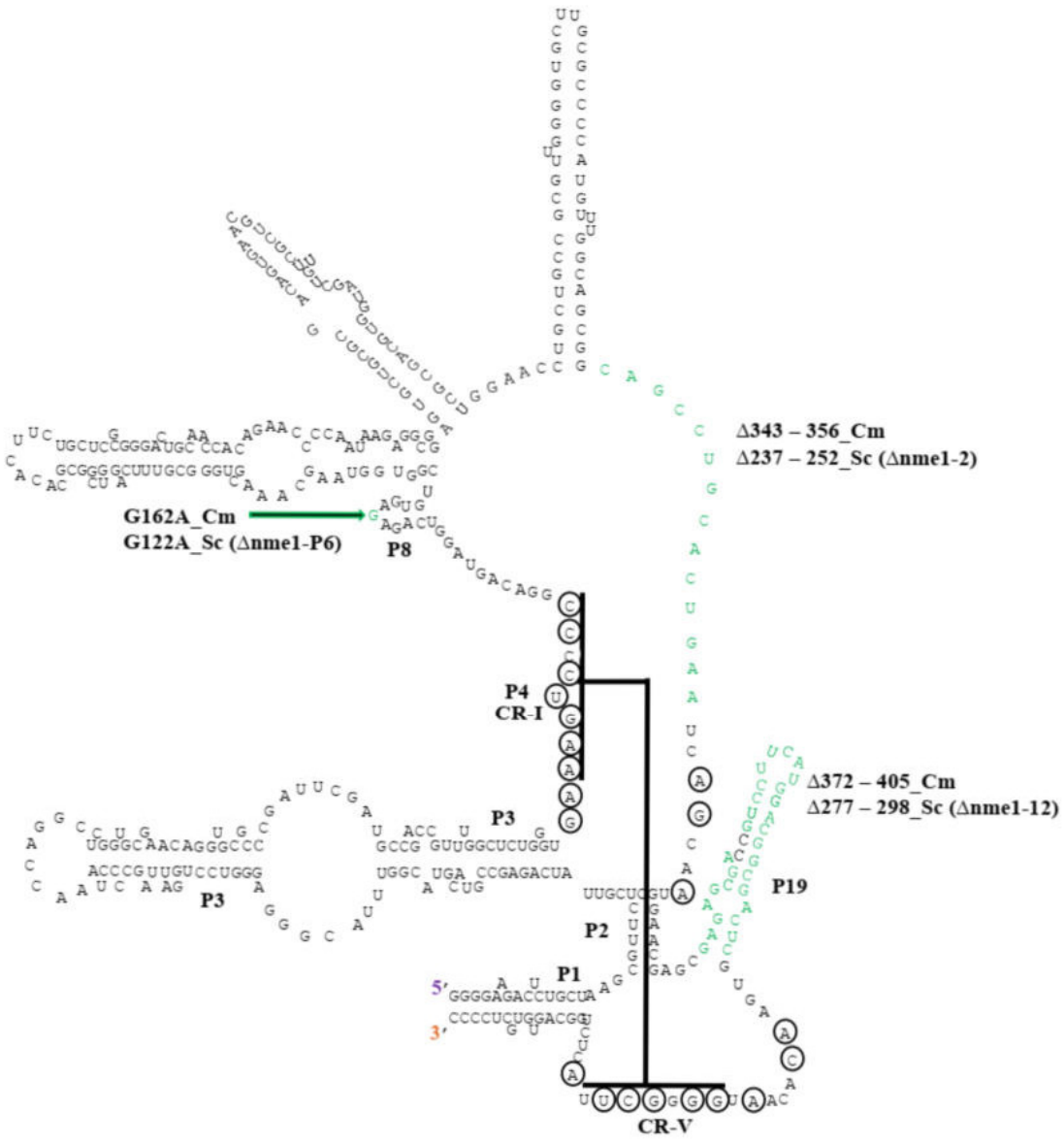

Figure 5.20: Predicted secondary structure of RNase MRP RNA in *Cyanidioschyzon merolae* with mutation sites highlighted. The mutation sites are marked in green, with the corresponding equivalent sites in *S. cerevisiae* (Sc) indicated.

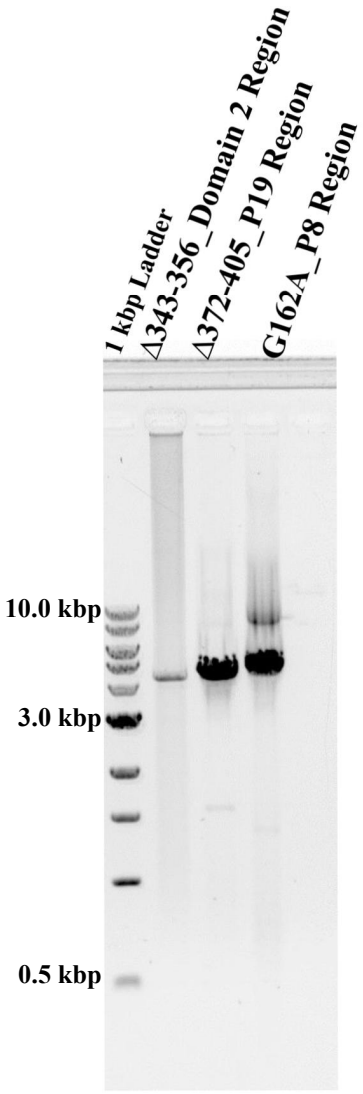

Figure 5.21: PCR results from site-directed mutagenesis of RNase MRP RNA in *Cyanidioschyzon merolae*. The resulting amplicons are 4,558 bp for the Δ343–356 deletion, 4,538 bp for the Δ372–405 deletion, and 4,572 bp for the G162A point mutation. The 1 kb DNA ladder is used as a size marker.

The mutagenized PCR products were digested with DpnI and ligated, as detailed in the Materials and Methods section. To preliminarily verify successful mutagenesis before sequencing, PCR amplification was performed. This allowed for an initial assessment of differences in product size between the mutagenized plasmids, using the non-mutagenized plasmid as a control. The results are shown in Figure 5.22 with Δ372–405 deletions (1,2,3,4,5) yielding the expected 157 bp band.

.

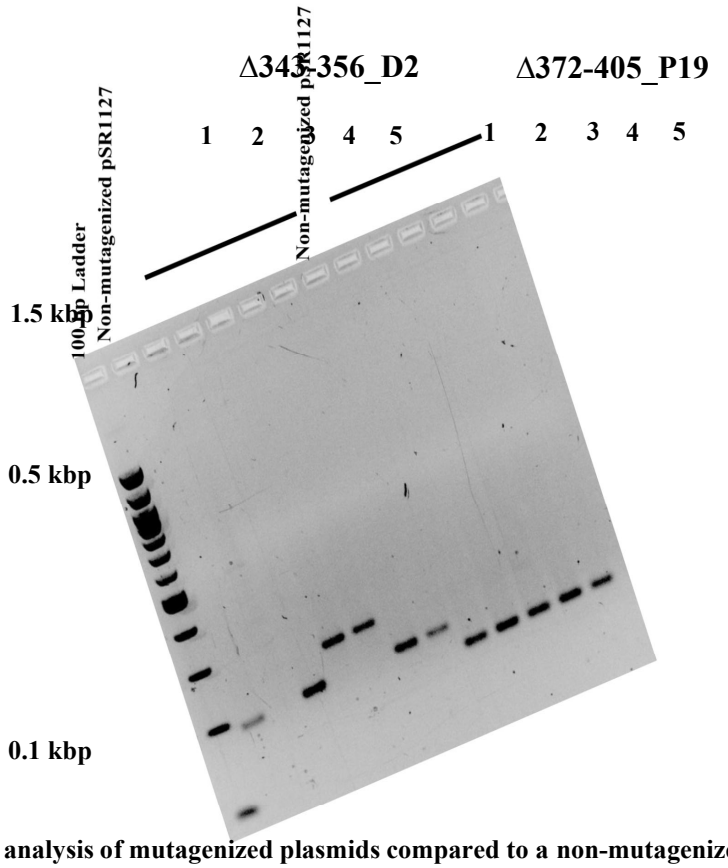

Figure 5.22: PCR analysis of mutagenized plasmids compared to a non-mutagenized control, displayed on a 2% agarose gel stained with ethidium bromide. The control plasmid produced the expected 191 bp band, while the Δ372–405 deletions (1,2,3,4,5) yielded the expected 157 bp band. Unexpected variable bands of 191 bp (2,5) and ~250 bp (3,4) were observed for the Δ343–356 deletion, instead of the anticipated 177 bp band. A 100 bp DNA ladder was used as a size reference.

Samples of the Δ372–405 deletion and the G162A point mutants, were sent for sequencing. Repeated attempts to achieve successful mutagenesis of the Δ343–356 deletion were unsuccessful.

Following sequencing confirmation of successful mutagenesis, the plasmids were digested, and the mutated regions were excised (Figure 5.23), as described in the Materials and Methods section. The corresponding region from pSR1124 was also excised and replaced with the mutated fragments through ligation, resulting in the construction of pSR1128 (Δ372–405

deletion) and pSR1130 (G162A mutation). The successful integration of the insert was confirmed by restriction digest analysis using PmeI and AgeI (Figure 5.24).

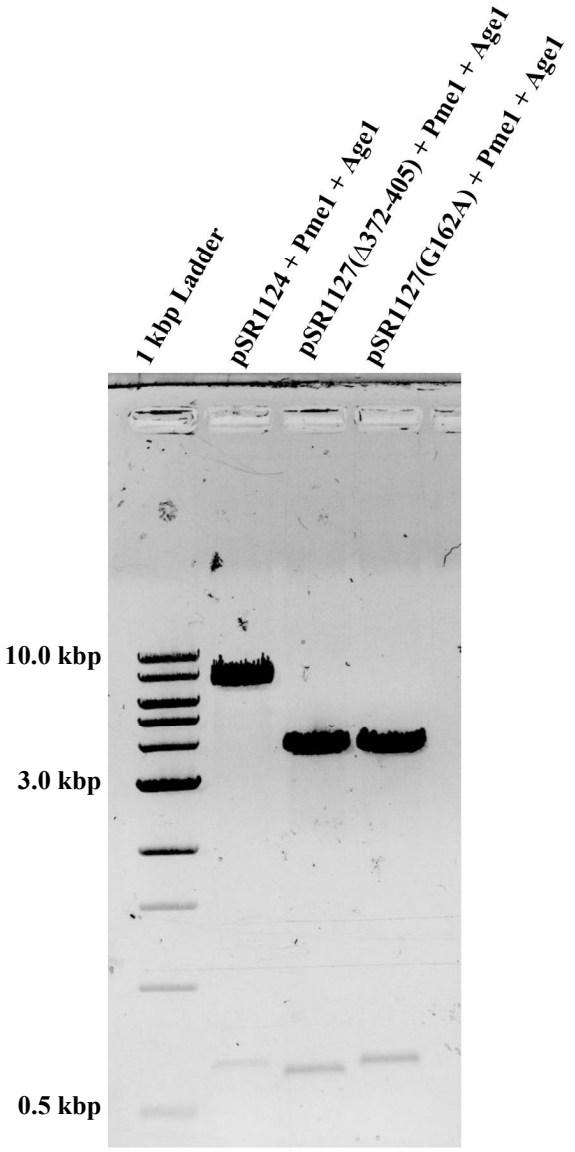

Figure 5.23 Restriction enzyme digestion and ligation process for constructing pSR1128 and pSR1130. A 0.7% agarose gel stained with ethidium bromide shows; digested pSR1124 yielding a backbone of interest fragment of 7,231 bp and inserts of interest measuring 636 bp and 669 bp from Δ372–405 deletion and G162A mutation respectively. The 1 kb DNA ladder is used as a size marker.

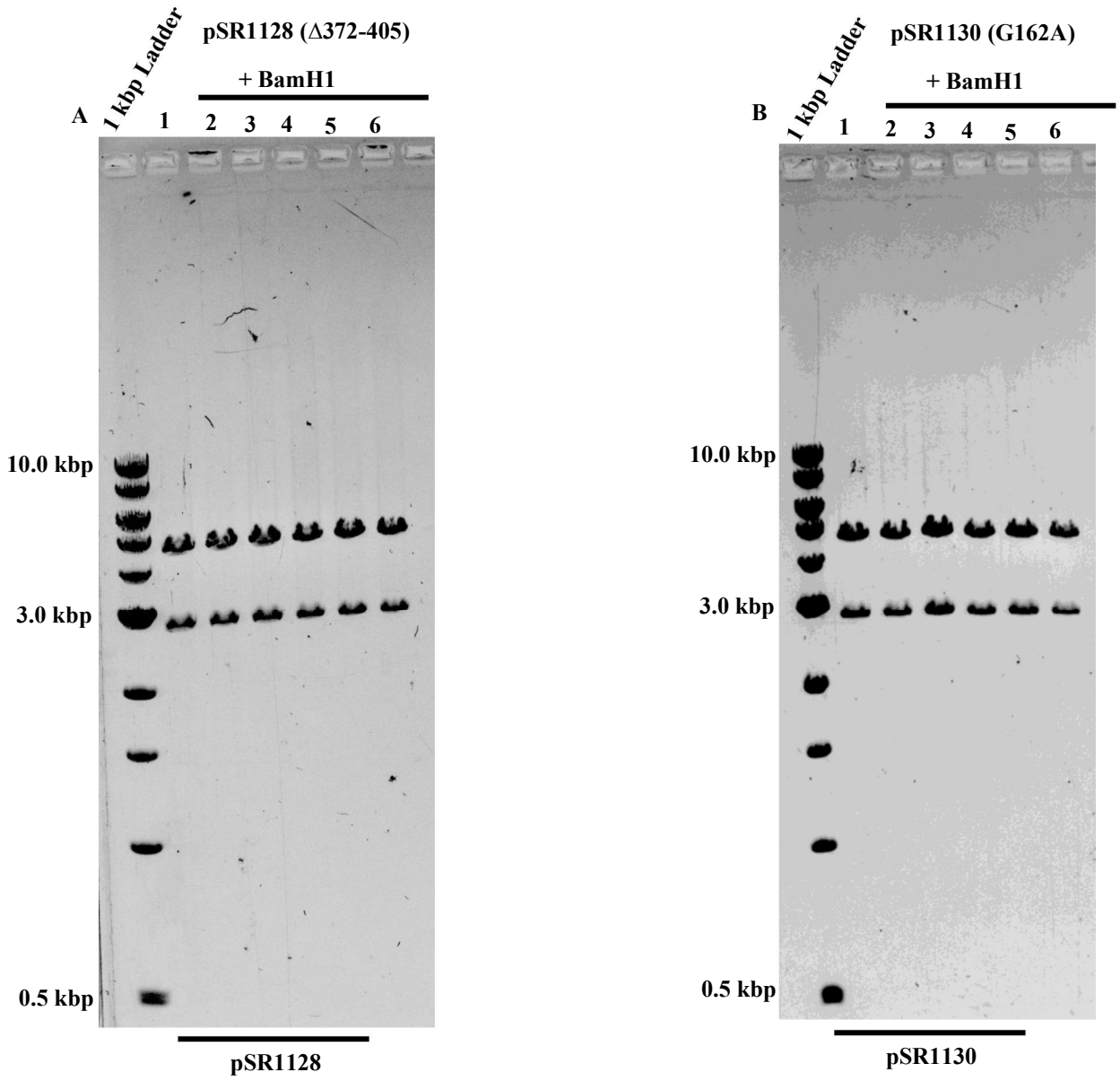

Figure 5.24. Restriction Digest of pSR1128 and pSR1130. A 0.7% agarose gel stained with ethidium bromide shows **(a)** Restriction digest of pSR1128 with BamHI, displaying the expected 4,932 bp and 2,932 bp fragments. **(b)** Restriction digest of pSR1130 with BamHI, displaying the expected 4,954 bp and 2,943 bp fragments. The 1 kb DNA ladder is used as a size marker.

After confirmation of the correct mutant constructs with the expected sizes for each mutation (pSR1128 displaying the expected 4,932 bp, and 2,932 bp fragments and pSR1130 the expected 4,954 bp and 2,943 bp fragments). Mutants were transformed into *C. merolae.*

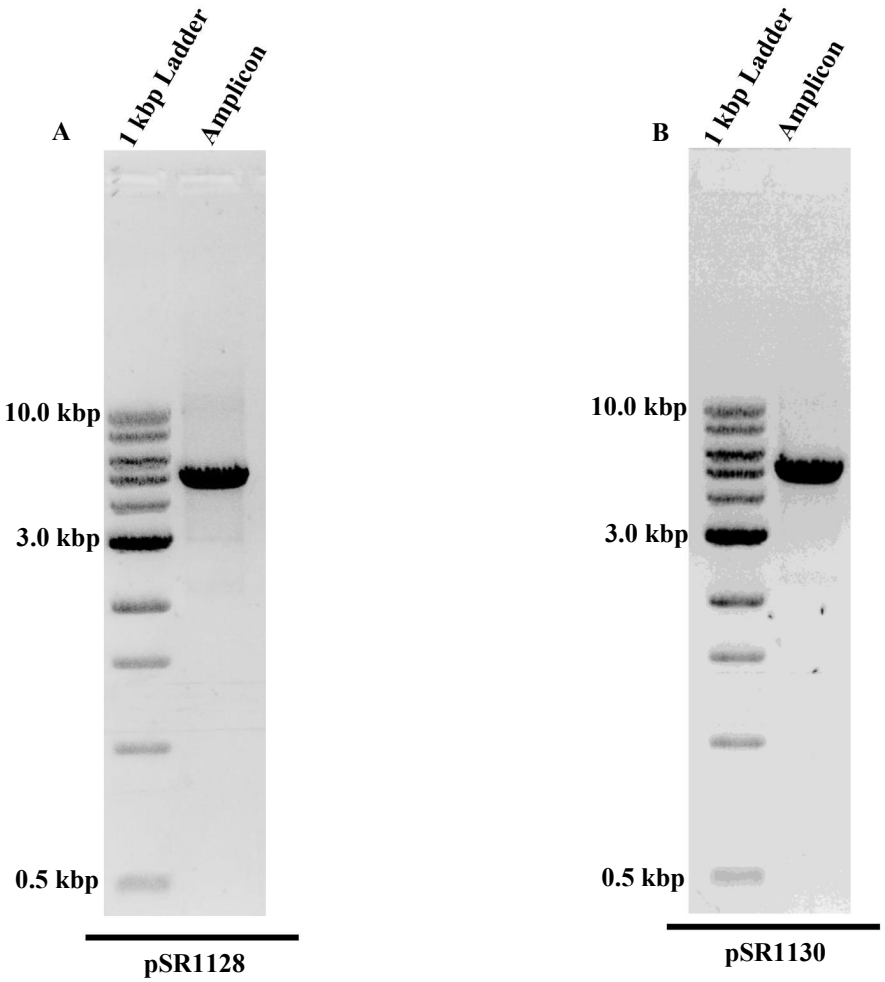

Figure 5.25: **Amplification of linear DNA from plasmids used for the transformation of *Cyanidioschyzon merolae***. A 0.7% agarose gel stained with ethidium bromide displays (a) the 4,986 bp PCR product from pSR1128 used for the transformation of *C. merolae*, and (b) the 5,018 bp PCR product from pSR1130 used for *C. merolae* transformation. A 1 kb DNA ladder was used as a size reference.

After 12 days post-transformation, multiple chloramphenicol-resistant colonies were observed. Twelve colonies picked from the pSR1128 (Δ372 – 405) transformants were screened for homologous recombination using colony PCR (Figure 5.26) with each transformant tested with two different sets of primers making a total of 24 screens. The colony PCR analysis identified several promising candidates, two of which were further analyzed by extracting genomic DNA and subjecting them to additional PCR tests.

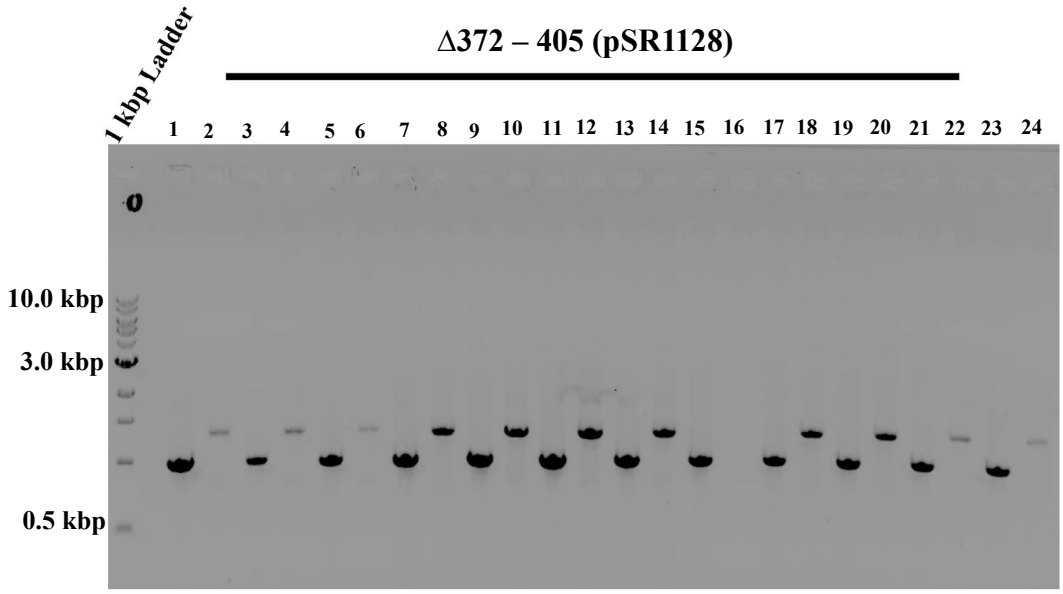

Figure 5.26 Initial colony PCR screening for genomic integration of pSR1128 (Δ372–405). A 0.7% agarose gel stained with ethidium bromide shows colony PCR results for 24 *C. merolae* colonies, tested with two primer sets. The expected bands of 1,318 bp and 995 bp, indicating successful genomic insertion, are displayed. A 1 kb DNA ladder was used as a size marker for reference.

This subsequent test was to confirm successful recombination and integration into the CMK142 locus and wild-type *C. merolae* genomic DNA was used as a control (Figure 5.27). The successful transformants' clear resistance to chloramphenicol confirmed the functionality of the APCC promoter, demonstrating its ability to drive the expression of the *CAT* gene.

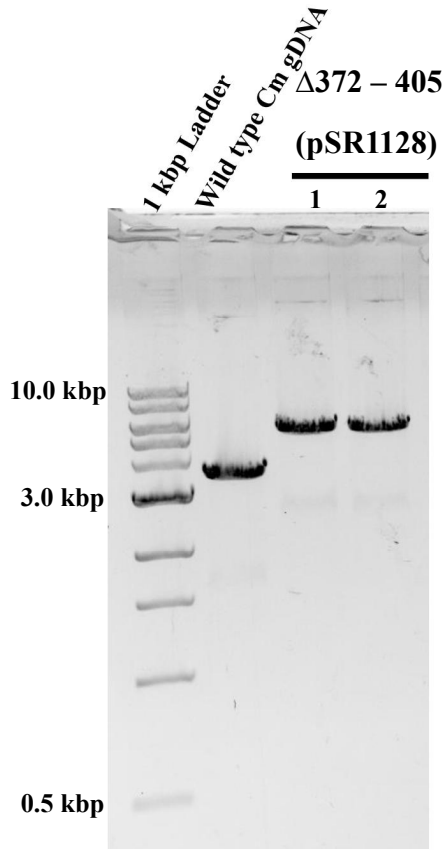

Figure 5.27. Final PCR confirming the successful genomic integration of pSR1128 (Δ372–405) into CMK142 locus. A 0.7% agarose gel containing ethidium bromide showing the PCR results for two promising Δ372–405 *C. merolae* candidates (1 and 2) showing the expected 5,609 bp band for successful integration while the wild-type (WT) sample acting as a negative control displays the expected 3,738 bp band. A 1 kb DNA ladder was used as a size reference.

Similarly, for pSR1130 (G162A), multiple chloramphenicol-resistant colonies were observed after 12 days post-transformation. Seven colonies picked from the pSR1130 (G162A) transformants were screened for homologous recombination using colony PCR (Figure 5.28) with each transformant tested with two different sets of primers making a total of 14 screens. The colony PCR analysis identified several promising candidates, three of which were further analyzed by extracting genomic DNA and subjecting them to additional PCR tests.

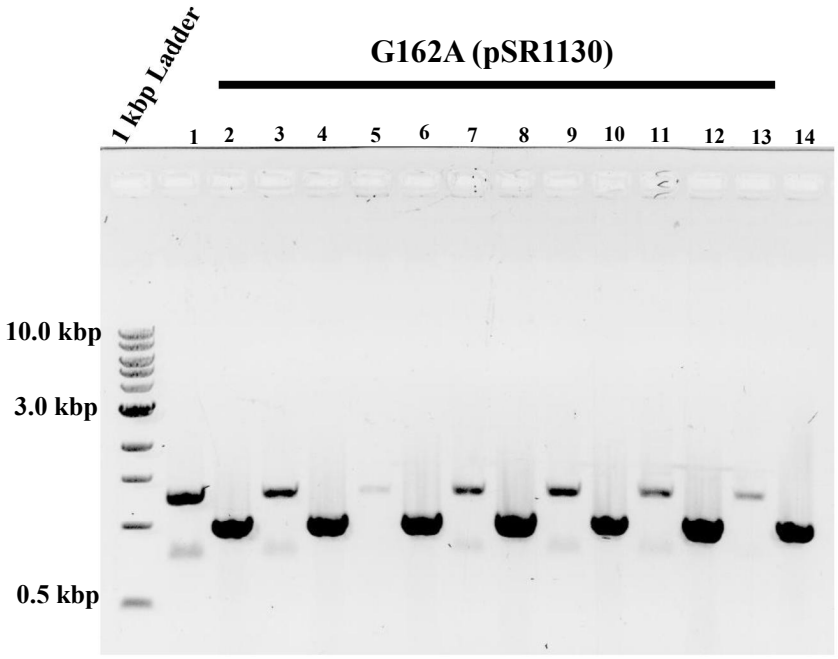

Figure 5.28 Initial colony PCR screening for genomic integration of pSR1130 (G162A). A 0.7% agarose gel stained with ethidium bromide shows colony PCR results for 14 *C. merolae* colonies, tested with two primer sets. The expected bands of 1,318 bp and 995 bp, indicating successful genomic insertion are displayed. A 1 kb DNA ladder was used as a size marker for reference.

Although some bands corresponding to nonspecific amplification were present, the expected bands were still observed, indicating successful recombination and integration into the *CMK142* locus, with wild-type *C. merolae* genomic DNA used as a control (Figure 5.29). The clear chloramphenicol resistance observed in the successful transformants further confirmed the functionality of the APCC promoter, demonstrating its ability to drive CAT gene expression.

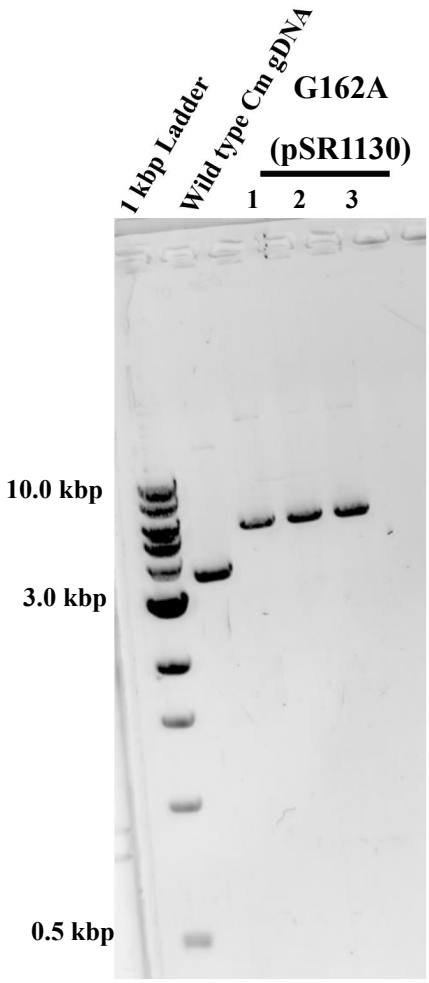

Figure 5.29. Final PCR confirming the successful genomic integration of pSR1130 (G162A) into CMK142 locus. A 0.7% agarose gel containing ethidium bromide showing the PCR results for three promising G162A *C. merolae* candidates (1, 2, and 3) showing the expected 5,641 bp band for successful integration while the wild-type (WT) sample acting as a negative control displays the expected 3,738 bp band. A 1 kb DNA ladder was used as a size reference.

5.3.2 Northern Blot Analysis

Following successful recombination and integration of the mutant RNase MRP RNA, I conducted northern blot analysis to evaluate potential alterations in the stoichiometry of the two forms of 5.8S rRNA. Figure 5.30 presents the results of this analysis.

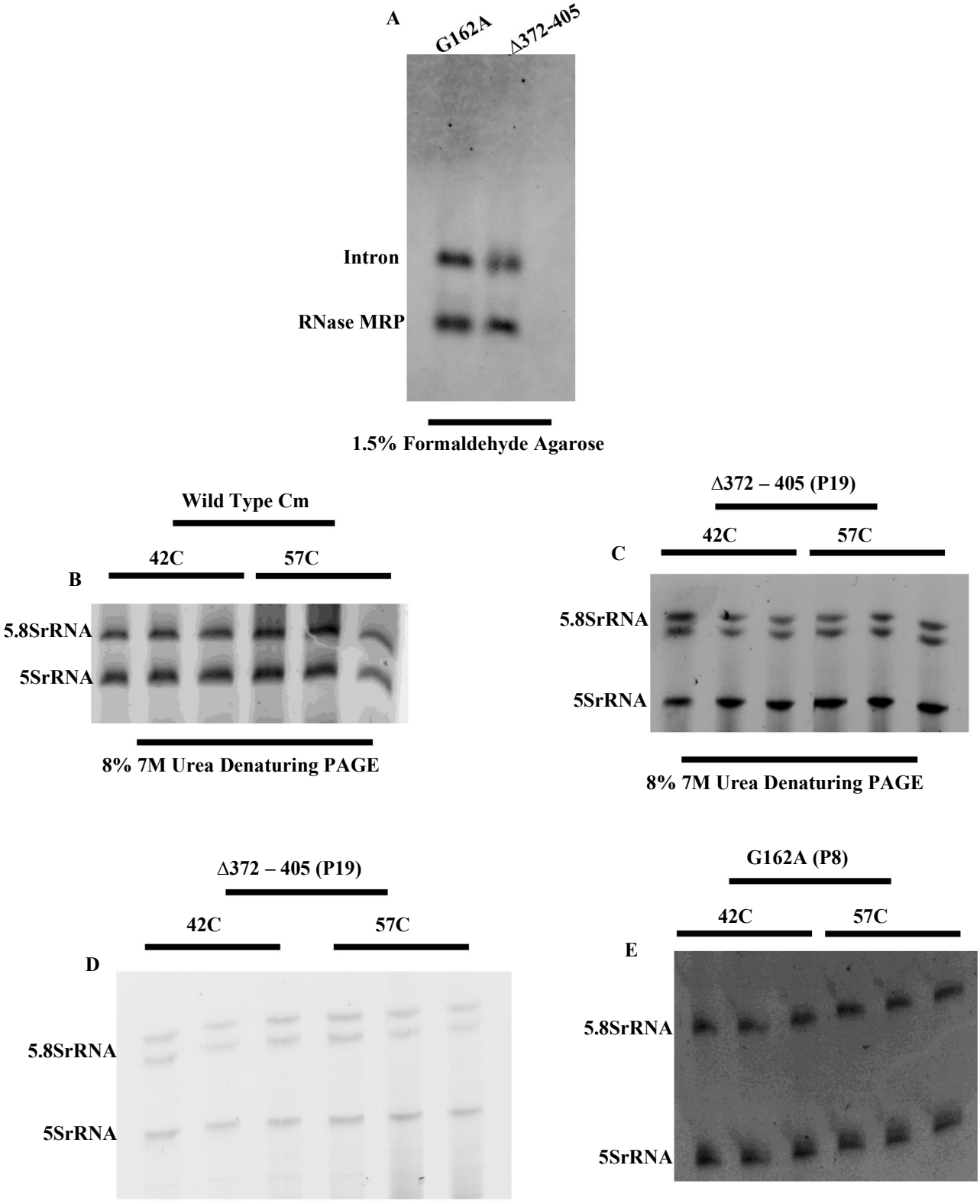

Figure 5.30 Changes in the stoichiometry of the two forms of 5.8S rRNA following RNase MRP RNA mutations in *Cyanidioschyzon merolae*. (a) Total RNA from the Δ372–405 and G162A mutant strains was analyzed for RNase MRP expression using a 1.5% formaldehyde agarose gel **(b)** Total RNA from wild-type cells analyzed on an 8% PAGE gel, stained with ethidium bromide to visualize the two forms of 5.8S rRNA. **(c-d)** Total RNA from the Δ372–405 mutant strain and **(e)** from the G162A mutant strain were analyzed using 8% PAGE gels and ethidium bromide staining to observe the 5.8S rRNA forms. The probes used were oSDR2487 = 5.8S and oSDR2479 = RNase MRP.

The northern blot analysis results reveal that deletion of the P19 region (Δ372–405) in *C. merolae*'s RNase MRP RNA leads to a notable shift in the stoichiometry of the two forms of 5.8S rRNA (Figures 5.30 c and d). The shift observed between Figure 2.7 and Figures 30c and 30d highlights a change in the relative abundance of the two forms of 5.8S rRNA after mutating RNase MRP. In Figure 2.7, the short form of 5.8S rRNA is predominant, with the long form being less visible. However, following the mutation of RNase MRP, the two forms appear in equal amounts, as shown in Figures 30c and 30d. This suggests that the mutation affects the processing of 5.8S rRNA, leading to altered stoichiometry between the long and short forms. However, the same change in stoichiometry between the long and short forms of 5.8S rRNA is observed at both 42 C and 57 C (Figures 5.30 c and d), suggesting that temperature does not play a role in this shift. The equal amounts of both forms after RNase MRP mutation are consistent across different temperature conditions, indicating that the observed change in stoichiometry is driven by the mutation rather than by heat stress.

In contrast, the G162A mutant strain exhibited no discernible effect on 5.8S rRNA processing, indicating that mutating this region does not impair RNase MRP functionality in *C. merolae*.

5.3.3 Establishing Plasmid Shuffling System in *C. merolae*

Even though the direct replacement via homologous recombination worked successfully (section 5.3.2 and Figures 5.30c and d) I attempted to use the plasmid shuffling system used in *S. cerevisiae* to see if that gives the same result in *C. merolae* and 8as an attempt to establish this system in *C. merolae*. The plasmid shuffling system involves transiently introducing a second copy of the *CMK142* gene on a plasmid containing a selectable marker, *URA5.3*. This step enables the knockout of the endogenous *CMK142* gene through homologous recombination using a different selectable marker, *Sulfadiazine*. After successfully disrupting the native gene, the plasmid-encoded *CMK142* copy is transiently replaced or "shuffled out" with a mutant version of *CMK142* carried on another plasmid with a distinct selectable marker, *CAT*. This transient process ensures selective pressure throughout each phase, allowing for the replacement of the wild-type gene with the desired mutant.

To achieve this, I transiently transformed *Cyanidioschyzon merolae* T1 strains with a plasmid containing a copy of the *CMK142* gene (pSR1114), harboring the *URA5.3* selectable marker. The *URA5.3* gene encodes orotidine-5'-phosphate decarboxylase, an essential enzyme in the de novo pyrimidine (uracil) synthesis pathway. Since the T1 strains are auxotrophic for uracil, they rely on external uracil for survival, allowing cells transformed with the plasmid to survive in uracil-deficient conditions. After confirming the successful transformation, a linear DNA product was amplified from pSR1117 (Figure 5.31) to facilitate the replacement of the endogenous *CMK142* gene via homologous recombination.

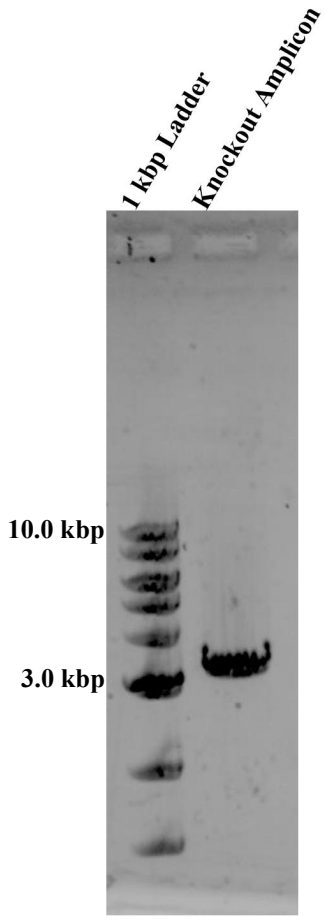

Figure 5.31 Amplification of linear DNA from pSR1117 used for the transformation of *Cyanidioschyzon merolae*. A 0.7% agarose gel stained with ethidium bromide displays the expected 3,329 bp PCR product from pSR1117 used for the transformation of C. merolae. A 1 kb DNA ladder was used as a size reference.

The integration was first selected using sulfadiazine, ensuring that only cells transformed with the sulfadiazine-resistant marker survived in the presence of the sulfadiazine (Figure 5.32 and Figure 5.33).

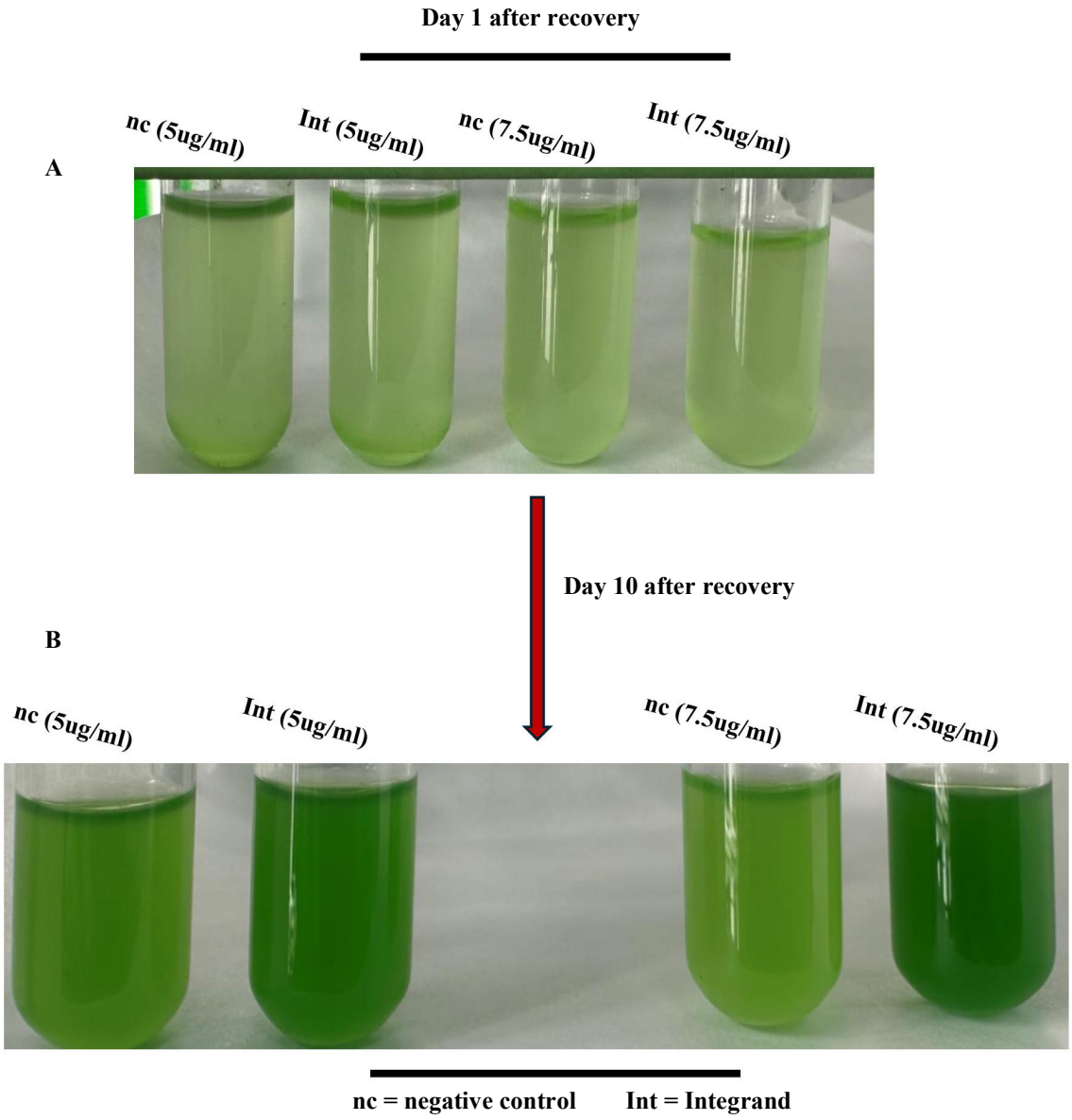

Figure 5.32. Selection of transformed cells with sulfadiazine. (a-b) Transformed *C. merolae* cells were cultured in the presence of 5 µg/mL and 7.5 µg/mL sulfadiazine from day one post-transformation until day 10. Control groups were included for reference, demonstrating the selective growth of cells carrying the sulfadiazine-resistant marker. nc= negative control, and Int = Integrand.

After 10 days of selection, the concentration of sulfadiazine was increased to 10 µg/mL for all cultures (Figure 5.33). This increase in sulfadiazine concentration heightened the stringency of the selection process, favoring cells with the successful integration of the selectable marker. As a

result, non-transformed cells that persisted at the lower concentrations were effectively eliminated, enriching the population of transformed cells.

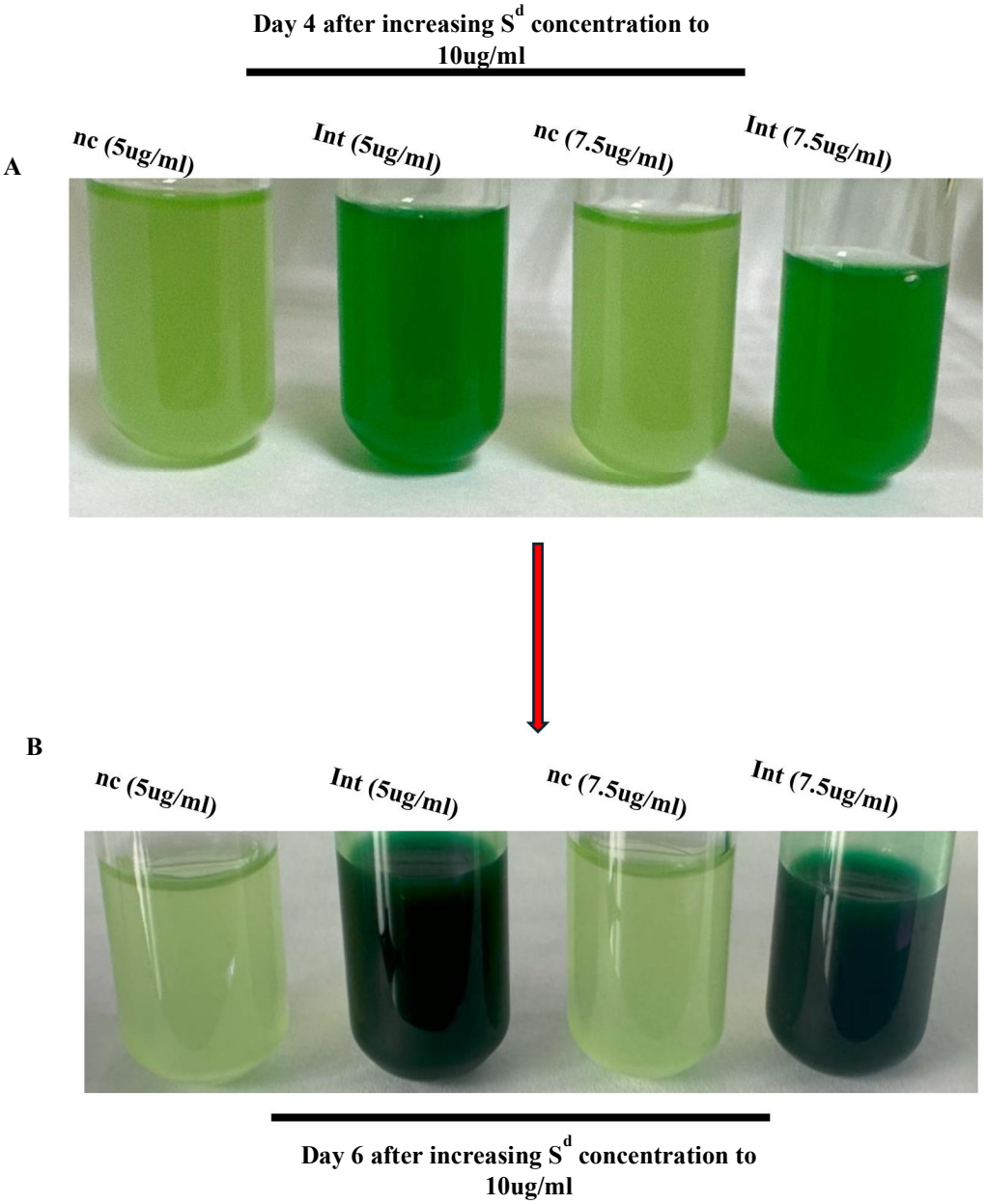

Figure 5.33 Growth of transformed *C. merolae* cells under increasing sulfadiazine concentration. Transformed *C. merolae* cells were grown in the presence of 10 µg/mL sulfadiazine from day 10 post-transformation, following initial selection with 5 µg/mL and 7.5 µg/mL. **(a and b**) display 4 days and 6 days after increasing sulfadiazine concentration respectively. Control groups were included for reference, demonstrating the selective growth of cells carrying the sulfadiazine-resistant marker. nc= negative control, and Int = Integrand.

After day 6 of stringent selection, cells were grown on an MA2G media plate for single colonies as described in the materials and methods section. Four colonies were screened with two different sets of primers making a total of 8 screens (Figure 5.34). The colony PCR analysis identified promising candidates, two of which were further analyzed by extracting genomic DNA and subjecting them to additional PCR tests.

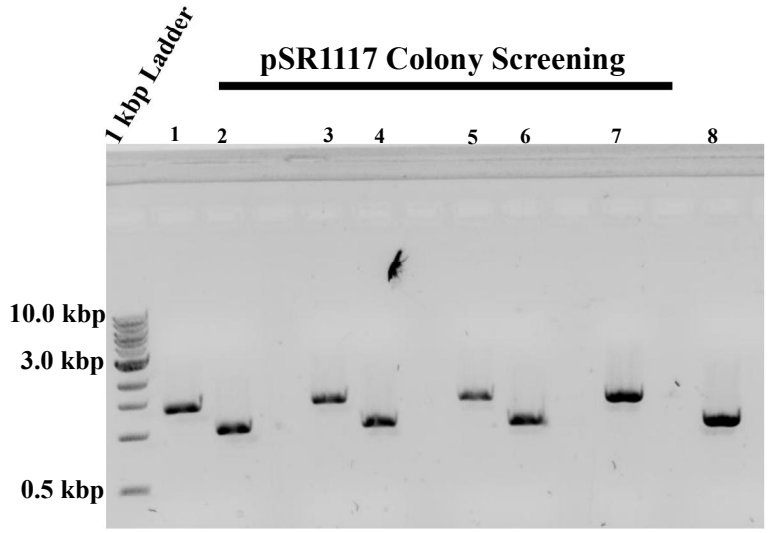

Figure 5.34 Initial colony PCR screening for genomic integration of pSR1117. A 0.7% agarose gel stained with ethidium bromide shows colony PCR results for 8 *C. merolae* colonies, tested with two primer sets (1,3,5,7 sets – oSDR2637 and oSDR2607) and (2,4,6,8 sets - oSDR2259 and oSDR2645). The expected bands of 1,358 bp and 979 bp, indicating successful genomic insertion, are displayed. A 1 kb DNA ladder was used as a size marker for reference.

This follow-up experiment aimed to confirm successful recombination and integration into the *CMK142* locus, using wild-type *C. merolae* genomic DNA as a control (Figure 5.35).

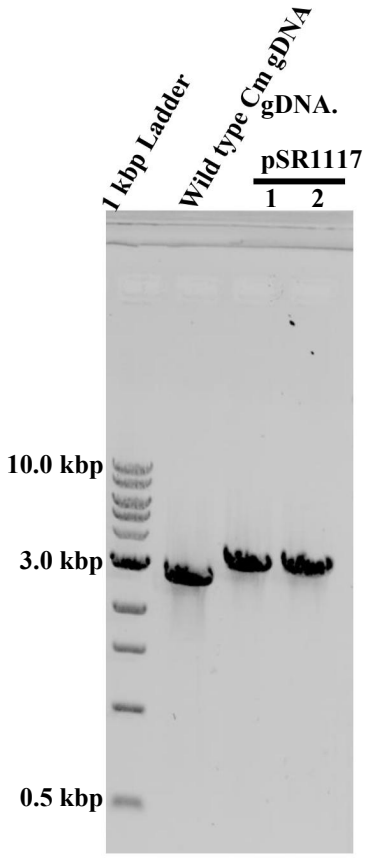

Figure 5.35. PCR confirming genomic integration of pSR1117. A 0.7% agarose gel containing ethidium bromide showing the PCR results for two promising CMK142 knockout candidates (1 and 2) showing the expected 2,822 bp band for wild-type (WT) genomic DNA sample and 3,329 bp band for integrands. A 1 kb DNA ladder was used as a size reference.

Cells were cultured and transiently transformed with the pSR1128 (Δ372–405) strain carrying the *CAT* gene. By day 9 post-transformation, a distinct difference between the control and the transformed cells was observed, and by day 12, the control cells had died while the transformants appeared dark green (Figure 5.36).

Figure 5.36. Chloramphenicol resistance in transformed *C. merolae* cells. Cells were transiently transformed with the pSR1128 (Δ372–405) strain harboring the *CAT* gene, with 150 µg/mL of chloramphenicol added every three days. By day 9 post-transformation, clear differences between control and transformed cells were visible. By day 12, control cells had died, while transformants exhibited a dark green coloration, confirming chloramphenicol resistance driven by the APCC promoter. nc = negative control Int = Integrands.

A final PCR analysis was performed to definitively confirm the knockout of *CMK142* and assess whether the prior transformation with sulfadiazine successfully disrupted *CMK142* or if the plasmid was merely integrated into the genome without knockout. This test ensured that the targeted homologous recombination event effectively removed the endogenous *CMK142* gene, validating the transformation process.

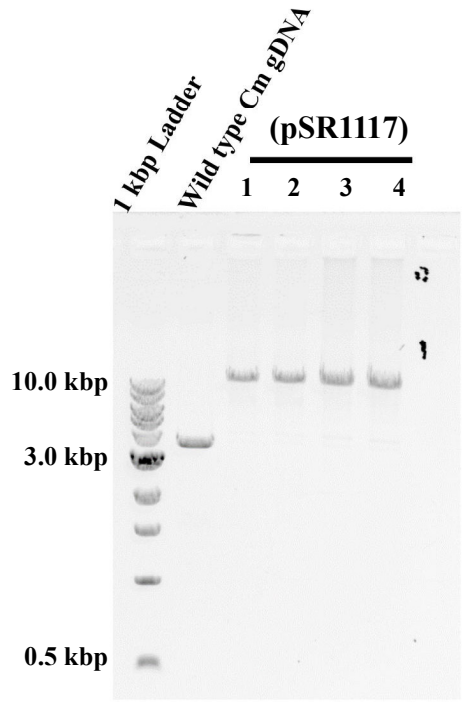

Figure 5.37. Final PCR analysis revealed unsuccessful integration of pSR1117 into the *CMK142* locus. A 0.7% agarose gel stained with ethidium bromide shows PCR results for four *CMK142* knockout candidates (lanes 1-4), each displaying an unexpected band above 10,000 bp. The wild-type (WT) sample, serving as a negative control, exhibits the expected 3,738 bp band. A 1 kb DNA ladder was used as a molecular size reference.

The appearance of an unexpected 10,000 bp band, rather than the expected 4,167 bp, indicates that the *CMK142* gene was not successfully knocked out during the transformation. The ability of the cells to grow in the presence of sulfadiazine suggests that while the selection marker was integrated into the genome, it did not disrupt the *CMK142* locus as intended. Subsequent

screenings of additional colonies yielded similar unsuccessful results. These findings suggest that, although integration occurred elsewhere in the genome, the desired knockout of *CMK142* was unsuccessful, necessitating further optimization of the plasmid shuffling technique approach in *C. merolae*.

5.4. Discussion

The Northern blot analysis results presented in this chapter revealed that the deletion of the P19 region (Δ372–405) in the RNA component of *Cyanidioschyzon merolae* RNase MRP results in a significant alteration in the stoichiometry of the two forms of 5.8S rRNA (Figure 5.30c and d). This observation underscores the role of RNase MRP in the biogenesis of 5.8S rRNA, aligning with its established function in *Saccharomyces cerevisiae* and *Drosophila melanogaster*. In these model organisms, mutations in RNase MRP lead to a shift in the ratio between the long and short forms of 5.8S rRNA (5.8S_L and 5.8S_S), typically maintained in a 10:1 ratio (long: short) (Schmitt and Clayton 1993; Schneider et al., 2010; Shadel et al., 2000). In *S. cerevisiae*, RNase MRP cleaves precursor rRNA at the A3 site, facilitating the generation of the shorter form of 5.8S rRNA (5.8S_S). The shift in stoichiometry observed in the *C. merolae* Δ372–405 mutant suggests that this region of RNase MRP RNA is required for similar rRNA processing, pointing to a conserved functional role of RNase MRP across eukaryotes.

Interestingly, in contrast to the P19 region deletion, the G162A mutant strain did not exhibit any noticeable effect on 5.8S rRNA processing (Figure 5.30e). This finding indicates that the G162A mutation does not disrupt RNase MRP functionality in *C. merolae*, as the stoichiometry of 5.8S rRNA remains unchanged. This observation mirrors studies in *S. cerevisiae*, where mutations in non-essential regions of RNase MRP RNA do not necessarily impair rRNA processing (Shadel et al., 2000; Figure 5.1 and Table 5.1). The lack of an effect in the G162A mutant suggests that

this region is not essential for the RNA-protein interactions or catalytic activity necessary for 5.8S rRNA processing. This also implies that certain regions of RNase MRP RNA are functionally redundant or dispensable, providing a more nuanced understanding of the structural and functional dynamics of RNase MRP.

An array of mutations in the RNA component of RNase MRP, each exhibiting distinct phenotypes, will be instrumental in future studies aimed at identifying the protein constituents of the MRP complex and elucidating the mechanisms that regulate its cellular localization and enzymatic function. By dissecting how different mutations impact RNase MRP activity, researchers can better understand the RNA-protein interactions and structural features required for the enzyme's role in rRNA processing.

These findings further support the hypothesis that the fundamental role of RNase MRP in 5.8S rRNA maturation is evolutionarily conserved across eukaryotes. As seen in other organisms, *C. merolae* depends on RNase MRP for precise regulation of 5.8S rRNA forms, with specific regions, such as the P19 region, playing an essential role in this process. The G162A mutation's lack of impact on 5.8S rRNA processing highlights that not all regions of the RNase MRP RNA are equally required, adding valuable insights into the structure-function relationship within the MRP complex.

Chapter 6 – General Conclusion and Remarks

I successfully clarified the role of RNase MRP in *C. merolae*, highlighting its conserved function in the processing of ribosomal RNA (rRNA), particularly in the generation of the two forms of 5.8S rRNA. This work has provided significant insights into the function and adaptation of RNase MRP in *C. merolae*. It was confirmed that *C. merolae* possesses two distinct forms of 5.8S rRNA in a 10:1 ratio (small: large), highlighting the role of RNase MRP in regulating rRNA stoichiometry, which is essential for ribosome biogenesis. Additionally, the study demonstrated that heat stress-induced intronic accumulation within the CMK142T gene does not affect RNase MRP's catalytic activity or the stoichiometry of 5.8S rRNA forms. This finding indicates that *C. merolae* maintains rRNA processing efficiency despite environmental stress.

Also, despite a reduction in pre-rRNA levels under heat stress, the unaltered levels of mature 28S and 18S rRNAs in *C. merolae* suggest a sophisticated regulatory mechanism that ensures ribosome function is maintained even under extreme conditions. One possibility is that mature rRNAs, once formed, are highly stable and resistant to degradation, allowing their levels to remain constant even when rDNA transcription is inhibited (Grünberger et al., 2023). Additionally, *C. merolae* may possess an efficient rRNA processing machinery that maximizes the conversion of available pre-rRNA into mature rRNAs, compensating for the reduced precursor synthesis. Moreover, the organism may regulate rRNA turnover, slowing down the degradation of mature rRNAs during stress to preserve essential ribosomal components. These adaptive mechanisms, which may include specialized pathways that protect and stabilize rRNA, highlight the resilience of *C. merolae* and its ability to maintain cellular functions in the face of environmental challenges. This contrasts with other organisms, where a short heat shock inhibits pre-rRNA transcription and processing into mature rRNAs in mammals (Ghosha and Jacob 1996), heat stress inhibits rDNA transcription in animal cells (Ghosha and Jacob 1996; Coccia *et*

al.,2017), and In *Arabidopsis thaliana*, where heat stress disturbs nucleolar structure, inhibits pre-rRNA processing, and provokes imbalanced ribosome profiles leading to undetectable precursors of 18S, 5.8S, and 25S RNAs (Darriere *et al*., 2022), underscoring the evolutionary diversity in stress response strategies.

I also explored the impact of specific mutations on RNase MRP function and the results show that deletion of the P19 region (Δ372–405) in the RNase MRP RNA component causes a shift in the stoichiometry of the two forms of 5.8S rRNA, confirming RNase MRP's role in this process. In contrast, the G162A mutation did not affect 5.8S rRNA processing, indicating that this specific mutation does not interfere with the enzyme's functionality. These findings support the hypothesis of evolutionary conservation of RNase MRP's role in rRNA processing, aligning with what has been observed in other organisms, such as yeast and humans (Piccinelli *et al*., 2005, Schmitt and Clayton 1993, Rosenblad et al., 2006; Lopez *et al*. 2009, Goldfarb *et al.,* 2017).

Furthermore, computational analyses revealed that RNase MRP RNA in *C. merolae* retains conserved structural regions similar to those in other eukaryotes, supporting the evolutionary conservation of its function. The RNase MRP complex in *C. merolae* comprises a reduced set of five protein constituents compared to eleven in *Saccharomyces cerevisiae*, reflecting an evolutionary adaptation to its unique cellular context.

The significance of this research lies in its contribution to understanding the fundamental role of RNase MRP in eukaryotic biology. Studying *C. merolae*, a red alga with a streamlined genome, provides valuable insights into how core cellular mechanisms function in simpler organisms, free from the genetic redundancies often seen in more complex systems. The evolutionary conservation of RNase MRP suggests that findings from this study could have broad biological implications, extending to more complex organisms, including humans where RNase MRP

mutations in humans are linked to genetic disorders such as cartilage-hair hypoplasia (CHH) (Hirose *et al*.,2006) a condition characterized by skeletal abnormalities, immunodeficiency, and increased cancer susceptibility. Understanding the role of RNase MRP in *C. merolae* again helps to deepen our knowledge of how similar mutations may affect their function in humans.

Looking forward, this study opens several new avenues for research. Further exploration of RNase MRP's molecular mechanisms, especially how specific regions of the enzyme interact with its protein components, will provide a deeper understanding of its function. Comparative studies between *C. merolae* and other organisms can help to delineate conserved and divergent aspects of RNase MRP across species. Also, structural studies using techniques like cryo-electron microscopy could offer high-resolution insights into the structure-function relationship of RNase MRP in *C. merolae*, advancing our understanding of this complex. Additionally, investigating the molecular mechanisms by which *C. merolae* maintains rRNA processing and ribosome function under heat stress could uncover novel regulatory pathways and stress response strategies. By addressing these areas, future research can build on the findings of this thesis to further elucidate the roles and adaptations of RNase MRP in eukaryotes, contributing to a more comprehensive understanding of ribosome biogenesis and cellular stress responses.

In conclusion, my research has significantly advanced our understanding of RNase MRP in *C. merolae*, reinforcing the enzyme's complex role in rRNA processing across species. The evolutionary conservation of RNase MRP underscores its importance in cellular processes and highlights its potential as a target for therapeutic intervention in diseases associated with rRNA processing dysfunction.

References

Altman, S. A view of RNase P. Mol. Biosyst. 3, 604–607 (2007).

Altschul, S.F. and Koonin, E.V. (1998) Iterated profile searches with PSI-BLAST—a tool for discovery in protein databases. Trends Biochem. Sci., 23, 444–447.

Altschul, S.F., Madden, T.L., Schaffer, A.A., Zhang, J., Zhang, Z., Miller, W. and Lipman, D.J. (1997) Gapped BLAST and Nucleic Acids Research, 2006, Vol. 34, No. 18 5155 Downloaded from https://academic.oup.com/nar/article/34/18/5145/3112050 by guest on 24 January 2022PSI-BLAST: a new generation of protein database search programs. Nucleic Acids Res., 25, 3389–3402.

An, W.; Du, Y.; Ye, K. Structural and functional analysis of Utp24, an endonuclease for processing 18S ribosomal RNA. *PLoS ONE* **2018**, *13*, e0195723. [CrossRef] [PubMed]

Aulds, J., Wierzbicki, S., McNairn, A. & Schmitt, M. E. Global identification of new substrates for the yeast endoribonuclease, RNase mitochondrial RNA processing (MRP). J. Biol. Chem. 287, 37089–37097 (2012).

Benson, D.A., Karsch-Mizrachi, I., Lipman, D.J., Ostell, J. and Wheeler, D.L. (2006) GenBank. Nucleic Acids Res., 34, D16–D20.

Bleichert, F.; Granneman, S.; Osheim, Y.N.; Beyer, A.L.; Baserga, S.J. The PINc domain protein Utp24, a putative nuclease, is required for the early cleavage steps in 18S rRNA maturation. *Proc. Natl. Acad. Sci. USA* **2006**, *103*, 9464–9469. [CrossRef] [PubMed]

Boulon S, Westman BJ, Hutten S, et al. The nucleolus under stress. Mol Cell. 2010;40(2):216–227.

Cai, T.; Aulds, J.; Gill, T.; Cerio, M.; E Schmitt, M. The Saccharomyces cerevisiae RNase mitochondrial RNA processing is critical for cell cycle progression at the end of mitosis. *Genetics* **2002**, *161*, 1029–1042.

Chamberlain, J. R., Lee, Y., Lane, W. S. & Engelke, D. R. Purification and characterization of the nuclear RNase P holoenzyme complex reveals extensive subunit overlap with RNase MRP. Genes Dev. 12, 1678–1690 (1998).

Chang, D.D.; Clayton, D.A. A mammalian mitochondrial RNA processing activity contains nucleus-encoded RNA. *Science* **1987**, *235*, 1178–1184. [CrossRef] *Biomolecules* **2020**, *10*, 783 24 of 28

Chang, D.D.; Clayton, D.A. Mouse RNAase MRP RNA is encoded by a nuclear gene and contains a decamer sequence complementary to a conserved region of mitochondrial RNA substrate. *Cell* **1989**, *56*, 131–139. [CrossRef]

Cherry JM, Adler C, Ball C, Chervitz SA, Dwight SS, Hester ET, Jia Y, Juvik G, Roe T, Schroeder M, Weng S, Botstein D. SGD: Saccharomyces Genome Database. Nucleic Acids Res. 1998 Jan 1;26(1):73-9. doi: 10.1093/nar/26.1.73. PMID: 9399804; PMCID: PMC147204.

Chu, S.; Archer, R.H.; Zengel, J.M.; Lindahl, L. The RNA of RNase MRP is required for normal processing of ribosomal RNA. *Proc. Natl. Acad. Sci. USA* **1994**, *91*, 659–663. [CrossRef] [PubMed]

Clayton, D.A. A nuclear function for RNase MRP. *Proc. Natl. Acad. Sci. USA* **1994**, *91*, 4615–4617. [CrossRef][PubMed]

Coccia M, Rossi A, Riccio A, et al. Human NF-kappaB repressing factor acts as a stress-regulated switch for ribosomal RNA processing and nucleolar homeostasis surveillance. Proc Natl Acad Sci U S A. 2017;114(5):1045–1050

Cui, P., Zhang, S., Ding, F., Ali, S., Xiong, L., and Li, L. The RNA polymerase I subunit RPA12p interacts with the stress response protein Msn2p and regulates its transcriptional activity. Current Genetics. **2017**, 63(3), 523-531.

Eddy, S.R. (1998) Profile hidden Markov models. Bioinformatics, 14, 755–763

Emsley, P., Lohkamp, B., Scott, W. & Cowtan, K. Features and development of Coot. Acta Crystallography. Sec. D Biol. Crystallography. 66, 486–501 (2010).

Esakova, O. & Krasilnikov, A. S. Of proteins and RNA: the RNase P/MRP family. RNA. **2010**, 16, 1725–1747.

Esakova, O., Perederina, A., Berezin, I. & Krasilnikov, A. S. Conserved regions of ribonucleoprotein ribonuclease MRP are involved in interactions with its substrate. Nucleic Acids Res. 41, 7084–7091 (2013).

Esakova, O., Perederina, A., Quan, C., Berezin, I. & Krasilnikov, A. S. Substrate recognition by ribonucleoprotein ribonuclease MRP. RNA 17, 356–364 (2011).

Esakova, O., Perederina, A., Quan, C., Schmitt, M. E. & Krasilnikov, A. S. Footprinting analysis demonstrates extensive similarity between eukaryotic RNase P and RNase MRP holoenzymes. RNA 14, 1558–1567 (2008).

Fabian, Sievers., Desmond, G., Higgins. (2013). 2. Clustal Omega, accurate alignment of very large numbers of sequences.. Methods of Molecular Biology, doi: 10.1007/978-1-62703-646-7_6

Fabian, Sievers., Andreas, Wilm., David, Dineen., Toby, J., Gibson., Kevin, Karplus., Weizhong, Li., Rodrigo, Lopez., Hamish, McWilliam., Michael, Remmert., Johannes, Söding., Julie, D., Thompson., Desmond, G., Higgins. (2010). 5. Fast, scalable generation of high-quality protein multiple sequence alignments using Clustal Omega. Molecular Systems Biology, doi: 10.1038/MSB.2011.75

Fujiwara, T., Ohnuma, M. (2017). Procedures for Transformation and Their Applications in *Cyanidioschyzon merolae*. In: Kuroiwa, T., *et al.* Cyanidioschyzon merolae. Springer, Singapore. https://doi.org/10.1007/978-981-10-6101-1_7

Garcia, P. D. et al. Stability and nuclear localization of yeast telomerase depend on protein components of RNase P/MRP. Nat. Commun. 11, 2173 (2020).

Ghoshal K, Jacob ST. Heat shock inhibits pre-rRNA processing at the primary site in vitro and alters the activity of some rRNA binding proteins. J Cell Biochem. 1996;62(4):506–515.

Gill, T.; Cai, T.; Aulds, J.; Wierzbicki, S.; Schmitt, M.E. RNase MRP cleaves the CLB2 mRNA to promote cell cycle progression: Novel method of mRNA degradation. *Mol. Cell Biol.* **2004**, *24*, 945–953. [CrossRef]

Gold, H.; Topper, J.; Clayton, D.; Craft, J. The RNA processing enzyme RNase MRP is identical to the Th RNP and related to RNase P. *Science* **1989**, *245*, 1377–1380. [CrossRef]

Goldfarb, K.C.; Cech, T.R. Targeted CRISPR disruption reveals a role for RNase MRP RNA in human preribosomal RNA processing. *Genes Dev.* **2017**, *31*, 59–71. [CrossRef]

Gopalan, V., Jarrous, N. & Krasilnikov, A. S. Chance and necessity in the evolution of RNase P. RNA 24, 1–5 (2018).

Grant, T., Rohou, A. & Grigorieff, N. cisTEM, user-friendly software for single-particle image processing. eLife 7, e35383 (2018).

Grünberger F, Schmid G, El Ahmad Z, Fenk M, Vogl K, Reichelt R, Hausner W, Urlaub H, Lenz C, Grohmann D. Uncovering the temporal dynamics and regulatory networks of thermal stress response in a hyperthermophile using transcriptomics and proteomics. mBio. 2023 Dec 19;14(6): e0217423. Doi: 10.1128/mbio.02174-23. Epub 2023 Oct 16. PMID: 37843364; PMCID: PMC10746257.

Hayashi K, Matsunaga S. Heat and chilling stress induce nucleolus morphological changes. J Plant Res. 2019;132(3):395–403.

Henras AK, Plisson-Chastang C, O'Donohue MF, et al. An overview of pre-ribosomal RNA processing in eukaryotes. Wiley Interdiscip Rev RNA. 2015;6(2):225–242.

Hermanns P, Tran A, Munivez E, *et al*. RMRP mutations in cartilage-hair hypoplasia. Am J Med Genet A 2006 **140**:2121-2130

Hirose Y, Nakashima E, Ohashi H, *et al*. Identification of novel RMRP mutations and specific founder haplotypes in Japanese patients with cartilage-hair hypoplasia. J Hum Genet 2006; **51**:706-710

Hui, J. Regulation of mammalian pre-mRNA splicing. *SCI CHINA SER C* **52**, 253–260 (2009). https://doi.org/10.1007/s11427-009-0037-0

Jarrous, N. & Gopalan, V. Archaeal/eukaryal RNase P: subunits, functions and RNA diversification. Nucleic Acids Res. 38, 7885–7894 (2010)

JC Venter MD Adams EW Myers PW Li RJ Mural *et al.* (2001) The sequence of the human genome. *Science* **291** 1304–1351 1:CAS:528:DC%2BD3MXhtlSgsbo%3D 11181995

Kalinina NO, Makarova S, Makhotenko A, et al. The multiple functions of the nucleolus in plant development, disease and stress responses. Front Plant Sci. 2018;9:132.

Karen, R., Christie., Shuai, Weng., Rama, Balakrishnan., Maria, C., Costanzo., Kara, Dolinski., Selina, S., Dwight., Stacia, R., Engel., Becket, Feierbach., Dianna, G., Fisk., Jodi, E., Hirschman., Eurie, L., Hong., Laurie, Issel-Tarver., Robert, S., Nash., Anand, Sethuraman., Barry, Starr., Chandra, L., Theesfeld., Rey, Andrada., Gail, Binkley., Qing, Dong., Christopher, Lane., Mark, Schroeder., David, Botstein., J., Michael, Cherry. (2003). Saccharomyces Genome

Database (SGD) provides tools to identify and analyze sequences from Saccharomyces cerevisiae and related sequences from other organisms.. Nucleic Acids Research, doi: 10.1093/NAR/GKH033.

Karwan, R., Bennett, J. L. & Clayton, D. A. Nuclear RNase MRP processes RNA at multiple discrete sites: interaction with an upstream G box is required for subsequent downstream cleavages. Genes Dev. 5, 1264–1276 (1991).

Kazantsev, A. V. et al. Crystal structure of a bacterial ribonuclease P RNA. Proc. Natl Acad. Sci. USA 102, 13392–13397 (2005).

Khanova, E., Esakova, O., Perederina, A., Berezin, I. & Krasilnikov, A. S. Structural organizations of yeast RNase P and RNase MRP holoenzymes as revealed by UV-crosslinking studies of RNA-protein interactions. RNA 18, 720–728 (2012).

Kim, J. S., Mizoi, J., Yoshida, T., Fujita, Y., Nakajima, J., Ohori, T., and Shinozaki, K. Heat stress-responsive transcriptome analysis in heat-tolerant and sensitive genotypes of Arabidopsis thaliana. Journal of Plant Research. **2012**, 125(4), 611-618.

Kobayashi, Y., Ohnuma, M., Kuroiwa, T., Tanaka, K., & Hanaoka, M. The basics of cultivation and molecular genetic analysis of the unicellular red alga *Cyanidioschyzon merolae*. *Journal of Endocytobiosis and Cell Research*, 2010;*20*, 53-61.

Krasilnikov, A. S., Xiao, Y., Pan, T. & Mondragon, A. Basis for structural diversity in homologous RNAs. Science 306, 104–107 (2004).

Kressler, D., Hurt, E., and Bassler, J. Driving ribosome assembly. Biochimica et Biophysica Acta (BBA)-Molecular Cell Research. **2010,** 1803(6), 673-683.

Kufel, J.; Dichtl, B.; Tollervey, D. Yeast Rnt1p is required for cleavage of the pre-ribosomal RNA in the 3*0* ETS but not the 5*0* ETS. *RNA* **1999**, *5*, 909–917. [CrossRef] [PubMed]

Lamolle, G., Musto, H. Why do Prokaryote's Genomes Lack Genes with Introns Processed by Spliceosomes? *J Mol Evol* **86**, 611–612 (2018). https://doi.org/10.1007/s00239-018-9874-4

Lan, P. et al. Structural insight into precursor tRNA processing by yeast ribonuclease P. Science 362, pii: eaat6678 (2018).

Lander E, et al. Initial sequencing and analysis of the human genome. Nature. 2001; 409:860–921. [PubMed: 11237011]

Lefort MC, Brown S, Boyer S, Worner S, Armstrong K. The PGI enzyme system and fitness response to temperature as a measure of environmental tolerance in an invasive species. PeerJ. 2014 Nov 25;2: e676. Doi: 10.7717/peerj.676. PMID: 25469320; PMCID: PMC4250065.

Lemieux, B. et al. Active yeast telomerase shares subunits with ribonucleoproteins RNase P and RNase MRP. Cell 165, 1171–1181 (2016

Li, X., Zaman, S., Langdon, Y., ZengelJ.M. & Lindahl. Identification of a functional core in the RNA component of RNase MRP of budding yeasts. Nucleic Acids Res. 32, 3703–3711 (2004).

Li, X.; Zengel, J.M.; Lindahl, L. A Novel Model for the RNase MRP-Induced Switch Between the Formation of Different Forms of 5.8S rRNA. *Int. J. Mol. Sci.* **2021**, *22*, 6690. https://doi.org/10.3390/ijms22136690

Liebschner, D. et al. Macromolecular structure determination using X-rays, neutrons, and electrons: recent developments in Phenix. Acta Crystallography. Sec. D Biol. Crystallogr. 75, 861–877 (2019).

Lindahl, L. et al. RNase MRP is required for the entry of 35S precursor rRNA into the canonical processing pathway. RNA 15, 1407–1416 (2009).

Lindahl, L.; Archer, R.H.; Zengel, J.M. A new rRNA processing mutant of Saccharomyces cerevisiae. *Nucleic Acids Res.* **1992**, *20*, 295–301. [CrossRef] [PubMed]

Lindahl, L.; Archer, R.H.; Zengel, J.M. A new rRNA processing mutant of Saccharomyces cerevisiae. *Nucleic Acids Res.* **1992**, *20*, 295–301. [CrossRef] [PubMed]

Lindahl, L.; Fretz, S.; Epps, N.; Zengel, J.M. Functional equivalence of hairpins in the RNA subunits of RNase MRP and RNase P in Saccharomyces cerevisiae. *RNA* **2000**, *6*, 653–658. [CrossRef]

Lopez, M. D., Rosenblad, M. A. & Samuelsson, T. Conserved and variable domains of RNase MRP RNA. RNA Biol. 6, 208–220 (2009).

Lygerou, Z., Allmang, C., Tollervey, D. & Seraphin, B. Accurate processing of a eukaryotic precursor ribosomal RNA by Ribonuclease MRP in vitro. Science 272, 268–270 (1996).

Lygerou, Z., Mitchell, P., Petfalski, E., Seraphin, B. & Tollervey, D. The POP1 gene encodes a protein component common to the RNase MRP and RNase P ribonucleoproteins. Genes Dev.**1994**, 8, 1423–1433.

Lygerou, Z.; Allmang, C.; Tollervey, D.; Seraphin, B. Accurate processing of a eukaryotic precursor ribosomal RNA by ribonuclease MRP in vitro. *Science* **1996**, *272*, 268–270.[CrossRef]

Marcela Dávila López, Magnus Alm Rosenblad & Tore Samuelsson (2009) Conserved and variable domains of RNase MRP RNA, RNA Biology, 6:3, 208-221, DOI: 10.4161/ rna.6.3.8584

McKusick VA. Mendelian inheritance in man. A catalog of human genes and genetic disorders. Baltimore: Johns Hopkins University Press, 1998; Online Mendelian Inheritance in Man (OMIM) is hosted at http://www.ncbi.nlm.nih.gov/omim/.

Mitchell, P.; Petfalski, E.; Shevchenko, A.; Mann, M.; Tollervey, D. The exosome: A conserved eukaryotic RNA processing complex containing multiple 3*0!5*0 exoribonucleases. *Cell* **1997**, *91*, 457–466. [CrossRef]

Nozaki, H., Takano, H., Misumi, O., Terasawa, K., Matsuzaki, M., Maruyama, S., Nishida, K., Yagisawa, F., Yoshida, Y., Fujiwara, T., Takio, S., Tamura, K., Chung, S. J., Nakamura, S., Kuroiwa, H., Tanaka, K., Sato, N., & Kuroiwa, T. (2007). A 100%-complete sequence reveals unusually simple genomic features in the hot-spring red alga Cyanidioschyzon merolae. *BMC Biology*, *5*(1), 28. https://doi.org/10.1186/1741-7007-5-28

Perederina, A., Esakova, O., Quan, C., Khanova, E. & Krasilnikov, A. S. Eukaryotic ribonucleases P/MRP: the crystal structure of the P3 domain. EMBO J. 29, 761–769 (2010).

Perederina, A., I. Berezin, I. & Krasilnikov, A. S. In vitro reconstitution and analysis of eukaryotic RNase P RNPs. Nucleic Acids Res. 46, 6857–6868 (2018).

Perederina, A., Li, D., Lee, H. *et al.* Cryo-EM structure of catalytic ribonucleoprotein complex RNase MRP. *Nat Commun* **11**, 3474 (2020). https://doi.org/10.1038/s41467-020-17308-z

Pettersen, E. F. et al. UCSF Chimera visualization system for exploratory research and analysis. J. Comput. Chem. 25, 1605–1612 (2004).

Piccinelli P, Rosenblad MA, Samuelsson T. Identification and analysis of ribonuclease P and MRP RNA in a broad range of eukaryotes. Nucleic Acids Res. 2005 Aug 8;33(14):4485-95. doi: 10.1093/nar/gki756. PMID: 16087735; PMCID: PMC1183490.

Piccinelli, P., Rosenblad, M. A. & Samuelsson, T. Identification and analysis of Ribonuclease P and MRP RNA in a broad range of eukaryotes. Nucleic Acids Res. 33, 4485–4495 (2005).

Puig, O. et al. The tandem affinity purification (TAP) method: a general procedure of protein complex purification. Methods 24, 218–229 (2001).

Raje HS, Lieux ME, DiMario PJ. R1 retrotransposons in the nucleolar organizers of Drosophila melanogaster are transcribed by RNA polymerase I upon heat shock. Transcription. 2018;9 (5):273–285.

Reddy, R.; Li, W.Y.; Henning, D.; Choi, Y.C.; Nohga, K.; Busch, H. Characterization and subcellular localization of 7-8 S RNAs of Novikoff hepatoma. *J. Biol. Chem.* **1981**, *256*, 8452–8457.

Reich, C.; Olsen, G.; Pace, B.; Pace, N. Role of the protein moiety of ribonuclease P, a ribonucleoprotein enzyme. *Science* **1988**, *239*, 178–181. [CrossRef]

Reimer, G.; Raška, I.; Scheer, U.; Tan, E.M. Immunolocalization of 7-2-ribonucleoprotein in the granular component of the nucleolus. *Exp. Cell Res.* **1988**, *176*, 117–128. [CrossRef]
Lygerou, Z.; Allmang, C.; Tollervey, D.; Séraphin, B. Accurate processing of a eukaryotic precursor ribosomal RNA by ribonuclease MRP in vitro. *Science* **1996**, *272*, 268–270. [CrossRef]

Reiter, N. J. et al. Structure of a bacterial ribonuclease P holoenzyme in complex with tRNA. Nature 468, 784–789 (2010).

Reiter, N. J., Can, C. W. & Mondragón, A. Emerging structural themes in large RNA molecules. Curr. Opin. Struct. Biol. 21, 319–326 (2011).

Ridanpa¨a, M. et al. Mutations in the RNA component of RNase MRP cause a pleiotropic human disease, cartilage-hair hypoplasia. Cell 104, 195–203(2001). Guerrier-Takada, C., Gardiner, K., Marsh, T., Pace, N. & Altman, S. The RNA moiety of ribonuclease P is the catalytic subunit of the enzyme. Cell 35, 849–857 (1983).

Rogozin, I.B., Carmel, L., Csuros, M. *et al.* Origin and evolution of spliceosomal introns. *Biol Direct* **7**, 11 (2012). https://doi.org/10.1186/1745-6150-7-11

Rosenblad, M. A., Lopez, M. D., Piccinelli, P. & Samuelsson, T. Inventory and analysis of the protein subunits of the ribonucleases P and MRP provides further evidence of homology between the yeast and human enzymes. Nucleic Acids Res. 34, 5145–5156 (2006).

Rudenko, V.; Korotkov, E. Study of Dispersed Repeats in the Cyanidioschyzon merolae Genome. Int. J. Mol. Sci. 2024, 25, 4441. https:// doi.org/10.3390/ijms25084441

Saito, Y. et al. RNase MRP cleaves pre-tRNASer-Met in the tRNA maturation pathway. PLoS ONE 9, e112488 (2014).

Salinas, K.; Wierzbicki, S.; Zhou, L.; Schmitt, M.E. Characterization and purification of Saccharomyces cerevisiae RNase MRP reveals a new unique protein component. *J. Biol. Chem.* **2005**, *280*, 11352–11360. [CrossRef]

Schmitt, M. E. & Clayton, D. A. Characterization of a unique protein component of yeast RNase MRP: an RNA-binding protein with a zinc-cluster domain. Genes Dev. 8, 2617–2628 (1994).

Schmitt, M. E. & Clayton, D. A. Nuclear RNase MRP is required for the correct processing of pre-5.8S rRNA in Saccharomyces cerevisiae. Mol. Cell. Biol. 13, 7935–7941 (1993).

Schmitt, M.E.; Bennett, J.L.; Dairaghi, D.J.; Clayton, D.A. Secondary structure of RNase MRP RNA as predicted by phylogenetic comparison. *FASEB J.* **1993**, *7*, 208–213. [CrossRef] [PubMed]

Schmitt, M.E.; Clayton, D.A. Characterization of a unique protein component of yeast RNase MRP: An RNA-binding protein with a zinc-cluster domain. *Genes Dev.* **1994**, *8*, 2617–2628. [CrossRef]

Schmitt, M.E.; Clayton, D.A. Nuclear RNase MRP is required for correct processing of pre-5.8S rRNA in Saccharomyces cerevisiae. *Mol. Cell Biol.* **1993**, *13*, 7935–7941. [CrossRef] [PubMed]

Schneider MD, Bains AK, Rajendra TK, Dominski Z, Matera AG, Simmonds AJ. Functional characterization of the Drosophila MRP (mitochondrial RNA processing) RNA gene. RNA. 2010 Nov;16(11):2120-30. doi: 10.1261/rna.2227710. Epub 2010 Sep 20. PMID: 20855541; PMCID: PMC2957052.

Scott C. Walker, Johanna M. Avis, Secondary structure probing of the human RNase MRP RNA reveals the potential for MRP RNA subsets, Biochemical and Biophysical Research Communications, Volume 335, Issue 2, 2005, Pages 314-321, https://doi.org/10.1016/j.bbrc.2005.07.074

Shadel GS, Buckenmeyer GA, Clayton DA, Schmitt ME. Mutational analysis of the RNA component of Saccharomyces cerevisiae RNase MRP reveals distinct nuclear phenotypes. Gene. **2000** Mar 7;245(1):175-84. doi: 10.1016/s0378-1119(00)00013-5. PMID: 10713458.

Shadel GS, Clayton DA. Mitochondrial DNA maintenance in vertebrates. Annu Rev Biochem 1997; **66**:409-435.

Sharma S, Lafontaine DL. 'view from a bridge': a new perspective on eukaryotic rRNA base modification. Trends Biochem Sci. 2015;40(10):560–575.

Sloan KE, Warda AS, Sharma S, et al. Tuning the ribosome: the influence of rRNA modification on eukaryotic ribosome biogenesis and function. RNA Biol. 2017;14(9):1138–1152.

Stark MR, Dunn EA, Dunn WS, Grisdale CJ, Daniele AR, Halstead MR, Fast NM, Rader SD. Dramatically reduced spliceosome in Cyanidioschyzon merolae. Proc Natl Acad Sci U S A. 2015 Mar 17;112(11): E1191-200. doi: 10.1073/pnas.1416879112. Epub 2015 Mar 2. PMID: 25733880; PMCID: PMC4371933.

Stepinski D. Functional ultrastructure of the plant nucleolus. Protoplasma. 2014;251(6):1285-1306

T. Darriere, E. Jobet, D. Zavala, M.L. Escande, N. Durut, A. de Bures, F. Blanco-Herrera, E.A. Vidal, M. Rompais, C. Carapito, S. Gourbiere & J. Sáez-Vásquez (2022) Upon heat stress processing of ribosomal RNA precursors into mature rRNAs is compromised after cleavage at primary P site in Arabidopsis thaliana, RNA Biology, 19:1, 719-734, DOI: 10.1080/15476286.2022.2071517

Tomecki R, Sikorski PJ, Zakrzewska-Placzek M. Comparison of preribosomal RNA processing pathways in yeast, plant, and human cells - focus on the coordinated action of endo- and exoribonucleases. FEBS Lett. 2017;591(13):1801–1850.

Topper, J.N.; Clayton, D.A. Characterization of human MRP/Th RNA and its nuclear gene: Full-length MRP/Th RNA is an active endoribonuclease when assembled as an RNP. *Nucleic Acids Res.* **1990**, *18*, 793–799. [CrossRef] [PubMed]

Torres-Larios, A., Swinger, K. K., Krasilnikov, A. S., Pan, T. & Mondragón, A. Crystal structure of the RNA component of bacterial ribonuclease P. Nature 437, 584–587 (2005).

Venema J, Tollervey D. Ribosome synthesis in *Saccharomyces cerevisiae*. Annu Rev Genet 1999; **33**:261-311

Walker, S.C.; Avis, J.M. A conserved element in the yeast RNase MRP RNA subunit can participate in a long-range base-pairing interaction. *J. Mol. Biol.* **2004**, *341*, 375–388. [CrossRef] [PubMed]

Wan, F. et al. Cryo-electron microscopy structure of an archaeal ribonuclease P holoenzyme. Nat. Commun. 10, 2617 (2019).

Ward, N. and Moreno-Hagelsieb, G. 2014. Quickly finding orthologs as reciprocal best hits with BLAT, LAST, and UBLAST: How much do we miss? PLoS ONE. 9(7): e101850.

Welting TJ, Kikkert BJ, Van Venrooij WJ, Pruijn GJ: Differential association of protein subunits with the human RNase MRP and RNase P complexes. RNA 2006, 12:1373-1382.

Woodhams, M.D., Stadler, P.F., Penny, D. *et al.* RNase MRP and the RNA processing cascade in the eukaryotic ancestor. *BMC Evol Biol* **7** (Suppl 1), S13 (2007). https://doi.org/10.1186/1471-2148-7-S1-S13

Wu, J. et al. Cryo-EM structure of the human ribonuclease P holoenzyme. Cell 175, 1393–1404 (2018).